The Influence of Steel Fibres on the Strength and Deformation Capacity of Reinforced Concrete Connections Using Nonlinear Finite Element Analysis

Jane Middlemiss

Abstract

The structural connections in a building transfer the load from one element to the next and are critical to the integrity of the structure. The load is transferred through the reinforcement and requires a suitable lap length to transfer the forces. There is debate on how long lap lengths should be and the design codes have major inconsistencies. The 2010 Model Code will be used in the new Eurocode 2 and requires a much larger lap length than the current Eurocode 2, which will be harder to work with and cost more to construct.

In design, steel fibres are only occasionally used due to limited knowledge around their behaviour within concrete and how they can be properly mixed during casting. This investigation looks at the influence of steel fibres on the strength and deformation capacity of reinforced concrete connections using nonlinear finite element analyses and examines the possibility of reducing the required lap length. A study of the equations in Eurocode 2 and the 2010 Model Code was undertaken to determine which is the most suitable for use in design. Small-scale concrete experiments were performed alongside the modelling to support the investigation and assess how the fibres behaved in practice.

It was found that steel fibres have a significant role in increasing the strength and deformation capacity of a reinforced concrete connection by preventing a brittle failure. The greater strength allows a shorter lap length to reach yield which could be advantageous in reducing the quantity of materials while still ensuring a sufficient transfer of load throughout the structure. The experiments concluded that steel fibres do increase the ductility of a concrete connection and therefore impede a sudden failure. However, due to the unpredictable behaviour of the fibres during concrete casting, the strength was lower than expected.

Table of Contents

List of Tables

List of Figures

List of Symbols and Abbreviations

Roman Uppercase Letters

$\mathbf{A_c}$	cross-sectional area
$\boldsymbol{A_{c,eff}}$	effective tension area
$\boldsymbol{A_{cb,eff}}$	effective tension area for lower surface
$\boldsymbol{A_{ct,eff}}$	effective tension area for upper surface
$\mathbf{A_h}$	hardening ductility parameter 1 in CDPM2
$\mathbf{A_s}$	ductility parameter during damage in CDPM2
$\mathbf{A_{steel}}$	area of steel
$\mathbf{B_h}$	hardening ductility parameter 2 in CDPM2
$\mathbf{B_s}$	damage ductility exponent during damage in CDPM2
C	concrete cover
$\mathbf{C_s}$	strain rate parameter in MAT_PLASTIC_KINEMATIC material model for reinforcement
$\mathbf{C_h}$	hardening ductility parameter 3 in CDPM2
D	diameter
$\mathbf{D_f}$	flow rule parameter in CDPM2
$\mathbf{D_h}$	hardening ductility parameter 4 in CDPM2
E	Young's modulus
$\mathbf{E_c}$	Young's modulus of concrete
$\mathbf{E_{ci}}$	Young's modulus at the concrete age of 28 days
$\mathbf{E_s}$	Young's modulus of Steel
F	force
$\mathbf{F_b}$	force of reinforcement bond
$\mathbf{F_{c0}}$	rate dependent parameter in CDPM2
$\mathbf{F_{ci}}$	compressive stress at which the initial yield surface is reached in CDPM2
$\mathbf{F_{max}}$	maximum load at failure
$\mathbf{F_s}$	steel force
$\mathbf{F_{strain}}$	effective plastic strain for eroding elements in MAT_PLASTIC_KINEMATIC material model for reinforcement

$\mathbf{F_y}$	rebar strength
$\mathbf{G_f}$	fracture energy of concrete
$\mathbf{H_p}$	hardening parameter in CDPM2
L	length
$\mathbf{L_b}$	lap length
$\mathbf{L_{b,rqm}}$	mean required lap length
$\mathbf{L_f}$	fibre length
$\mathbf{L_s}$	specimen length
N	axial force
$\mathbf{P_s}$	strain rate parameter in MAT_PLASTIC_KINEMATIC material model for reinforcement
$\mathbf{V_f}$	volume fraction of fibres

Roman Lowercase Letters

b	breadth
$\boldsymbol{c}$	speed of sound
$\boldsymbol{c_{3D-continuum}}$	speed of sound through a 3D-continuum in LS-DYNA
$\mathbf{c_{min}}$	minimum cover parameter
$\mathbf{c_{max}}$	maximum cover parameter
d	depth to rebar
$\mathbf{d_f}$	diameter of fibre
$\boldsymbol{e_{cc}}$	eccentricity parameter in CDPM2
$\boldsymbol{f_{bm}}$	ultimate bond stress
$\boldsymbol{f_c}$	uniaxial compressive strength
$\boldsymbol{f_{ck}}$	characteristic strength of concrete
$\boldsymbol{f_{cm}}$	mean compressive strength of concrete
$\boldsymbol{f_{ctm}}$	mean tensile strength of concrete
$\boldsymbol{f_{stm}}$	reinforcement stress for ribbed bars in a ‘good’ casting position
$\boldsymbol{f_t}$	tensile strength
$\boldsymbol{f_{t1}}$	tensile threshold value for bi-linear damage formulation in CDPM2
$\boldsymbol{f_y}$	yield stress of reinforcing steel

f_{yk}	characteristic value of yield stress of reinforcing steel
h	height
h_e	element length
k_1	coefficient which takes account of the bond properties of the bonded reinforcement in EC2
k_2	coefficient which takes account of the distribution of strain in EC2
k_3	coefficient in EC2
k_4	coefficient in EC2
k_m	represents the efficiency of confinement from transverse reinforcement
k_{tr}	density of transverse reinforcement relative to the anchored or lapped bars
n	number of bars
q_{h0}	initial hardening parameter in CDPM2
q_{h1}	hardening law dimensionless variable in CDPM2
q_{h2}	hardening law dimensionless variable in CDPM2
r	radius
s	slip
s_r	crack spacing
t_{min}	critical timestep
u	elongation
v_p	formulation for rate effects in MAT_PLASTIC_KINEMATIC material model for reinforcement
w_c	crack opening
w_f	tensile threshold value for linear tensile damage formulation in CDPM2
w_{f1}	tensile threshold value for the second part of bi-linear damage formulation in CDPM2
z	position along the beam

Greek Letters

α_1	coefficient for the effect of the form of the bars assuming adequate cover in EC2
α_2	coefficient for the effect of concrete minimum cover in EC2

α_3	coefficient for the effect of confinement by transverse reinforcement in EC2
α_5	coefficient for the effect of the pressure transverse to the plane of splitting along the design anchorage length in EC2
α_6	coefficient representing the percentage of lapped bars relative to the total cross-section area in EC2
β	hardening parameter in MAT_PLASTIC_KINEMATIC material model for reinforcement
β_1	orientation efficiency factor for 3D random fibre distribution
β_2	fraction of bond strength mobilized at cracking
γ_s	partial safety factor for steel
δ	displacement
δ_e	elastic displacement
δ_y	displacement at yield
ε_{fc}	parameter controlling compressive damage softening branch in CDPM2
ε	strain
η_1	coefficient related to the quality of the bond condition and the position of the bar during curing in EC2
η_2	coefficient relating to the bar diameter in EC2
$\dot{\varepsilon}$	strain rate
ε_{strong}	strain for strengthened section of reinforcement bar
θ	Lode angle
κ_p	hardening variable in CDPM2
λ_1	average pull-out length ratio
λ_2	factor accounting for post-cracking orientation efficiency
λ_3	group reduction factor
ρ	mass density
ρ_c	mass density of concrete
ρ_s	mass density of steel
σ	stress
σ_t	positive component of the effective stress

σ_c	negative component of the effective stress
σ_{cc}	cracking strength
σ_{mu}	tensile strength of concrete
σ_{pc}	post-cracking strength
σ_y	yield strength of reinforcement
τ	average bond strength at fibre concrete interface
τ_b	bond stress
ν	Poisson's ratio
ν_c	Poisson's ratio of concrete
ν_s	Poisson's ratio of steel
∅	diameter of reinforcement
ω_t	tensile scalar damage parameter in CDPM2
ω_c	compressive scalar damage parameter in CDPM2

Abbreviations

CDPM1	Concrete Damage Plasticity Model 1
CDPM2	Concrete Damage Plasticity Model 2
EC2	Eurocode 2
MC10	Model Code 2010
RC	Reinforced Concrete
RFC	Fibre Reinforced Concrete with Traditional Steel Bars
3D	Three-dimensional

Preface

This project was conducted in the School of Engineering at the University of Glasgow during the period from September 2018 to January 2019 to satisfy the requirements of the final year individual project for the Civil Engineering MEng Degree Programme.

I would like to thank my supervisor, Dr. Peter Grassl, for his guidance and support throughout the investigation. I would also like to express my thanks to Ian Gardner and Tim Montgomery for their assistance with the concrete experiments.

1 Introduction

1.1 Background

Providing safe and stable infrastructure is a key priority for civil engineers. The connections of structural members, both beam-beam connections and beam-column connections, within a piece of infrastructure are an integral part of the structure's stability. Reinforced concrete connections are designed with lapped reinforcement bars which transfers the steel force along the bars. One of the main objectives when designing connections is to ensure there is a large enough lap length to allow the connection to transfer the load at the ultimate limit state. The strength of a connection is related to the yield strength of the reinforcement bars which correlates to the maximum load that the connection can sustain. It is useful to understand how much displacement occurs at this yield load before failure as a connection can still have a brittle failure once the force redistribution starts. This is where fibres may be able to increase the deformation capacity of the connection. The use of fibres in a reinforced concrete connection may be able to reduce the lap length required, decreasing the cost of material and easing constructability.

Analysing the structural response of connections experimentally can be a challenging task. There are many requirements that hinder this process being carried out at a real-life scale such as the time taken; space required; cost of operation; and health and safety concerns. Due to these factors, computer modelling has become a very popular technique and using the correct simplifications, the building elements behaviour can be analysed. Using computer models, together with selected experiments, can ensure that the investigations are done in a more economical and timely manner. Nonlinear finite element modelling can provide an understanding of the response of reinforced concrete.

In previous University of Glasgow projects, the response of reinforced concrete using CDPM2 was investigated. As an example, Lockhart (2017) modelled the failure of reinforced concrete with and without fibres using CDPM2 in LS-DYNA. There is, however, little research to explain how the addition of steel fibres affects the structural response and how the steel fibres affect the length of the reinforcement laps.

1.2 Aim and Objectives

The aim is to investigate the influence of steel fibres on the strength and deformation capacity of reinforced concrete connections using nonlinear finite element analysis.

The main objectives are:

- To verify and validate the model for a reinforced concrete prism to ensure that the model is both implemented correctly and producing accurate results which are then able to represent more complex situations.
- To improve the understanding of reinforced concrete connections by investigating how the length of the reinforcement lap affects the strength and deformation capacity and investigate the difference in the design codes values for the required lap length.
- To investigate how the reinforced concrete connections strength and deformation capacity are influenced by the addition of steel fibres and how the required lap length is affected as well as analyse how the fibres affect the ductility of the specimen.

1.3 Methodology

In this investigation, the nonlinear finite element approach is used to investigate the aim as stated above. Within the nonlinear finite element framework the Concrete Damage Plasticity Model 2 (CDPM2) has been used which incorporates both damage mechanics and plasticity to describe the multiaxial failure of concrete. For steel, a simple elasto-plastic model is used. For the analyses, the conventional finite element programme LS-DYNA has been used.

Small-scale concrete experiments have been conducted in the laboratory to strengthen the understanding of the effect of steel fibres in a concrete specimen. They show the different failures for a plain concrete sample compared to samples with volume fractions of steel fibres of 0.5 % and 1 %.

1.4 Outline of Report

This report consists of six chapters as follows:

- Chapter 2 is a literature review which explains the concepts and theory behind the project.
- Chapter 3 details the theory behind the nonlinear finite modelling, the constitutive models, the design of the required lap length and the maximum crack spacing.
- Chapter 4 explains the analyses including the geometry of each analysis; the input parameters; the results obtained; and then discusses and explains the results in relation to the theory.
- Chapter 5 describes how the concrete experiments were conducted and tested and explains the results in relation to the theory.
- Chapter 6 concludes the investigation and gives suggestions for further research.

2 Literature Review

This chapter explains the background and theory behind this investigation by means of a literature study. The material properties of concrete, steel reinforcement and steel fibres has been discussed as well as an explanation of how these materials behave together. The behaviour of connections has been explained along with nonlinear finite element modelling methods for the interaction of reinforcement with concrete and the processes of verification and validation.

2.1 Plain Concrete

Fresh concrete is made up of three main constituents which are cement, aggregate and water. In the hardened state, it has a high compressive strength and a low tensile strength. Due to this low tensile strength, plain concrete will normally be reinforced with steel bars which help to resist the tensile forces which arise in the concrete (Grassl, 2014).

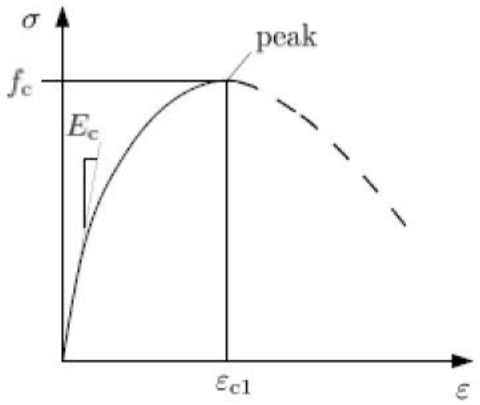

Figure 2.1: Schematic of a stress-strain curve for concrete subjected to compression (Grassl, 2018)

A generalized stress-strain curve for concrete subjected to compression is shown in Figure 2.1. This figure highlights that in the stress-strain space, the peak strength can be found. This implies that the strength of the concrete is a function of the stress state and therefore the concrete strength can be illustrated in the stress space by a strength envelope. Jirásek and Bažant (2002) explains that in the principal stress space the strength envelope of concrete is a deformed cone which has three planes of symmetry that intersect at the hydrostatic axis. A schematic of this is shown in Figure 2.2. The deviatoric sections of the failure surface are the shape of a rounded triangle which changes from triangular for tensile and low compressive hydrostatic pressures to circular for high compressive hydrostatic pressures.

Two meridians can be used to describe the change of shape in this deviatoric section. The tensile meridian resembles the stress states with two equal principal stresses smaller than the third one which

has a Lode angle, $\theta = 0$. The compressive meridian has a Lode angle, $\theta = \frac{\pi}{3}$ and corresponds to the stress states with two equal principal stresses larger than the third one. The Lode angle is defined by Jirásek and Bažant (2002) as "the deviatoric projection of the angle between the radius vector of the current stress point and the axis σ_1".

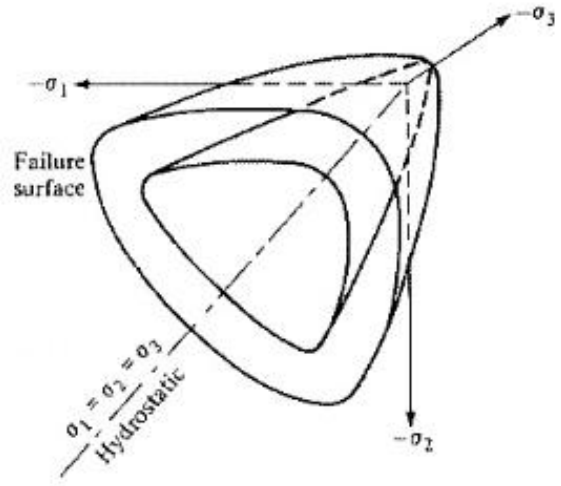

Figure 2.2: Failure surface of concrete in three-dimensional stress space (Chen, 2007)

Grassl et al. (2013) explains that concrete is a heterogeneous material and displays a "complex nonlinear mechanical behaviour". When subject to tension, the failure can be described as softening, which is a decrease of stress with an increase of deformation. These irreversible deformations occur during the plastic region of concrete failure and show up as cracks on a concrete specimen.

Under uniaxial tension, the stress-strain curves will behave elastically initially up to high stresses. Chen (2007) states that microcracks are found in concrete where interfaces form between coarse aggregates and mortar. A weak link is formed at this aggregate-mortar interface due to it having a lower tensile strength than the mortar and this is where failure will occur. According to Chen (2007), these microcracks will start to propagate when the stress is over 60% of the uniaxial tensile strength, f_t. When the load is increased, the microcracks will start to connect and create a localised zone at the weakest section. At 75% of f_t the specimen has reached the maximum load that it can resist and the cracks bridge together. The cracks that form will be perpendicular to the stress and the failure will be due to a small number of bridging cracks.

Figure 2.3(a) shows the load-displacement curve for a concrete sample under uniaxial tension. This relation can be converted into a stress-strain graph when there is a uniform deformation of stress. This can be done by dividing the displacement by the length of the concrete sample.

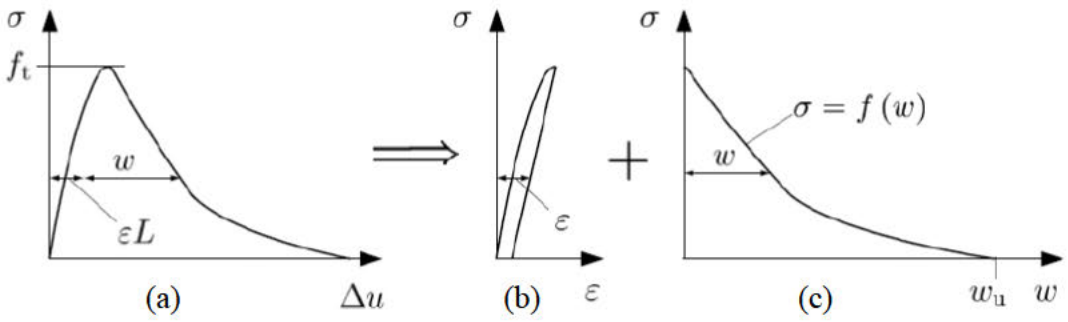

Figure 2.3: (a) stress-displacement relation for a uniaxial tension test; (b) the uniform displacement expressed in the form of a stress-strain curve; (c) the stress-displacement relation for localised deformations (modified from Grassl, 2018)

However, Grassl (2018) explains that this is not feasible when the deformations are localised due to the stress-strain relation depending on the sample length. A solution is to split the graph into (b) a stress-strain relation for the uniform deformations outside the fracture zone and (c) a stress-crack opening displacement relation from deformations in the fracture zone as shown in Figure 2.3. This shows that the total displacement Δu is the sum of the strain ε and the crack opening w_c. A significant parameter used in fracture mechanics of concrete is called the fracture energy, G_F. The fracture energy is defined in Grassl (2018) as the volume of energy dissipated during the fracture process and can be calculated from the area under the stress-crack opening curve (Figure 2.3(c)).

2.2 Concrete with Fibres

Fibres are able to modify the mechanical properties of concrete and are important for controlling crack growth. The fibres slow down the development of cracks and transfer load in this cracked area which influences the deformation behaviour of a cracked concrete member (Maidl and Dietrich, 1995). According to CEB-FIP (2013), the addition of fibres in concrete can reduce the brittle nature when in compression, however they have little effect on the elastic properties and the compressive strength unless a large volume of fibres is used. Conversely, when used in tension they can increase the tensile strength as well as the brittleness of the sample (Maidl and Dietrich, 1995).

Figure 2.4 shows a typical load elongation response for concrete with steel fibres subjected to tension. Naaman (1987) explains that the first stage is linear up to the cracking stress and will very closely match that of normal reinforced concrete. When cracking occurs there will be a drastic change in the slope. The next stage of the graph represents the failure and pull-out of the fibres and occurs when the post-cracking stress is lower than the cracking stress.

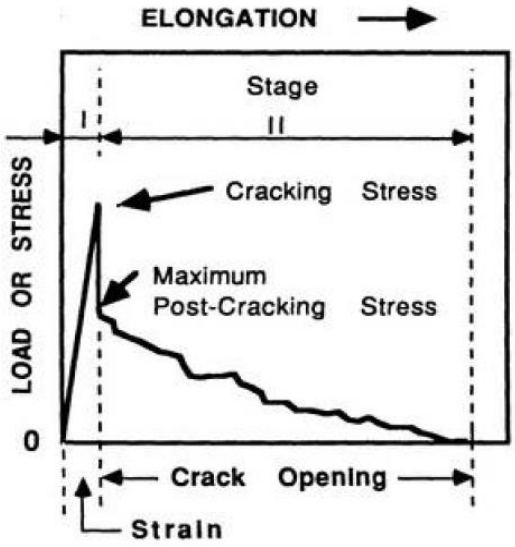

Figure 2.4: Typical load elongation response in tension of steel fibre reinforced concrete (Naaman, 1987)

Failure of concrete with steel fibres can occur from either the pull-out or the splitting of the fibre. Both failure mechanisms depend on a number of factors which are: the aspect ratio; anchorage; tensile strength; and bonding strength of the fibres to the concrete (Maidl and Dietrich, 1995).

2.2.1 Bond of Concrete to Fibres

Bond characteristics depend on a number of factors which are: the orientation of the fibres; the embedded length of the fibres; the shape of the fibres; and the strength of the concrete (Aslani and Nejadi, 2012). The bond stress also depends on the make-up of the surface of the fibre as a rougher surface allows more bond stress to transfer from the fibre to the concrete (Maidl and Dietrich, 1995). The mechanical properties of the concrete are influenced by the bond characteristics between the fibres and the concrete. The load at which the fibre either pulls out or fractures is related to the transfer of the bond stress between the fibres and the concrete and on the anchorage length of the fibres (Maidl and Dietrich, 1995).

2.3 Steel Reinforced Concrete

Steel reinforcement bars are often used in concrete structures to strengthen the structure against tensile forces. The bars are often ribbed which helps the concrete and reinforcement to bond together. The steel reinforcement bars are ductile which means that when subjected to loading, both elastic and plastic deformations occur (Grassl, 2014). The bar will initially behave elastically until the applied force reaches the elastic limit. The stress at the elastic limit is normally called the yield strength of the reinforcement. After the elastic limit has been reached, the behaviour of the bar will become plastic and any deformations that occur after this point will not be recoverable. The relationship between stress and strain can be represented in a simplified graph shown in Figure 2.5.

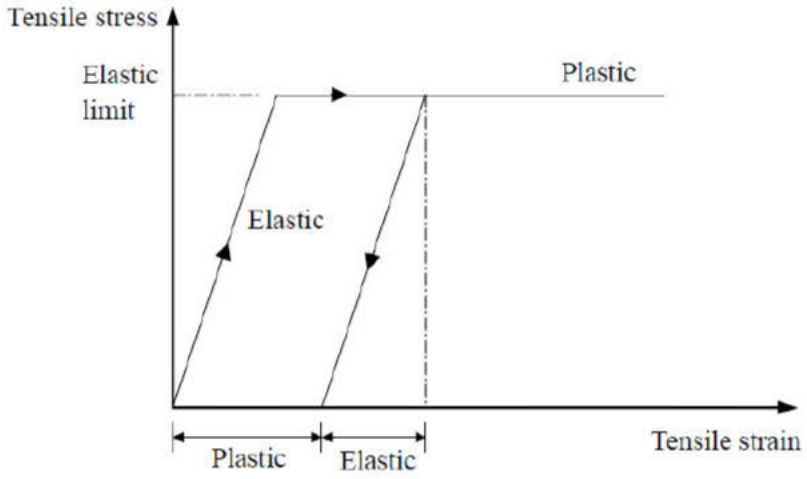

Figure 2.5: Stress-strain graph for reinforcing steel (Grassl, 2014)

Steel reinforced concrete has many important material properties which are advantageous when used as a construction material; and makes it one of the most popular materials used in construction today. Concrete has a very high strength and can withstand both compression and tension when reinforced with steel. A reinforced concrete element subjected to load will have a nonlinear load-deflection response. This nonlinear response is dictated by the cracking of the concrete and the plasticity of both the reinforcement and compression concrete as stated by Chen (2007). This cracking response can be portrayed in an idealized schematic as shown in Figure 2.6 for a reinforced concrete specimen. The cracking response of a reinforced concrete beam specimen subjected to a uniaxial tensile load can be split into a number of stages. The stages are the uncracked stage, initiation stage, cracking stage, stabilised cracking and yielding (Grassl, 2018).

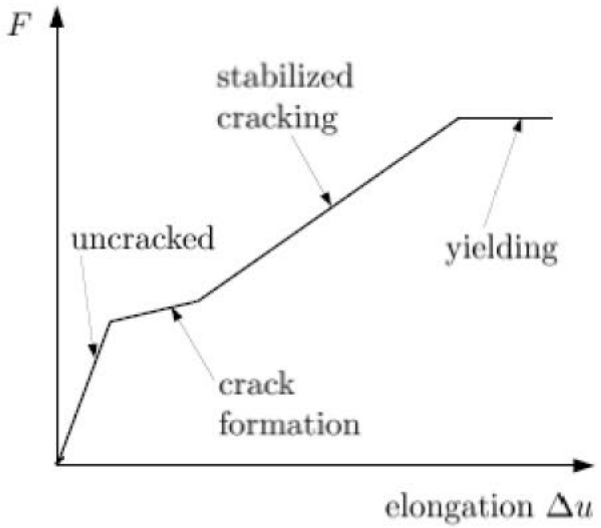

Figure 2.6: Idealized load-displacement graph for a cracked reinforced concrete specimen (modified from Grassl, 2018)

The first uncracked stage is linear and here the load is not high enough to initiate cracking. During the cracking stage, cracks continue to develop as the load increases until the cracks are close together and no new cracks can form between the existing cracks. Grassl (2018) explains that these new cracks

are unable to form due to the small transfer length between the already formed cracks. The tensile force is transferred from the reinforcement bar to the surrounding concrete by bond stresses and each new crack decreases the overall stiffness of the concrete member. The stage after the development of the cracks is called stabilised cracking where no new cracks form, but as the load continues to increase, the crack widths increase.

2.3.1 Bond of Concrete to Reinforcement

Bond is defined in CEB-FIP (2013) as the interaction and transfer of forces between reinforcement bars and concrete. The stresses at the interface between these two materials are called bond stresses. When the reinforcement bar slips, the bond stresses will then become active (Grassl, 1999). The bond between concrete and reinforcement is often improved by using ribbed bars which help to transfer force along the bar (Cairns, 2015).

The bond stress–slip relationship is influenced by rib geometry, concrete strength, position and orientation of the bar during casting, state of stress, boundary conditions and concrete cover as stated in CEB-FIP (2013). Figure 2.7 shows the bond stress–slip relationship for monotonic loading. CEB-FIP (2013) explains that the first part of the graph represents local crushing and microcracking in the concrete which then becomes constant for confined concrete where advanced crushing and shearing of the concrete between the ribs occurs. The last stage is where the bond stress decreases with increasing slip which happens as concrete between the ribs is sheared off. In unconfined concrete, splitting failure is shown on the graph by a sudden decrease in the bond stress with increasing slip.

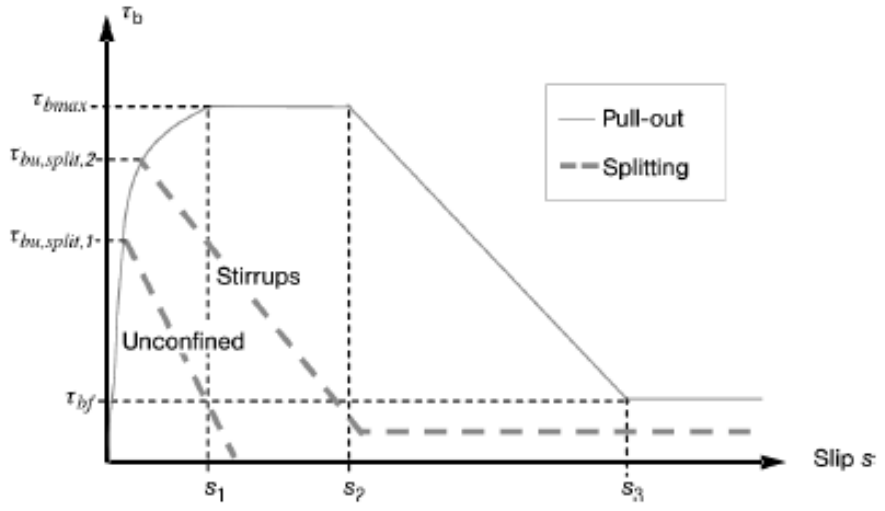

Figure 2.7: Analytical bond stress-slip relationship for monotonic loading (CEB-FIP, 2013)

2.3.2 Tension Stiffening

Bischoff (2001) explains that tension stiffening is when the concrete between cracks carries some of the tensile forces due to the bond action of the reinforcement and the concrete. The bond of the steel to the concrete is an important property which determines the amount of tension which is transferred to the concrete between the cracks (Bischoff, 2001). This will stiffen the member and hence reduce the deflections up to the yield limit of the reinforcement (Bischoff, 2003).

2.4 Steel Reinforced Concrete with Fibres

The advantage of using steel fibres in reinforced concrete is that they help to create a post-cracking residual tensile strength as well as a large tensile strain (CEB-FIP, 2013). The cracks in the concrete form perpendicular to the direction of the tensile stress and the fibres work most effectively when embedded in the concrete in the same direction as this tensile stress, therefore crossing the crack at right angles (Maidl and Dietrich, 1995). Aslani and Nejadi (2012) state that when fibres bridge the cracks, stress is allowed to transfer across cracked surfaces, slowing down the crack propagation.

2.4.1 Tension Stiffening

The definition of tension stiffening has been explained in Section 2.3.2 for steel reinforced concrete. The difference in the tension stiffening of a steel reinforced concrete member with fibres is that at the cracks the concrete is now able to carry some of the tensile forces due to the presence of the fibres as well as carrying tension between the cracks (Bischoff, 2003). This has many advantages which are that it increases the tension stiffening of the member; improves crack control; and provides additional strength to the member after the reinforcement has yielded. When fibres are used, they improve the bond conditions within the member. The addition of fibres will result in a reduced crack spacing as shown in Figure 2.8 due to the concrete having an increased tensile resistance at a crack. Figure 2.8 shows that the reinforced concrete member can only carry tensile forces in the concrete between cracks whereas the fibre reinforced concrete can carry tensile forces in the concrete at the cracks as well as between.

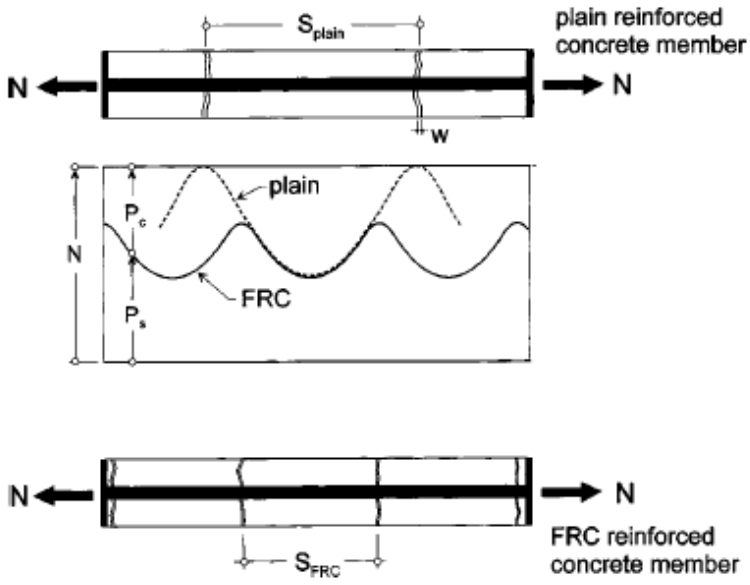

Figure 2.8: Axial force distribution for stabilized cracking (modified from Bischoff, 2003)

2.5 Behaviour of Connections

Reinforced concrete connections are an integral part of a building's design and ensure the sufficient transfer of the loads throughout the structure. The loads are transferred through the connection by the transfer of bond stresses in the lapped reinforcement. This requires an adequate lap length in order to allow the bond stresses to fully transfer the bond stresses from one bar to the other. The bond between concrete and reinforcement bars has been explained in Section 2.3.1.

Cairns (2015) explains that bond is related to the geometry of the section, the materials used and on the stress state. Bond can cause failure depending on the level of confinement in the connection (Cairns, 2015). The failure will either be due to shearing of the concrete in situations where there is more confinement, or due to splitting of the concrete cover from longitudinal cracks that develop (Cairns, 2015). Bond at the ultimate limit state affects the strength of the lapped reinforcement section in the connection as explained by Cairns (2015), implying that the higher the bond stresses, the higher the connection strength. This splitting failure that occurs is a brittle failure, which in design needs to be avoided and Cairns (2015) explains that there are two ways to guarantee a more ductile failure mode. More confinement can be provided to ensure that pull-out of the reinforcement bar is the main failure mode, or a sufficient reinforcement lap length should be provided so that yield can be achieved.

Reinforcement in concrete connections can vary between straight lapped reinforcement or looped reinforcement, with different lap lengths. Figure 2.9 shows the straight lapped reinforcement and Figure 2.10 shows the looped reinforcement bars.

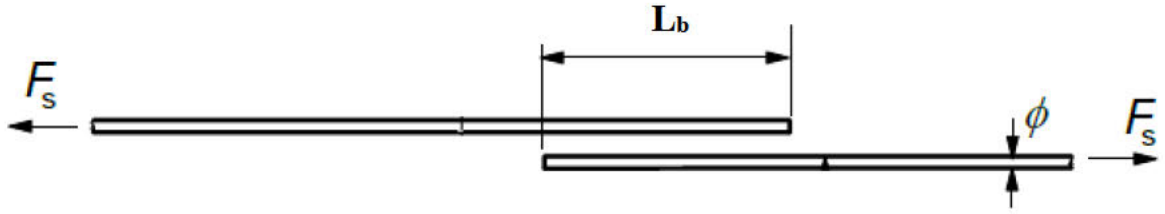

Figure 2.9: Straight lapped reinforcement (modified from BS EN1992-1-1:2004)

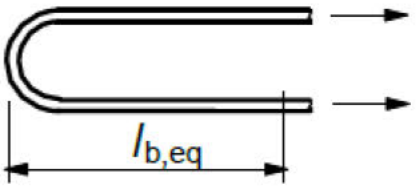

Figure 2.10: Looped reinforcement bar (BS EN1992-1-11:2004)

2.5.1 Straight Lapped Reinforcement

Straight lapped reinforcement such as that shown in Figure 2.9 is a conventional way of designing connections. The overlapping sections of the bar are able to transfer the bond stresses from one side of the connection to the other; combat spalling of the concrete; and prevent large cracks occurring in the concrete which are detrimental to the structural integrity of the connection (BS EN 1992-1-1:2004).

Micallef and Vollum (2017) conducted experiments on a range of reinforced concrete beams with different reinforcement lap lengths. The main concern was how the length of the reinforcement lap affected the failure behaviour of the connection and three main failure types were identified. Micallef and Vollum (2017) noted that all specimens first produced transverse flexural cracks near the loading point. In the lapped area, cracks were first identified at the ends of the lap and then further developed along the lapped section of the reinforcement. This was followed by the development of longitudinal cracks which followed the edge of the laps and developed at half of the failure load and continued to spread as the load increased towards failure. These cracks are clearly shown in Figure 2.11 which shows the cracks at the end of the experiments. The distinct cracks at the end of the lapped reinforcement are highlighted. Spalling of the concrete can be seen near to the support with the largest spalling occurring in the specimens with the longer laps.

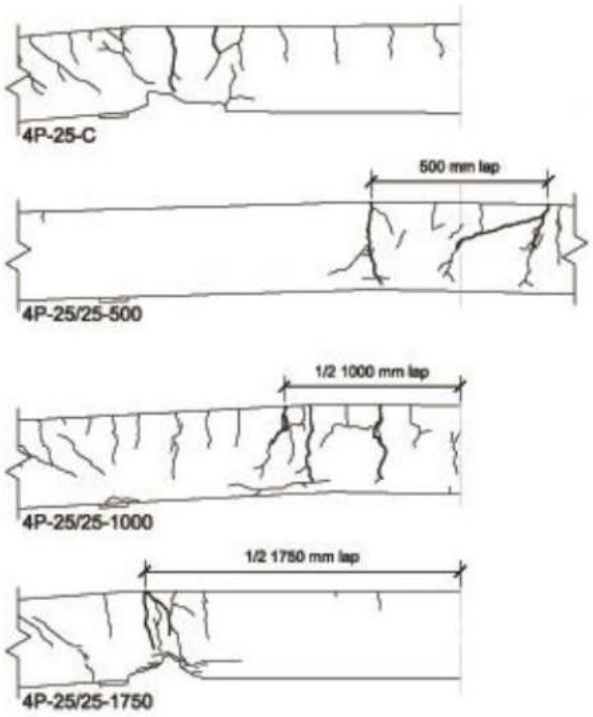

Figure 2.11: Crack patterns observed for series A laps in Micallef and Vollum (2017) experiments (Micallef and Vollum, 2017)

Micallef and Vollum (2017) observed that the shortest laps that were investigated had a brittle bond failure before the reinforcement had yielded. With the "long laps", at least one bar had yielded before the brittle bond failure occurred and for the "very long laps" a flexural failure occurred. The brittle failure occurred where the laps were not long enough to transfer the forces along one bar into the next and therefore the specimen failed before the reinforcement could reach the yield strength. The longitudinal cracks for the specimens that possessed this bond failure were widened and occurred over the whole length of the reinforcement lap at failure as seen by Micallef and Vollum (2017). As the length of the lap increased, Micallef and Vollum (2017) shows that the failure mode transitions from a very brittle failure for a "short lap" into a more ductile failure where the reinforcement for the longer laps can reach yield. After the longer laps reached yield, the failure was dependent on the length of the lap and on the bar diameter (Micallef and Vollum, 2017). The "long laps" failed suddenly with a bond failure whereas the "very long laps" had a flexure failure after a plastic hinge had developed in the sample. Nevertheless, both these long lap samples showed post-yield ductility before the subsequent failure mode; unlike the short laps which caused a brittle failure. Further information on these experiments can be found in Micallef and Vollum (2017).

2.5.2 Looped Reinforcement

Looped bars are often used as an alternative to straight lapped bars due to the advantages they have. One of the main advantages is that because of the curved loop, the anchorage capacity can be greatly

increased. The loops have three main failure modes which are a tensile splitting failure of the concrete; bond slip failure between the reinforcement and the concrete; and a concrete crushing failure (Grassl, 1999). The failure in the loops is due to the radial pressure that acts along the inside of the curved part of the bar which is then balanced by the force in the steel.

Grassl (1999) conducted experiments using looped reinforcement bars using a simply supported beam. The load was applied underneath the beam in order to view the crack patterns in the beams. The failure patterns observed from these experiments varied for the four beams tested. The four beams had different properties in order to determine how these factors affected the failure patterns. One specimen had a short loop splice; one had a longer splice length; one had double the beam width with the shorter loop splice; and the last had straight reinforcing bars. For these specimens, Grassl (1999) observed different crack patterns and failure.

For the specimen with the shorter loop splice, it was noted by Grassl (1999) that there was spalling of the outer concrete. The cracks for this specimen occurred in the region where the loop splice was and followed the shape closely with the largest spalling occurring around the loop. Grassl (1999) shows that the first cracks produced were flexural bending cracks which were then followed by cracks in the direction of the loop. The spalling of the concrete was avoided when the length of the straight splice was increased and therefore increased the stiffness of the specimen. This specimen was able to carry a higher load compared to the straight reinforcing splices due to the loops increasing the area of reinforcement in this central area. The crack pattern here is more regular and the cracks on the top of the specimen are perpendicular to the reinforcement direction. Flexural cracks were first observed, both inside and outside the splice zone, before the largest cracks continued to develop and followed the direction of the loop. With the straight reinforcement bars, Grassl (1999) noticed flexural bending cracks appear before changing to flexural shear cracks originating from the point where the load was applied. Grassl (1999) concluded that the looped reinforcement bars were able to withstand a higher load capacity than the alternative straight reinforcing bars. When a large enough loop splice is used, the spalling of the concrete can also be prevented.

2.6 Nonlinear Finite Element Analysis

2.6.1 Implicit and Explicit Schemes

Nonlinear finite element modelling can be based on either an implicit or explicit time integration scheme depending on the programme used and the type of analysis. Livermore Software Technology Corporation (2019) explains that an implicit analysis involves several iterations in the calculation of

the timestep whereas an explicit analysis solves the timestep at the nodes directly. An explicit analysis is more favourable when dynamic effects are involved in the analysis as it can efficiently solve the equations of motion. An explicit analysis requires a timestep less than the critical timestep, which is calculated as the time for a sound wave to travel in the continuum (Livermore Software Technology Corporation, 2019). An implicit analysis is time consuming as it involves the inversion of a stiffness matrix which therefore increases the computational expense.

2.6.2 Finite Elements

There are different types of elements which can be used in finite element analysis ranging from one-dimensional to three-dimensional. One-dimensional elements are known as beam or line elements and they normally have two nodes. Shell elements are two-dimensional and solid elements are three-dimensional. These different element shapes can be used to represent different materials or sections of the model and are analysed using different methods.

2.6.3 Modelling Reinforcement

Within finite element modelling there are many techniques to model the interaction between the concrete and the reinforcement. Schwer (2014) explains that there are two main ways to model the reinforcement either via shared nodes or by constraint techniques. The shared node method is where both the steel and concrete are modelled with the nodes of the elements merged together as shown in Figure 2.12. The bond can be modelled by modelling the ribbed parts of the bar using a very fine mesh, however this can cause the calculations in the model to be very time consuming. The other way to model the bond is by an interface where elements connect the coinciding nodes in the concrete. In the analyses in Grassl (1999) this method was used to model the reinforcement.

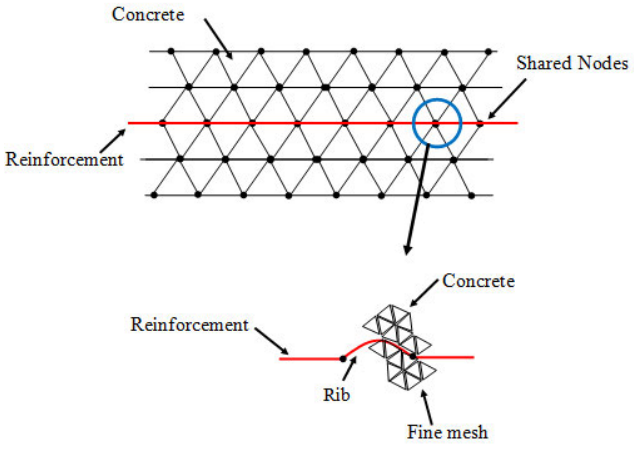

Figure 2.12: Schematic of shared nodes with ribs to model reinforcement

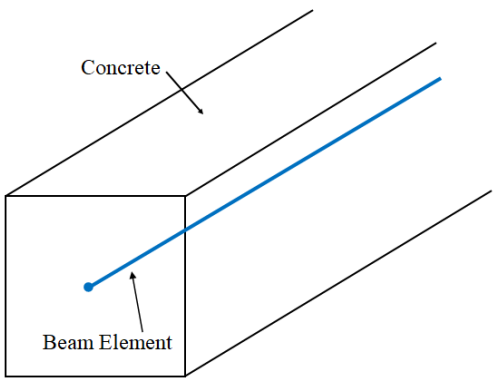

Figure 2.13: Schematic of beam element constrained in solid to model reinforcement

The constraint method allows the reinforcement to be defined independently of the concrete with separate nodes and this involves constructing the nodes separately for the concrete and the reinforcement and modelling the bond interaction by constraining the reinforcement within the solid. The simplest way to do this is using a beam element as shown in Figure 2.13. The issue with this method is that the model overcompensates the volume of concrete, which ultimately increases the stiffness and could lead to results which are not an accurate representation of the reality. This could then be compensated for by adjusting the stiffness and density.

2.6.4 Verification and Validation

Computer models are not always accurate and must be verified and validated in order to ensure that the results produced are reasonable and correctly represent the real-life problem. Assumptions are made when creating a computer model in order to simplify the real-life situation which are normally the main cause of error.

The verification process checks that the model has been implemented correctly (MacLeod, 2005). There are two types of verification that can be used as stated in Schaller et al. (2004) which are code verification and calculation verification. Schaller et al. (2004) defines code verification as the "process of determining that the computer code is correct and functioning as intended" by carrying out a software quality assurance. Calculation verification is defined by Schaller et al. (2004) as the "process of determining the solution accuracy of a particular calculation". Calculation verification is done by checking the convergence of a solution which assesses the error in the simulation, known as numerical error estimation (Schaller et al., 2004).

The validation process checks the accuracy of a given model and examines if it is capable of satisfying the investigation requirements (MacLeod, 2005). The validation of a model is carried out by comparing the model's numerical solutions to experimental data, which determines how close a model is to representing the real-life situation (Schaller et al., 2004).

3 Model Theory

In this chapter, the theory behind the nonlinear finite element analyses, including the constitutive models used in this investigation, are explained. It also describes and explains the equations used for the design of the reinforcement lap length from both EC2 and MC10.

3.1 Nonlinear Finite Element Analysis

3.1.1 Solution Method

An explicit analysis was carried out in the finite element programme LS-DYNA which has been defined in Section 2.6.1. The timestep size chosen in LS-DYNA affects the dynamic response of the element. A balance needs to be struck between using a small enough timestep size to minimize the dynamic effects whilst also ensuring the timestep size is not so small that the analyses take a very long time. Livermore Software Technology Corporation (2018c) explains how the timestep is calculated in LS-DYNA.

The way LS-DYNA works is by using the force on each node from the timestep before and then using this to find the acceleration of the node from $Force = Mass \times Acceleration$. The displacement can then be calculated from $Displacement = Velocity \times Time$. The stress on each node is then calculated and used to determine the applied force on the next node for the next timestep. These calculations behave like a wave moving through the mesh for every timestep with the wave travelling at the speed of sound. Equation 3.1 shows the equation for the speed of sound for a 3D Continuum Wave (Livermore Software Technology Corporation, 2018c).

$$c_{3D-continuum} = \sqrt{\frac{E(1-\nu)}{(1+\nu)(1-2\nu)\rho}} \tag{3.1}$$

Where, E is the Young's modulus, ν is the Poisson's ratio and ρ is the mass density. The critical timestep can be calculated from Equation 3.2 (Livermore Software Technology Corporation, 2018c).

$$\Delta t_{min} = \frac{h_e}{c} \tag{3.2}$$

Where, h_e is the element length and c is the speed of sound. This equation shows that the timestep is dependent on the mesh size and the speed at which the wave travels.

3.1.2 Displacement Method

The analyses involve prescribing a displacement to the prism instead of applying a force and pulling the specimen. The resulting load can then be determined from this prescribed displacement to analyse the load that the prism can sustain as explained in Section 3.1.1 on the timestep in LS-DYNA.

3.2 Constitutive Models

The finite element modelling involved three constitutive models to represent the concrete, the reinforcement and the bond between the concrete and the reinforcement. MAT_CDPM was used as a material model for the concrete; MAT_PLASTIC_KINEMATIC as a material model for the reinforcement; and CONSTRAINED_BEAM_IN_SOLID to represent the bond between these two materials. This section explains the input parameters required in each of these models and the values used in this investigation.

3.2.1 Constitutive Model for Concrete

The material model used for the concrete is the concrete damage plasticity model: MAT_CDPM. The Concrete Damage Plasticity Model 2 (CDPM2) is a constitutive material model for the failure of concrete under multiaxial loading which relies on both the use of damage mechanics and plasticity as explained by Grassl et al. (2013). This model can be input into the finite element software LS-DYNA for analyses of the failure of concrete. This model is an advancement on the previous model, Concrete Damage Plasticity Model 1 (CDPM1) developed by Grassl and Jiràsek (2006).

Previous constitutive models have been developed before CDPM1 using plasticity models, damage mechanics and a combination of the two (Grassl et al., 2013). However, none of these models were able to correctly describe the complete failure of concrete. The stress-based plasticity models were able to model concrete subject to triaxial stress states since the yield surface corresponds at a certain stage of hardening to the strength envelope of concrete. This model was unable to represent the reduction of stiffness that occurs during the unloading stage for the softening response of the concrete. Strain-based isotropic damage mechanics models can directly determine the stress state of the concrete due to the stress evaluation process being explicit but is incapable of expressing the irreversible deformations that are found in the concrete.

Grassl and Jiràsek (2006) combined both a stress-based plasticity model with a strain-based damage model in CDPM1. Grassl et al. (2013) explain that this model was capable of analysing concrete subjected to multiaxial stress states and obtaining mesh-independent results for the overall load-displacement response. However, by assuming a perfect plastic response, this created mesh-dependent results for the plastic strain profiles. This model was constructed with only one parameter to model both tension and compression which caused issues when trying to model the transition from tensile to compressive failure accurately. This led to the creation of CDPM2 which as shown in Grassl

et al. (2013) produces mesh independent results to explain the failure of concrete as well as accurately describing the transition between the tensile and compressive failure.

CDPM2 follows the stress-strain relationship:

$$\boldsymbol{\sigma} = (1 - \omega_t)\boldsymbol{\sigma_t} + (1 - \omega_c)\boldsymbol{\sigma_c} \tag{3.3}$$

Where, $\boldsymbol{\sigma_t}$ is the positive component of the effective stress; $\boldsymbol{\sigma_c}$ is the negative component of the effective stress; and ω_t and ω_c are scalar damage parameters. The scalar damage parameters have values which range from zero to one, where a value of zero represents the undamaged situation and a value of one represents the damaged situation. CDPM2 consists of two main frameworks: plasticity and damage mechanics which are discussed below.

The plasticity model is centred around the effective stress and is unrelated to damage. There are four components to the plasticity part which are the evolution law for the hardening variable, the flow rule, the hardening law, and the yield function (Grassl et al., 2013).

The yield surface can be represented by the cylindrical coordinates in the principal effective stress space, known as the Haigh-Westergaard coordinates. The hardening law dimensionless variables q_{h1} and q_{h2} are functions of the hardening variable κ_p, and control the size and shape of the yield surface. Grassl et al. (2013) also states that the evolution law for the hardening variable ensures that the rate of the hardening variable is equal to the norm of the plastic strain rate scaled by a hardening ductility parameter. The flow rule in CDPM2 is non-associated as the yield function does not correspond to the plastic potential which implies that the plastic flow will be normal to the yield surface. Grassl (2016) explains that having a non-associative flow rule is an important aspect of the model for concrete as if it was associative it would overestimate the maximum stress.

The damage component of the model can be split into both tensile damage and compressive damage. The tensile section of damage as shown in Grassl (2016) can be represented by a bi-linear stress – inelastic displacement law and the compressive section of damage can be presented as a stress – inelastic strain exponential relationship as shown in Figure 3.1.

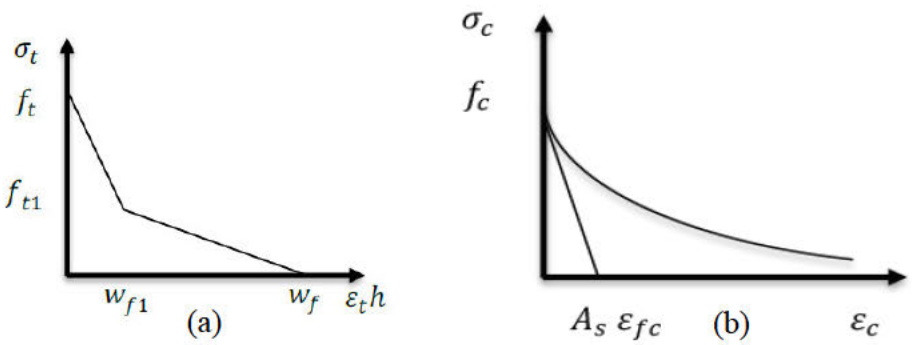

Figure 3.1: Stress-crack strain relationships for (a) tensile and (b) compressive section of damage (modified from Grassl, 2016)

This material model has 23 input parameters which are described below and are explained in Grassl (2016) and Livermore Software Technology Corporation (2018a). All the definitions described below have been taken from these two sources.

- **Mass Density, ρ_c:**

  The mass density of the concrete. CEB-FIP (2013) states the range for normal weight concrete as 2000-2600 kg/m^3. For all analyses a value of 2400 kg/m^3 has been used.

- **Young's Modulus, E_c:**

  The modulus of elasticity of concrete which gives an indication of the stiffness. CEB-FIP (2013) gives the following expression for calculating the Young's modulus:

$$E_{ci} = E_{c0} \times \alpha_E \times \left(\frac{f_{cm}}{10}\right)^{\frac{1}{3}} \tag{3.4}$$

  Where, f_{cm} is the compressive strength of concrete at 28 days and taken as 40 MPa. $E_{c0} = 21.5 \times 10^3$ MPa, and α_E is taken as 1.0 for quartzite aggregates as stated in CEB-FIP (2013).

- **Poisson's Ratio, ν_c:**

  Poisson's ratio of concrete. CEB-FIP (2013) gives a range for the Poisson's ratio of concrete as 0.14 – 0.26. BS EN 1992-1-1 (2004) states that the recommended value for the Poisson's ratio is 0.2 which has been used in all analyses.

- **Eccentricity Parameter, e_{cc}:**

  Jirásek and Bažant (2002) give the following expression for the eccentricity parameter:

$$ECC = \frac{1+\epsilon}{2-\epsilon}; \qquad \epsilon = \frac{f_t(f_b{}^2 - f_c{}^2)}{f_b(f_c{}^2 - f_t{}^2)}; \qquad f_b = 1.16 f_c \tag{3.5(a), (b), (c)}$$

- **Initial Hardening, q_{H0}:**

  The initial hardening of the material is defined by the following expression:

$$q_{H0} = \frac{F_{ci}}{F_C} \tag{3.6}$$

  Where, F_{ci} is the compressive stress at which the initial yield surface is reached. The default value for the initial hardening parameter is 0.3.

- **Uniaxial Tensile Strength, f_t:**

  The uniaxial tensile strength can be estimated from the expression given in CEB-FIP (2013):

$$f_{ctm} = 0.3(f_{ck})^{\frac{2}{3}} \tag{3.7}$$

- **Uniaxial Compression Strength, f_{cm}:**

  Taken as the mean value in all analyses.

- **Hardening Parameter, H_p:**

  LS-DYNA gives the default value for the hardening parameter as 0.5. However, for models without a strain rate effect, a recommended value of 0.01 is given as was used in Grassl et al. (2013).

- **Hardening Ductility Parameter 1, A_h:**

  The default value in LS_DYNA is given as 0.08.

- **Hardening Ductility Parameter 2, B_h:**

  The default value in LS_DYNA is given as 0.003.

- **Hardening Ductility Parameter 3, C_h:**

  The default value in LS_DYNA is given as 2.

- **Hardening Ductility Parameter 4, D_h:**

  The default value in LS_DYNA is given as 1×10^{-6}.

- **Ductility Parameter During Damage, A_s:**

  The default value in LS_DYNA is given as 15.

- **Flow Rule Parameter, D_f:**

  The default value in LS_DYNA is given as 0.85.

- **Rate Dependent Parameter, F_{c0}:**

  This parameter is only needed if the value of STRFLG = 1. If this is the case the recommended value is 10 MPa.

- **Flag for Tensile Damage Type (TYPE):**

  There are four different cases for this parameter: 0 is for linear damage formulation; 1 is for bi-linear damage formulation; 2 is for exponential damage formulation; and 3 is for no damage. The default value in LS-DYNA is given as 0 for a linear damage formulation, however results can be improved by using a value of 1 which represents the bi-linear damage formulation**.**

- **Damage Ductility Exponent During Damage, B_s:**

  The default value in LS_DYNA is given as 1.

- **Tensile Threshold Value for Linear Tensile Damage Formulation, w_f:**

  This parameter is used to control the tensile softening branch for the exponential tensile damage formulation.

  For TYPE = 1: $$w_f = 4.444\frac{G_f}{f_t} \tag{3.8}$$

  Where, G_f is the fracture energy.

  The fracture energy can be determined from an expression in CEB-FIP (2013):

  $$G_f = 73 \times {f_{cm}}^{0.18} \tag{3.9}$$

  Where, f_{cm} is the mean compressive strength in MPa. For all analyses a value for TYPE = 1 has been used. For tetrahedral meshes it is recommended that the value is altered by $0.56w_f$, which is the case for all analyses. This is due to the way the element length is computed which overestimates the fracture energy.

- **Tensile Threshold Value for the Second Part of the Bi-Linear Damage Formulation, w_{f1}:**

  The default value in LS_DYNA is given as $0.15w_f$.

- **Tensile Strength Threshold Value for Bi-Linear Damage Formulation, f_{t1}:**

  The default value in LS_DYNA is given as $0.3f_t$.

- **Strain Rate Flag (STRFLG):**

  There are two different cases for this parameter: 0 is no strain rate dependency and 1 is strain rate dependent. A value of 0 has been used in all analyses.

- **Failure Flag (FAILFLG):**

  There are two different cases for this parameter: 0 is not active and no erosion and the other case is a percentage of all integration points that must fail before erosion. A value of 0 has been used in all analyses.

- **Parameter Controlling Compressive Damage Softening Branch, ε_{fc}:**

  Used in the Exponential Compressive Damage Formulation shown in Figure 3.1(b). Default value in LS-DYNA is 1×10^{-4} m. A value of 1×10^{-3} m has been used for all analyses.

The fibre reinforced concrete with traditional steel bars (RFC) material parameters were estimated from Naaman (1987) and Bolander. The failure mechanism of the fibres was assumed as pull-out failure in all analyses. Naaman (1987) defines the cracking strength as

$$\sigma_{cc} = \sigma_{mu}\left(1 - V_f\right) + \beta_1\beta_2\tau V_f\frac{L_f}{d_f} \tag{3.10}$$

Where, σ_{mu} is the tensile strength of concrete and taken as 3 MPa; V_f is the volume fraction of fibres taken as 0.01; β_1 is the orientation efficiency factor for 3D random fibre distributions taken as 0.5;

β_2 is the fraction of bond strength mobilized at cracking which is assumed by Bolander as 20%; τ is the average bond strength at fibre concrete interface which is assumed by Bolander as 4; L_f is the length of fibre which is 35 mm; and d_f is the diameter of the fibre which is 0.55 mm.

The post-cracking strength is defined by Naaman (1987) as

$$\sigma_{pc} = \lambda_1 \lambda_2 \lambda_3 \tau V_f \frac{L_f}{d_f} \tag{3.11}$$

Where, λ_1 is the average pull-out length ratio which is 0.25; λ_2 is the factor accounting for post-cracking orientation efficiency which Bolander states as $\lambda_2 = \alpha_1$ and therefore taken as 0.5; and λ_3 is the group reduction factor which Bolander assumes a value of 4.

The cracking strength is then taken as the tensile strength of the fibre reinforced concrete, f_t and the post cracking strength is taken as the tensile strength threshold value, f_{t1}. The tensile softening branch parameter, w_f was estimated using the pull-out behaviour assumption.

$$w_f = \frac{L_f}{2} \tag{3.12}$$

Where, L_f is the fibre length. The parameter, w_{f1} was taken as the same value as for reinforced concrete (RC). These values have been plotted in a stress – crack opening curve and compared to the RC curve as shown in Figure 3.2. All other parameters were taken the same as for RC, defined above.

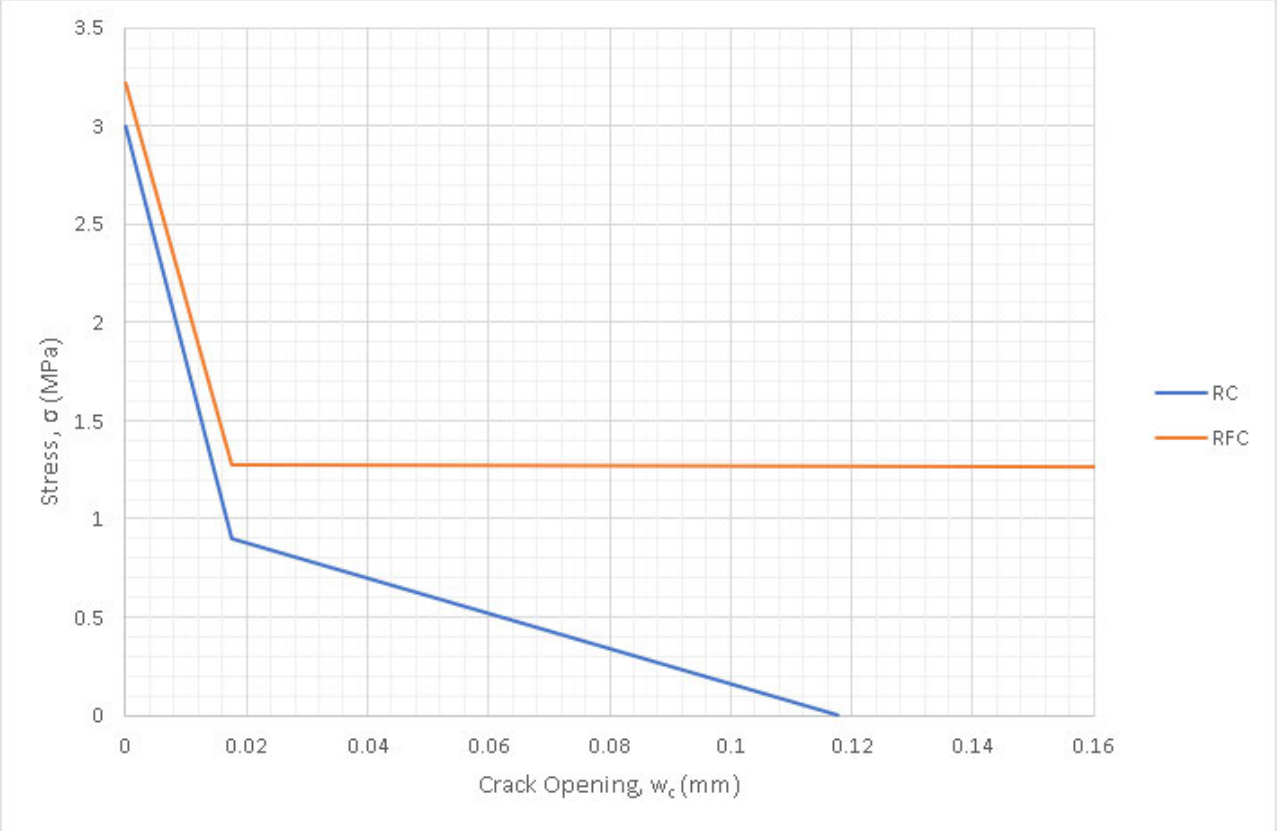

Figure 3.2: Stress – crack opening curves for RC and RFC

3.2.2 Constitutive Model for Reinforcement

The material model used for the reinforcement is the MAT_PLASTIC_KINEMATIC model. This model has 10 parameters which are described below and are explained in Livermore Software Technology Corporation (2018b). All the definitions described below have been taken from this source.

- **Mass Density, $\boldsymbol{\rho_s}$:**

  The mass density of the steel. BS EN 1992-1-1 (2004) gives the density of reinforcing steel as 7850 kg/m^3. This value has been used for all analyses.

- **Young's Modulus, $\boldsymbol{E_s}$:**

  The modulus of elasticity of reinforcing steel which gives an indication of the stiffness. CEB-FIP (2013) gives the Young's modulus of reinforcing steel as 200 GPa.

- **Poisson's Ratio, $\boldsymbol{\nu_s}$:**

  Bright and Roberts (2010) gives the value for the Poisson's ratio of reinforcing steel as 0.3.

- **Yield Stress, $\boldsymbol{f_y}$:**

  Bright and Roberts (2010) states that the yield stress of reinforcing steel for use in the UK is 500 MPa.

- **Tangent Modulus:**

  The default value in LS_DYNA is given as 0.

- **Hardening Parameter, $\boldsymbol{\beta}$:**

  The default value in LS_DYNA is given as 0 ($0 < \beta' < 1$).

- **Strain Rate Parameter, $\boldsymbol{C_s}$ and $\boldsymbol{P_s}$:**

  For Cowper Symonds strain rate model. If this value is 0, the rate effects are ignored in the analysis. The default value in LS_DYNA is given as 0. The yield stress is scaled by the factor, $1 + \left(\frac{\dot{\varepsilon}}{C}\right)^{\frac{1}{P}}$, in the Cowper and Symonds Model, where $\dot{\varepsilon}$ is the strain rate.

- **Effective Plastic Strain for Eroding Elements, $\boldsymbol{F_{strain}}$:**

  The default value in LS_DYNA is given as 1×10^{20}.

- **Formulation for Rate Effects, $\boldsymbol{v_p}$**:

  There are two different cases for this parameter: 0 is no strain rate dependency and 1 is strain rate dependent. A value of 0 has been used in all analyses.

3.2.3 Constitutive Model for Bond Between Concrete and Reinforcement

The keyword CONSTRAINED_BEAM_IN_SOLID has been used in LS-DYNA to model the bond between the concrete and reinforcement. This model has six parameters which are described below

as explained in Livermore Software Technology Corporation (2018a). All the definitions described below have been taken from this source.

- **Slave:**
  Defines the part set ID of the beam structure, where the beam structure represents the reinforcement.
- **Master:**
  Defines the part set ID of the solid element, where the solid element represents the concrete.
- **Coupling Direction:**
  There are two different cases for this parameter: 0 is a constraint applied along all directions and 1 is a constraint only applied along normal directions and along the beam axial direction there is no constraint. The default value in LS-DYNA is 0 which has been used in all analyses.
- **Start:**
  Start time for coupling. Default value in LS-DYNA is 0 which has been used in all analyses.
- **End:**
  End time for coupling. Default value in LS-DYNA is 0 which has been used in all analyses.
- **ID of a user defined function (axfor):**
  Defines the coupling force versus slip along the axial direction of the beam. A value of 0 in LS-DYNA turns the function off, which has been used in all analyses.

3.3 Reinforcement Lap Lengths

For the design of the reinforcement lap length in the connections, both BS EN 1992-1-1 (2004) and CEB-FIP (2013) were used and the results compared. The lap lengths calculated from these two methods vary considerably. The analyses involve using a range of lap lengths from the highest value larger than the recommended value from MC10 and the lowest value lower than the EC2 value.

The basic design equations have been explained in the following section and the calculations for both EC2 and MC10 can be found in Appendix A. Mean values have been used in the design instead of design values and hence the partial safety factors have all been taken as 1. This is so that the hand calculations can be compared to the finite element analysis where mean values were used.

3.3.1 Eurocode Design Equations

BS EN1992-1-1 (2004) Section 8 sets out the process and equations for the design of the lap length of reinforcement in concrete connections. The equations and parameter definitions have all come from BS EN1992-1-1 (2004).

The lap length is given by Equation 3.13.

$$L_b = \alpha_1\alpha_2\alpha_3\alpha_5\alpha_6 L_{b,rqm} \tag{3.13}$$

Where, α_1 is for the effect of the form of the bars assuming adequate cover; α_2 is for the effect of concrete minimum cover; α_3 is for the effect of confinement by transverse reinforcement; α_5 is for the effect of the pressure transverse to the plane of splitting along the design anchorage length; α_6 is a coefficient representing the percentage of lapped bars relative to the total cross-section area; and $L_{b,rqm}$ is the mean required lap length given by Equation 3.14.

$$L_{b,rqm} = \left(\frac{\emptyset}{4}\right)\left(\frac{\sigma_y}{f_{bm}}\right) \tag{3.14}$$

Where, $\emptyset$ is the diameter of the reinforcement bar; σ_y is the yield strength of the reinforcement given by Equation 3.15; and f_{bm} is the ultimate bond stress for ribbed bars given by Equation 3.19.

$$\sigma_y = \frac{f_{yk}}{\gamma_s} \tag{3.15}$$

Where, f_{yk} is the characteristic value of yield strength and γ_s is the partial safety factor for steel which has been taken as 1.

Equation 3.14 can be derived by considering the equilibrium between the forces along the reinforcement bar. The forces are shown in Figure 3.3.

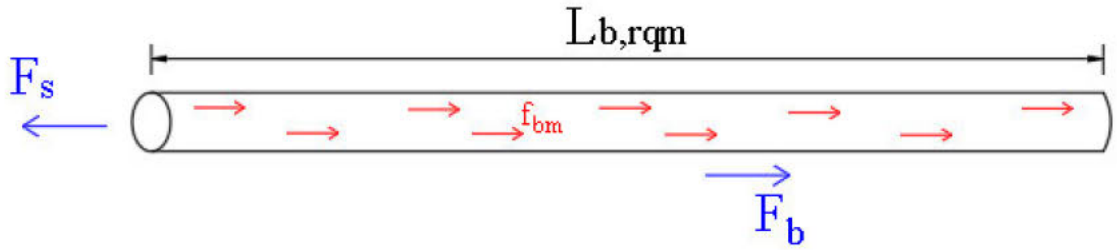

Figure 3.3: Force equilibrium along reinforcement bar

From Figure 3.3, the force of the steel is given by the area of steel multiplied by the yield strength of the steel shown by Equation 3.16.

$$F_s = A_{steel}\sigma_y = \pi r^2\sigma_y \tag{3.16}$$

The force of the bond of the steel is given by the length of the lap multiplied by the circumference of the bar multiplied by the forces in the reinforcement bar shown by Equation 3.17.

$$F_b = 2\pi r L_{b,rqm} f_{bm} \tag{3.17}$$

Using a force equilibrium, the lap length equation can be derived as shown by the steps below.

$$F_s = F_b$$

$$\pi r^2\sigma_y = 2\pi r L_{b,rqm} f_{bm}$$

$$r\sigma_y = 2L_{b,rqm} f_{bm}$$

$$L_{b,rqm} = \frac{r\sigma_y}{2f_{bm}}$$

$$\emptyset = 2r \Longrightarrow r = \frac{\emptyset}{2}$$

$$\therefore L_{b,rqm} = \frac{\emptyset\sigma_y}{4f_{bm}} \tag{3.18}$$

The mean value of ultimate bond stress for ribbed bars is given by Equation 3.19.

$$f_{bm} = 2.25\eta_1\eta_2 f_{ctm} \tag{3.19}$$

Where, f_{ctm} is the mean value of concrete tensile strength given by Equation 3.20; η_1 is a coefficient related to the quality of the bond condition and the position of the bar during curing; and η_2 is a coefficient relating to the bar diameter.

Mean value of concrete tensile strength:

$$f_{ctm} = 0.3 \times (f_{ck})^{2/3} \tag{3.20}$$

Where, f_{ck} is the characteristic value of concrete strength taken as $f_{ck} = f_{cm} - 8$ with $f_{cm} = 40$ MPa.

3.3.2 Model Code Design Equations

CEB-FIP (2013) has one equation, shown by Equation 3.21, which uses mean values and can be rearranged for the calculation of the lap length L_b. The equation and parameter definitions have all come from CEB-FIP (2013).

$$f_{stm} = 54\left(\frac{f_{cm}}{25}\right)^{0.25}\left(\frac{25}{\emptyset}\right)^{0.2}\left(\frac{L_b}{\emptyset}\right)^{0.55}\left[\left(\frac{c_{min}}{\emptyset}\right)^{0.25}\left(\frac{c_{max}}{c_{min}}\right)^{0.1} + k_m k_{tr}\right] \tag{3.21}$$

Where, f_{stm} is the reinforcement stress for ribbed bars in a 'good' casting position, c_{min} and c_{max} are cover parameters defined as shown in Figure 3.4, k_m represents the efficiency of confinement from transverse reinforcement and has been taken as 0 here, and k_{tr} is the density of transverse reinforcement relative to the anchored or lapped bars.

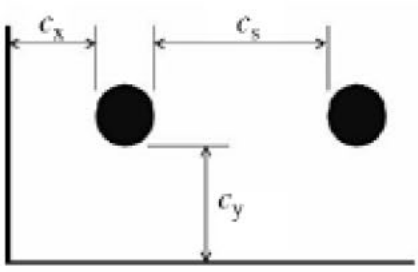

$c_{min} = \min(c_s/2, c_x, c_y)$
$c_{max} = \max(c_s/2, c_x)$

Figure 3.4: Cover parameters

3.4 Crack Spacing

The crack spacing of a reinforced concrete connection can be calculated from Section 7 of BS EN1992-1-1 (2004). CEB-FIP (2013) does not have specific equations for the calculation of the crack spacing.

3.4.1 Eurocode Design Equations

The calculations for the maximum crack spacing can be found in Appendix B. The equations and parameter definitions have all come from BS EN1992-1-1 (2004).

The maximum crack spacing is given by Equation 3.22.

$$S_{r,max} = k_3 C + k_1 k_2 k_4 \frac{\emptyset}{\rho_{s,eff}} \tag{3.22}$$

Where, k_1 is the coefficient which takes account of the bond properties of the bonded reinforcement; k_2 is the coefficient which takes account of the distribution of strain; k_3 is a coefficient with a recommended value in the National Annexe of 3.4; k_4 is a coefficient with a recommended value in the National Annexe of 0.425; $\emptyset$ is the bar diameter; C is the concrete cover; and $\rho_{s,eff}$ is given by Equation 3.23.

$$\rho_{s,eff} = \frac{A_{steel}}{A_{c,eff}} \tag{3.23}$$

For a member in tension, $A_{c,eff}$ is given by Equation 3.24.

$$A_{c,eff} = A_{ct,eff} + A_{cb,eff} \tag{3.24}$$

Figure 3.5 shows where the tension areas are for a member in tension and $A_{ct,eff}$ and $A_{cb,eff}$ are given by Equation 3.25.

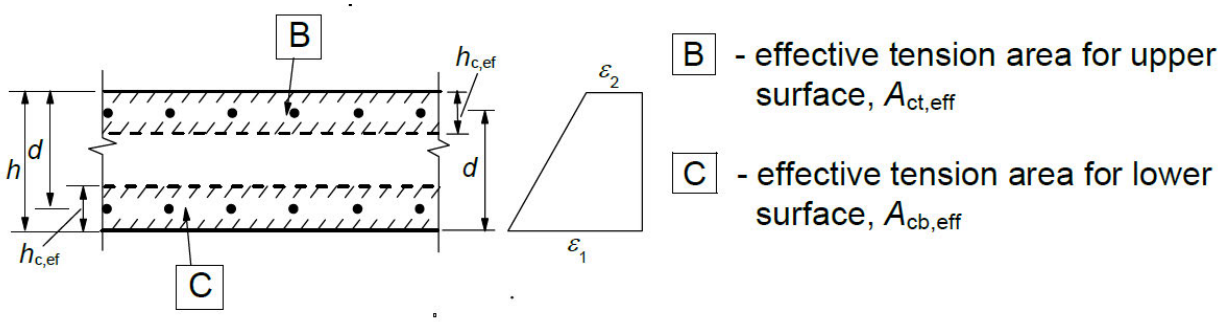

Figure 3.5: Effective tension area for a concrete member in tension (BS EN1992-1-1:2004)

$$A_{ct,eff} = A_{cb,eff} = \big(2.5(h-d)\big) \times b \tag{3.25}$$

Where, b is the breadth of the specimen.

4 Analyses

This section explains the analyses undertaken in this investigation and discusses and compares the results output for the beam and the reinforced concrete connection and how RFC behaves differently to RC. Appendix C shows an example of the input file used in the analyses.

4.1 Material Parameters

Material properties used in the analyses for the concrete and the reinforcement are shown in Table 4.1 and Table 4.2 respectively (other values used have been the defaults mentioned in Section 3.2.1 and 3.2.2). Appendix D shows how these parameters for both concrete and reinforcement were entered into the material file.

Table 4.1: Concrete material parameters for CDPM2

Model Parameter		RC	RFC
		Concrete	**Concrete**
Mass Density	ρ_c	2400 kg/m^3	2400 kg/m^3
Young's modulus	E_c	35 GPa	35 GPa
Poisson's Ratio	ν_c	0.2	0.2
Uniaxial Tensile Strength	f_t	3 MPa	3.22 MPa
Uniaxial Compression Strength	f_c	40 MPa	40 MPa
Tensile Threshold - linear damage	w_f	117.8×10^{-6} m	17.5×10^{-3} m
Tensile Threshold - second part of bi-linear damage	w_{f1}	17.67×10^{-6} m	17.67×10^{-6} m
Tensile Threshold - bi-linear damage	f_{t1}	0.9 MPa	1.27 MPa

The value of w_f for RC corresponds to a fracture energy of 142 N/m and for tetrahedral meshes it has been recommended to use a value that corresponds to $0.56w_f$, which has been used here. The value of w_f for RFC has been calculated according to Equation 3.12 defined in Section 3.2.1. The tensile strength and tensile threshold – bi-linear damage parameters have been calculated from Equations

3.10 and 3.11 respectively which are defined in Section 3.2.1. The other parameters have been calculated using the methods explained in Section 3.2.1.

Table 4.2: Reinforcement material parameters

Model Parameter		RC	RFC
		Reinforcement	**Reinforcement**
Mass Density	ρ_s	7850 kg/m^3	7850 kg/m^3
Young's Modulus	E_s	200 GPa	200 GPa
Poisson's Ratio	ν_s	0.3	0.3
Yield Stress	f_y	500 MPa	500 MPa

The reinforcement parameters have been calculated using the methods and equations detailed in Section 3.2.2.

4.2 Tetrahedral Mesh

The mesh used was a tetrahedral mesh created using the mesh creator programme T3D (Rypl, 2016). Three different mesh sizes have been used for the verification of the model. The mesh sizes used are shown in Table 4.3. All subsequent analyses after the verification check have used the medium mesh size unless stated otherwise.

Table 4.3: Mesh size

Mesh Name	Mesh Size (m)
Coarse	0.04
Medium	0.02
Fine	0.01

Figure 4.1 shows the tetrahedral mesh on the beam element for the coarse, medium and fine mesh sizes. The contour plots shown for the analyses have been plotted without the mesh to make the diagrams clearer and easier to understand.

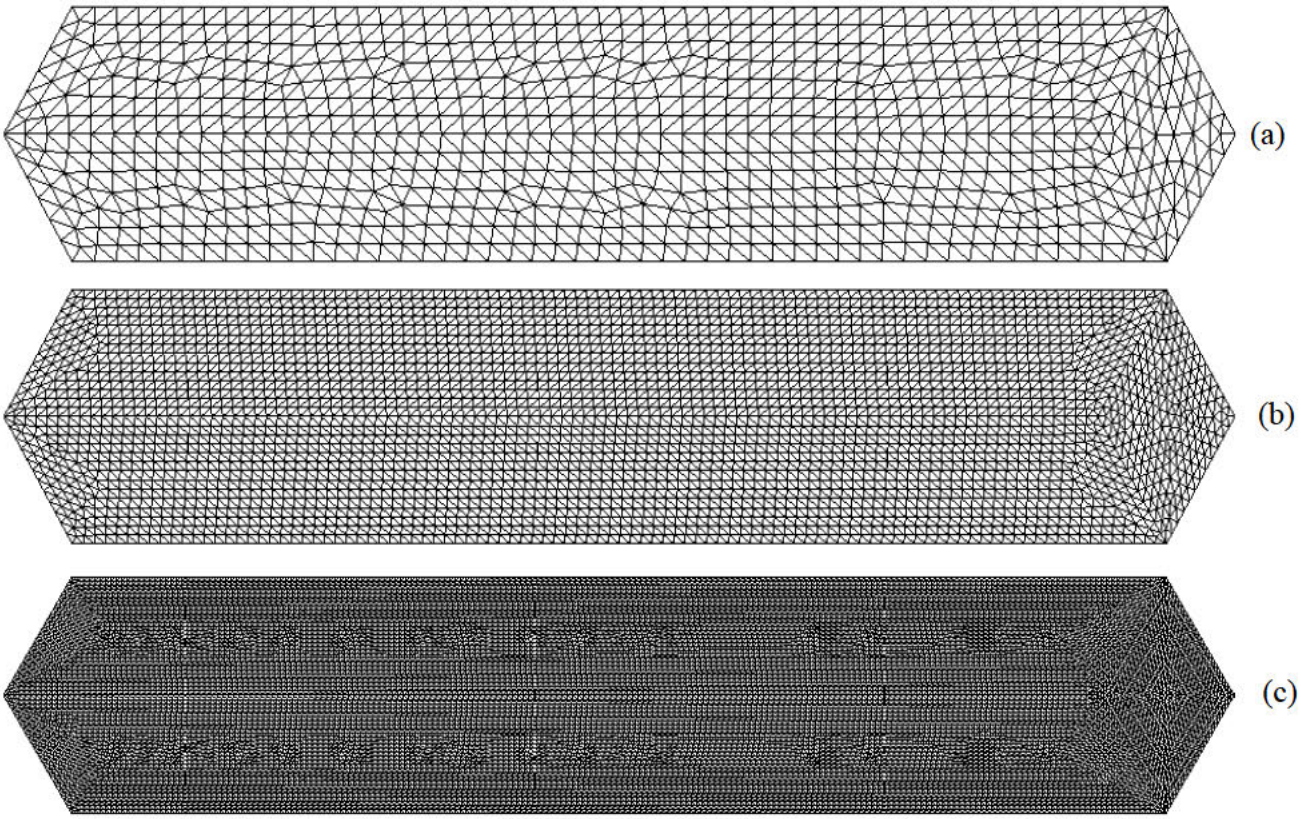

Figure 4.1: Tetrahedral mesh used in analyses - (a) coarse mesh; (b) medium mesh; and (c) fine mesh

4.3 Geometry

The analyses involved two different geometries to investigate the aim. A prism with four continuous straight reinforcement bars was used as a reference specimen to verify and validate the model and offer a comparison to the lapped reinforcement specimen. A concrete connection with four straight lapped reinforcement bars was subsequently analysed.

In order to see the bridging effects of the fibres, the ends of all the reinforcement bars were strengthened to double the diameter for the first and last 200 mm as shown in the figures by the green rebar lines. This allowed the response of the RFC specimens to be easily compared to the RC response.

4.3.1 Continuous Reinforcement Bars

The continuous reinforcement bars consisted of four straight reinforcement bars with 30 mm cover to reinforcement bar. The beam element modelled was 2 m long with a cross-section of 250 x 250 mm. The plan view, 3D view and cross-section of the geometry are shown in Figure 4.2, Figure 4.3 and Figure 4.4 respectively.

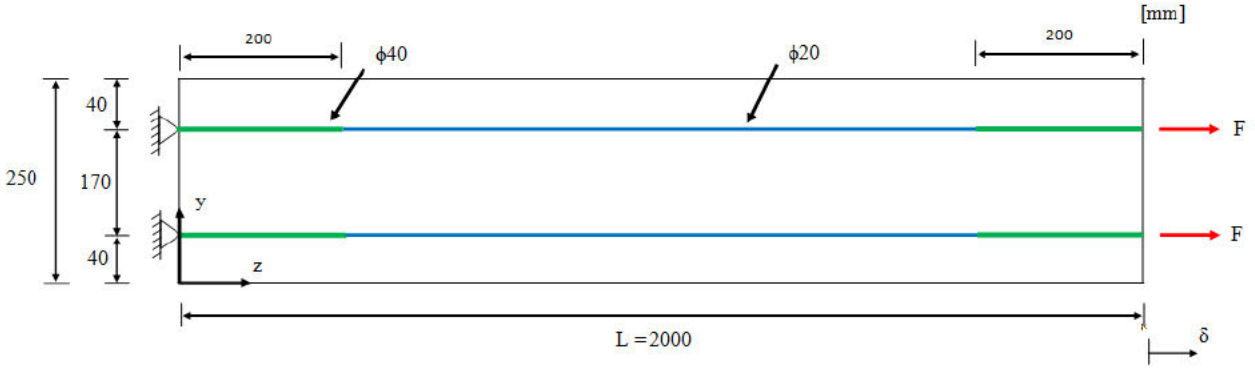

Figure 4.2: Continuous reinforcement bars plan view

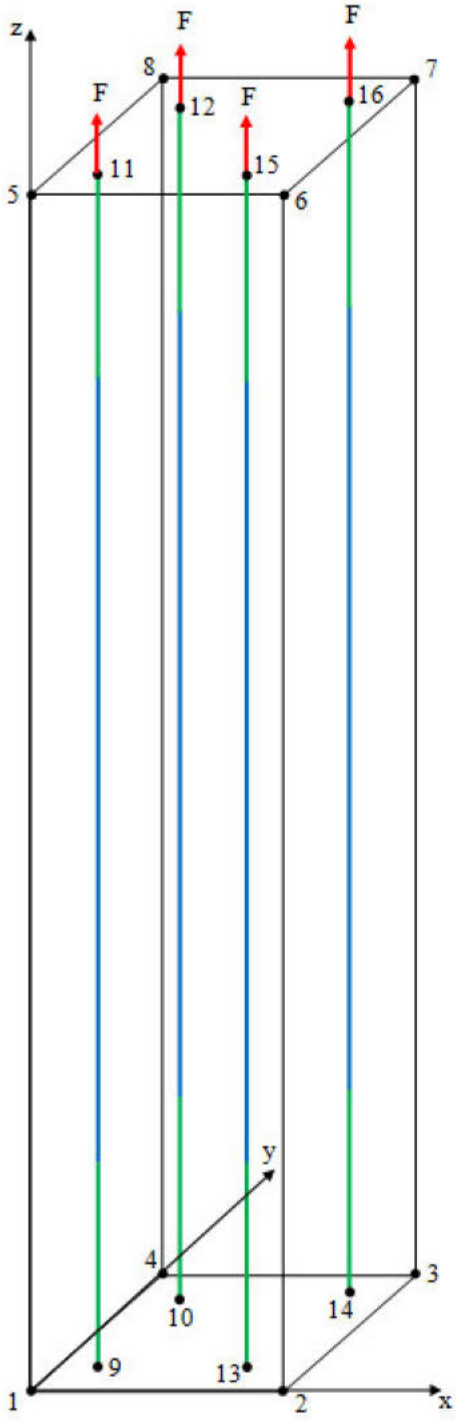

Figure 4.3: Continuous reinforcement bars 3D view

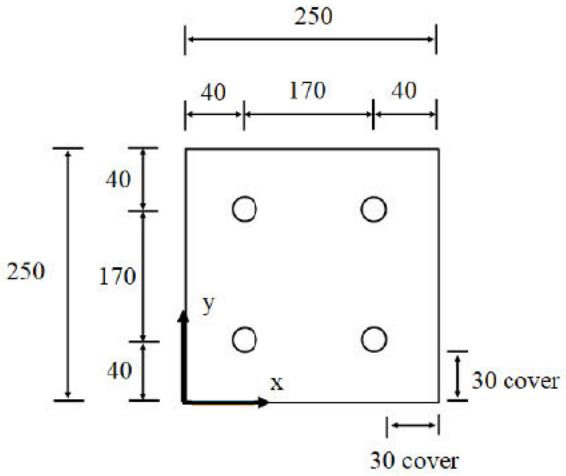

Figure 4.4: Continuous reinforcement bars cross-section view at z = 1000 mm

4.3.2 Connection with Straight Lapped Reinforcement

The connection modelled had lapped reinforcement bars with lap lengths shown in Table 4.4.

Table 4.4: Lap lengths

Lap Number	Lap Length, L_b (mm)
Lap 1	300
Lap 2	500
Lap 3	800
Lap 4	1200

The plan view, 3D view and cross-section of the geometry are shown in Figure 4.5, Figure 4.6 and Figure 4.7 respectively.

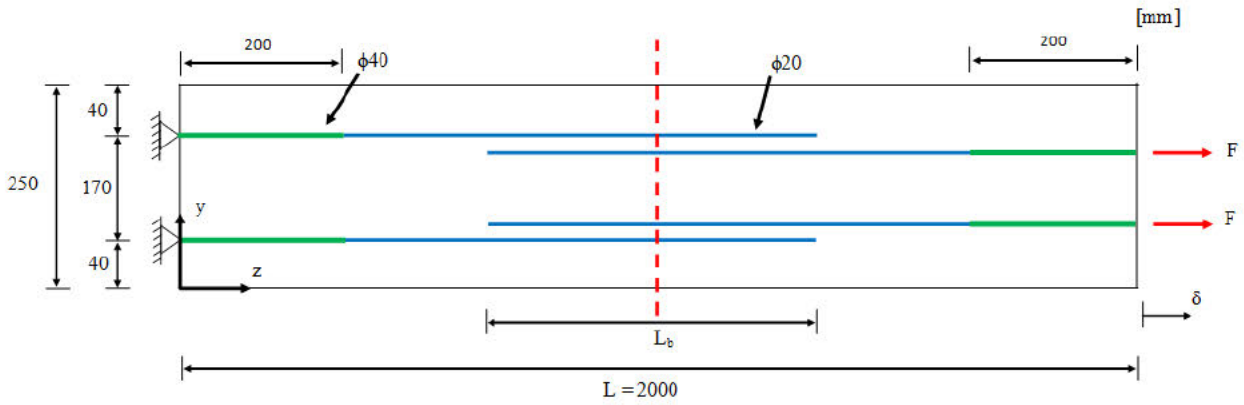

Figure 4.5: Connection with straight lapped reinforcement plan view

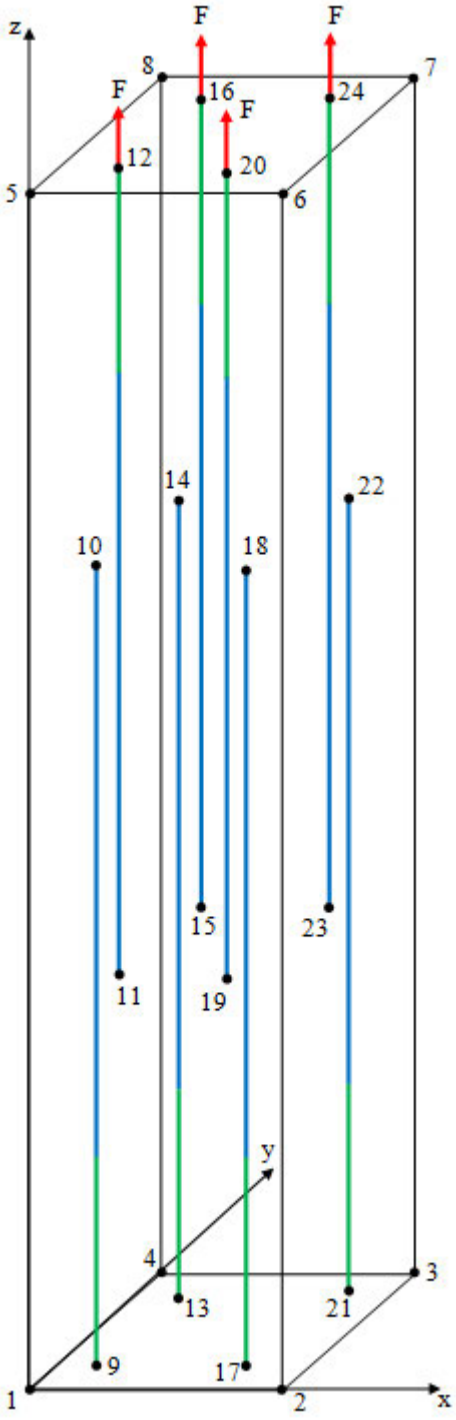

Figure 4.6: Connection with straight lapped reinforcement 3D view

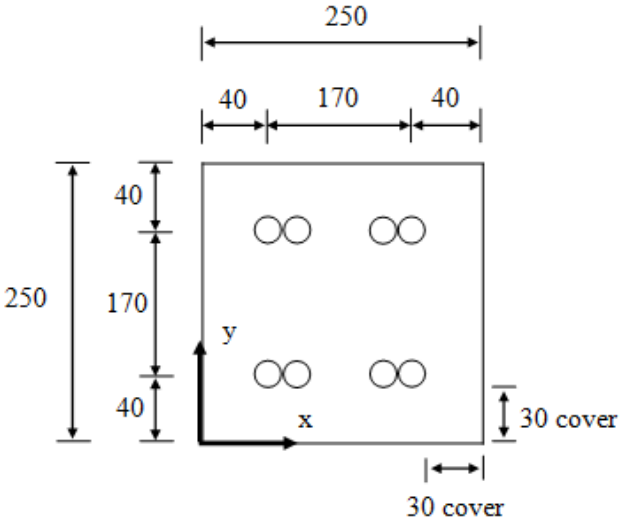

Figure 4.7: Connection with straight lapped reinforcement cross-section view at z = 1000 mm

4.4 Results

All contour plots have been plotted showing the maximum principal strain with black corresponding to a crack opening of 0.3 mm from Equation 4.1.

$$\varepsilon = \varepsilon_e + \varepsilon_i = 0 + \frac{w_c}{h_e} \tag{4.1}$$

Where, ε is the strain, w_c is the crack opening and h_e is the element length which has been taken as 20 mm for the medium mesh.

The following figures show the graphs and contour plots for the RC and RFC specimens. The load displacement curves for the different lap lengths and the continuous reinforcement bar have been compared and the steel force from one lapped reinforcement bar has been plotted and compared to one continuous bar. The crack evolution for the long lap and short lap have been shown. Here the long lap corresponds to L_b = 1200 mm which is well above the MC10 lap length value, and the short lap corresponds to L_b = 500 mm which is between the EC2 and MC10 lap length value. All graphs have been plotted dimensionless for easy comparison. The loads were divided by the rebar strength and the displacement divided by the displacement at yield.

The rebar strength is equal to the maximum load that the reinforced concrete member will be able to sustain. The reinforcement bars used in all analyses have 200 mm of strengthened ends which have double the diameter of reinforcement. The rebar strength will still be from the smaller diameter bars as these bars will yield first which ultimately determines the rebar strength. The lapped reinforcement bars will also have the same rebar strength due to the 20 mm diameter bars still reaching yield first. The rebar strength can be calculated from Equation 4.2.

$$F_y = \left(A_{steel} \times \sigma_y\right) \times n \tag{4.2}$$

Where, A_{steel} is the area of steel of one bar which is 314 mm^2; σ_y is the yield strength of steel which is 500 MPa; and n is the number of bars. The rebar strength for four 20 $\emptyset$ bars has been calculated to be 628 kN.

The displacement at yield was calculated by considering the strain for the normal diameter reinforcement bars and the strengthened reinforcement bars as shown in Figure 4.8.

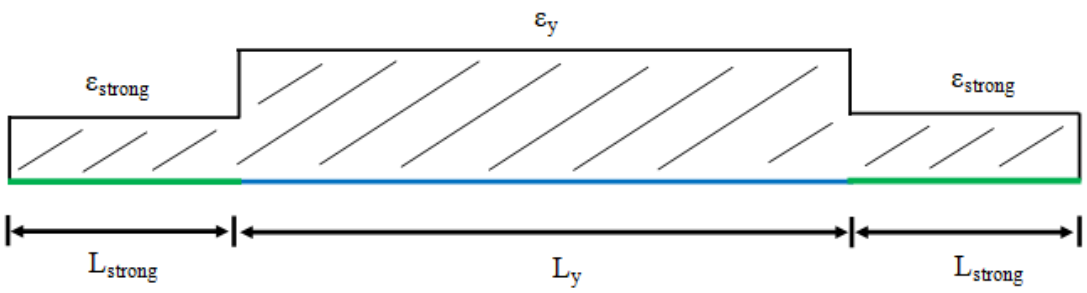

Figure 4.8: Strain for different sections of reinforcement bar

The strain for the 20 mm diameter bars can be calculated from Equation 4.3.

$$\varepsilon_y = \frac{\sigma_y}{E} \tag{4.3}$$

Where, σ_y is the yield strength of steel taken as 500 MPa and E is the Young's modulus of the steel taken as 200 GPa. Therefore, ε_y was calculated as 2.5×10^{-3}.

The strain for the strengthened ends can be calculated from a force balance, shown in Equation 4.4.

$$F = A_{steel}\varepsilon_y E = A_{steel,strong}\varepsilon_{strong} E \tag{4.4}$$

Where, A_{steel} has been taken as 314 mm^2 and $A_{steel,strong}$ has been taken as 1257 mm^2 . Therefore, ε_{strong} was calculated as 6.25×10^{-4}.

The displacement at yield can then be calculated from Equation 4.5.

$$\delta_y = 2L_{strong}\varepsilon_{strong} + L_y\varepsilon_y \tag{4.5}$$

Where, L_{strong} is 200 mm and L_y is 1600 mm. The displacement at yield is therefore 4.25 mm.

The comparison graph shows the maximum force for each lap for RC and RFC, where the lap length has been divided by the bar diameter of 20 mm. The long lap corresponds to $^{L_b}/_{\emptyset} = 60$ and the short lap corresponds to $^{L_b}/_{\emptyset} = 25$.

4.4.1 Reinforced Concrete

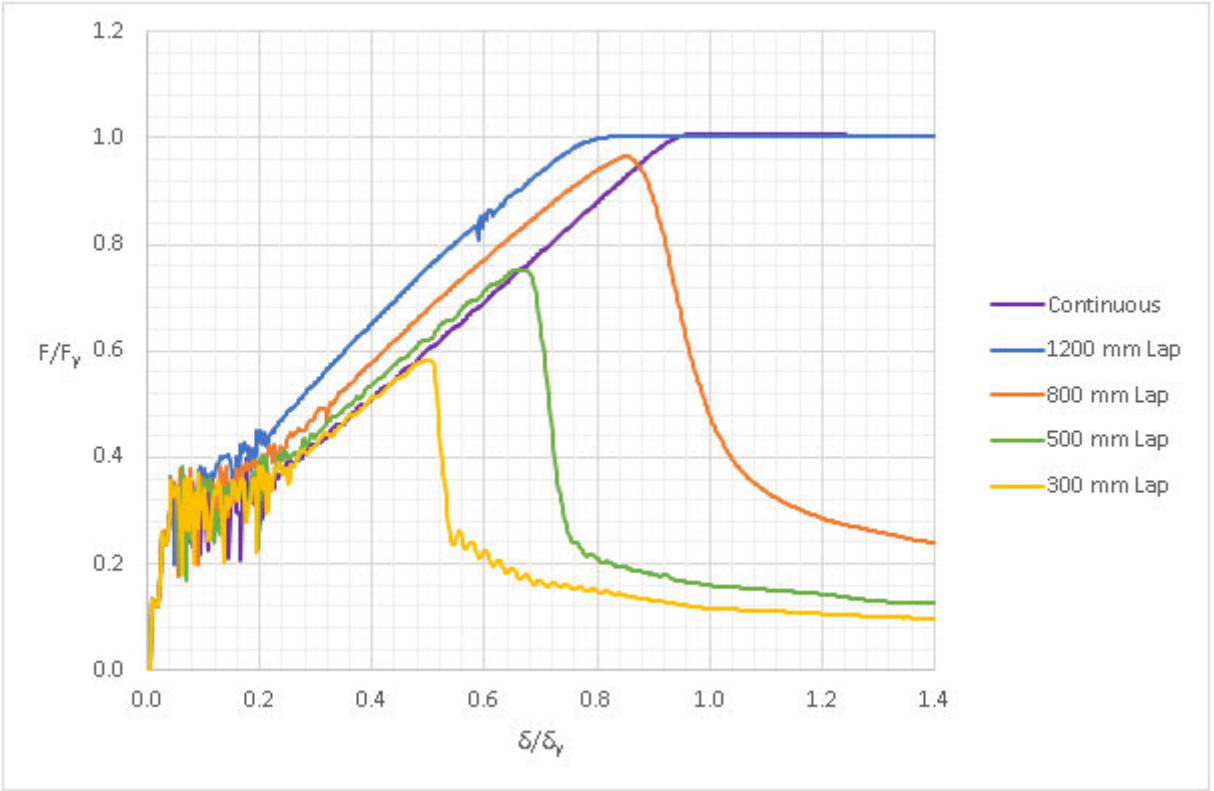

Figure 4.9: Reinforced concrete load displacement curve for lapped reinforcement bars

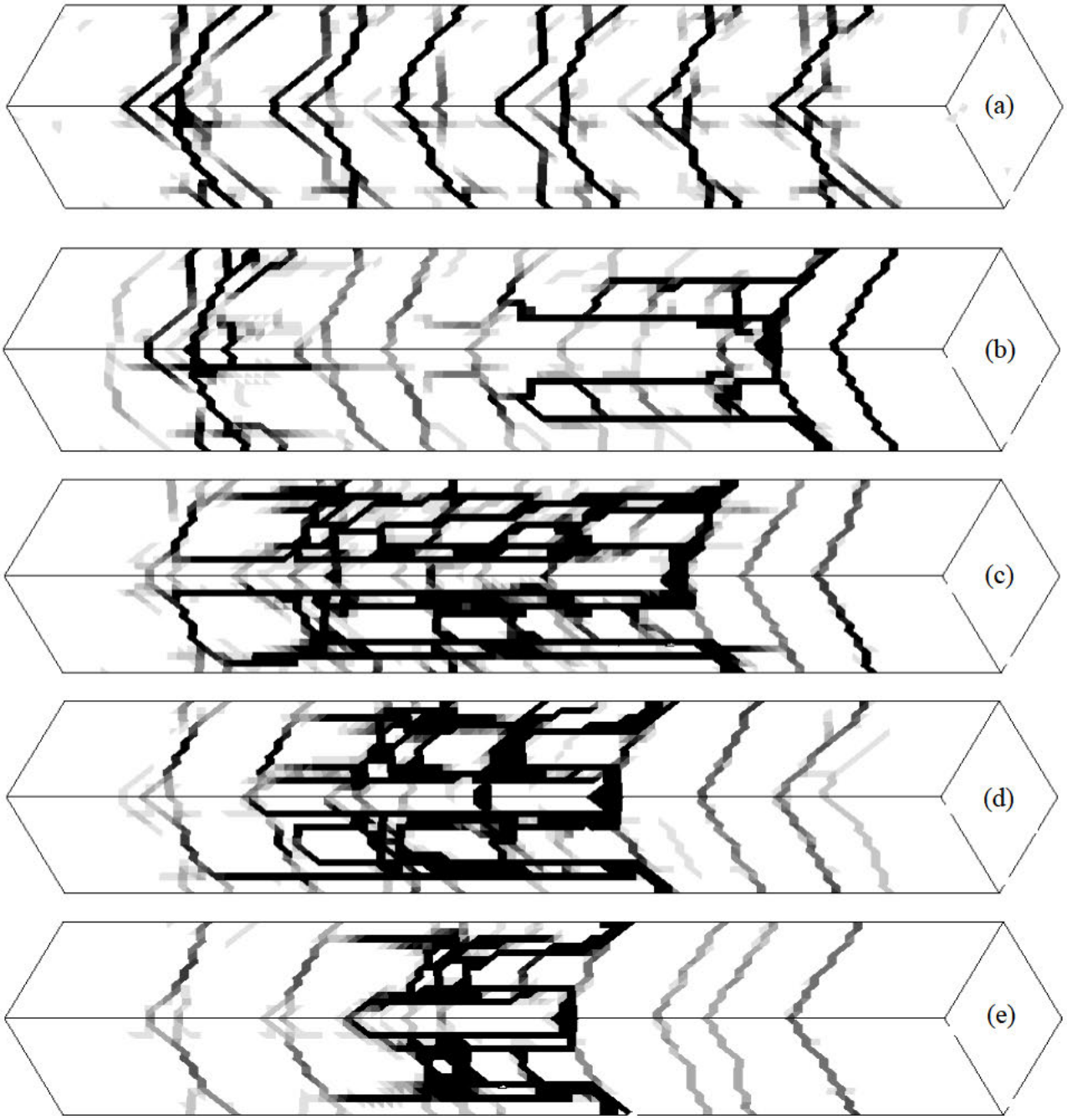

Figure 4.10: Reinforced concrete lapped reinforcement bar contour plots showing maximum principal strain at a normalised displacement of 1.4 where black corresponds to a crack width of 0.3 mm – (a) continuous reinforcement; (b) 1200 mm lap; (c) 800 mm lap; (d) 500 mm lap; and (e) 300 mm lap

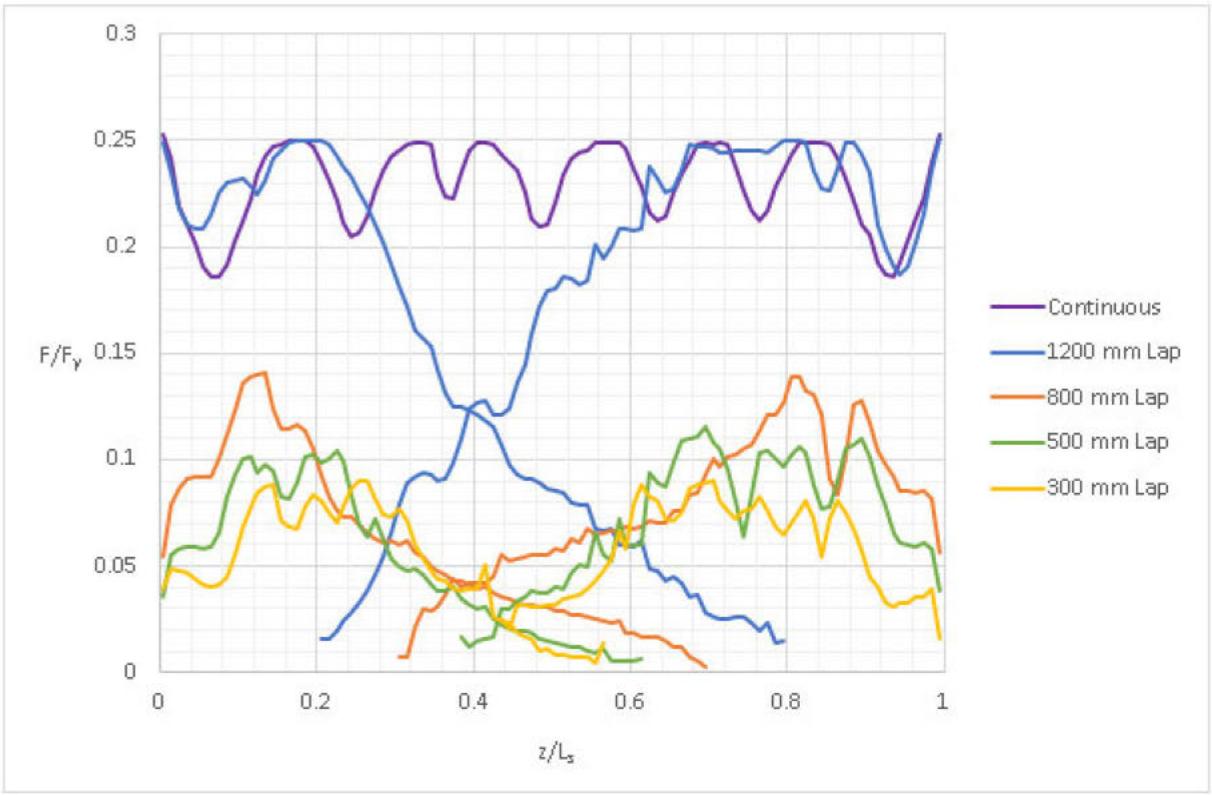

Figure 4.11: Steel force along lapped reinforcement bar for reinforced concrete

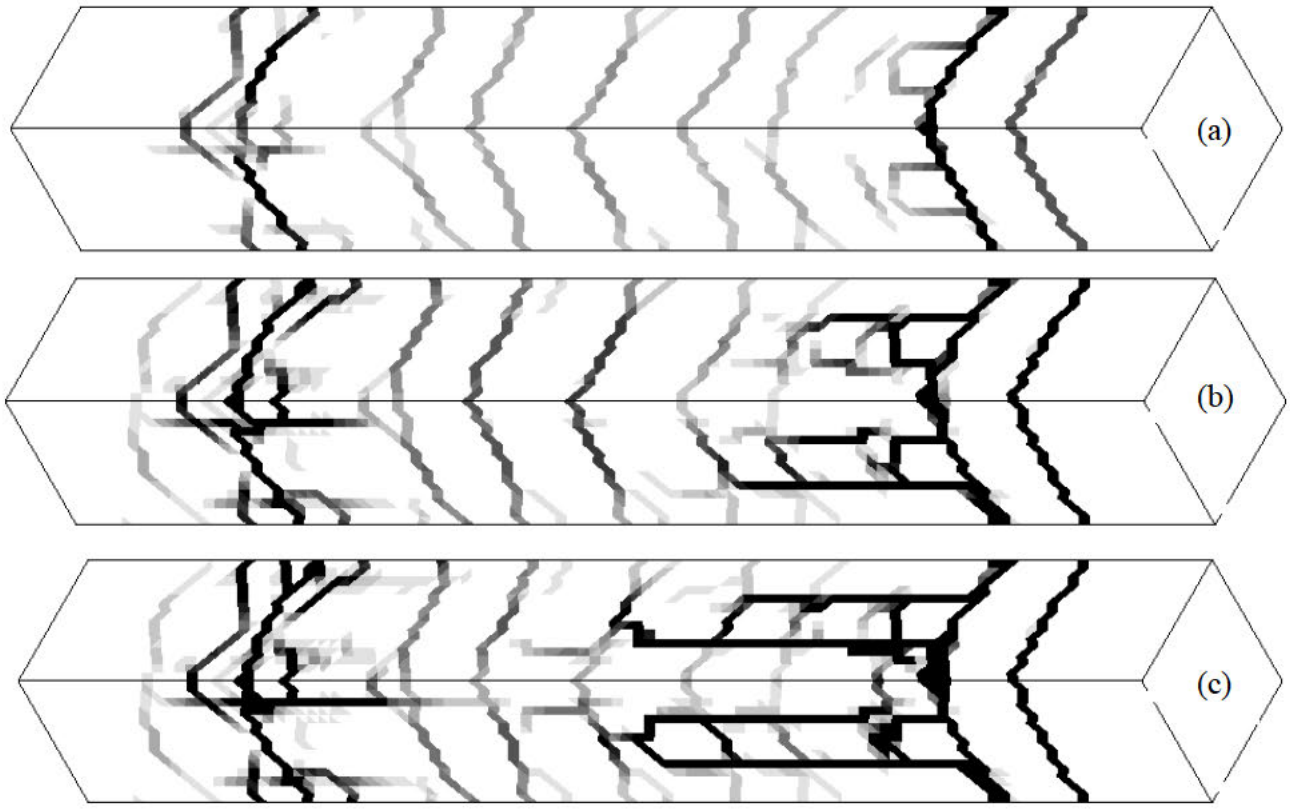

Figure 4.12: Reinforced concrete long lap (1200 mm) contour plots showing maximum principal strain where black corresponds to a crack width of 0.3 mm at normalised displacements of – (a) before yield (0.4); (b) yield (0.8); and (c) end (1.4)

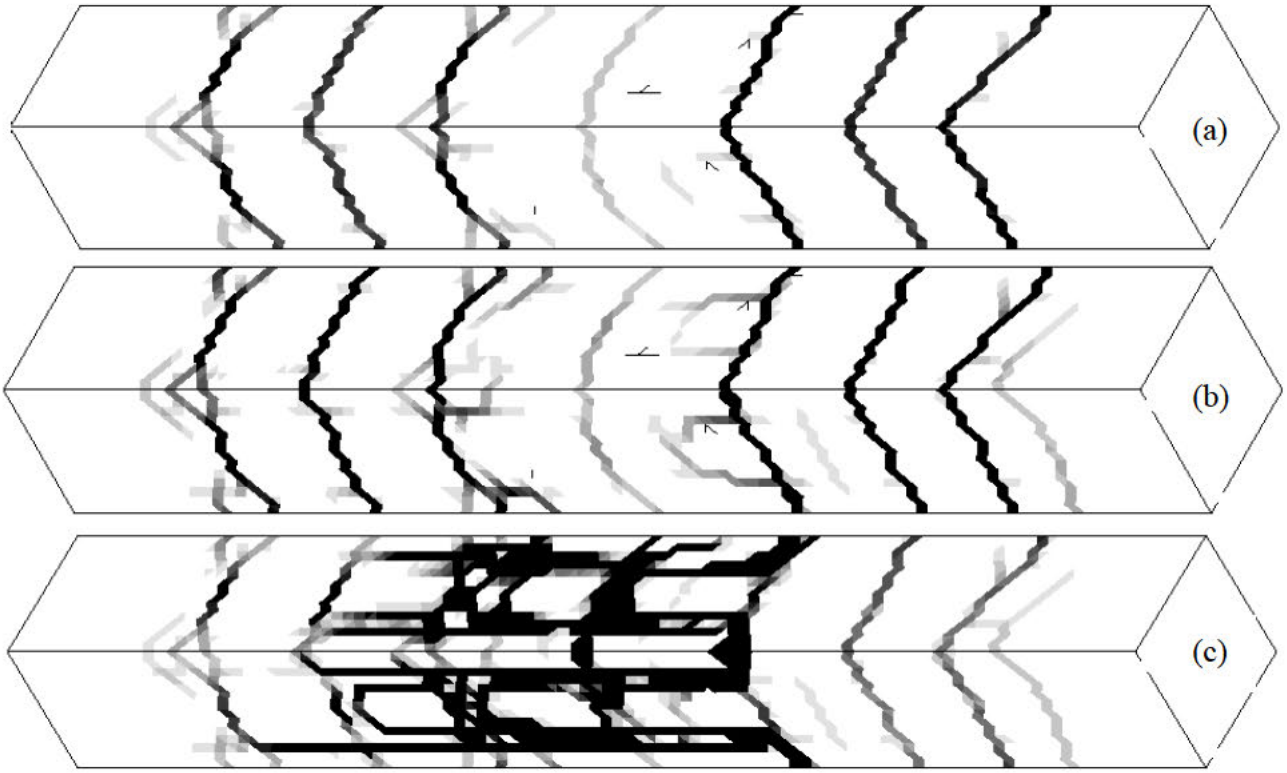

Figure 4.13: Reinforced concrete short lap (500 mm) contour plots showing maximum principal strain where black corresponds to a crack width of 0.3 mm at normalised displacements of – (a) before yield (0.4); (b) yield (0.6); and (c) end (1.4)

4.4.2 Fibre Reinforced Concrete with Traditional Steel Bars

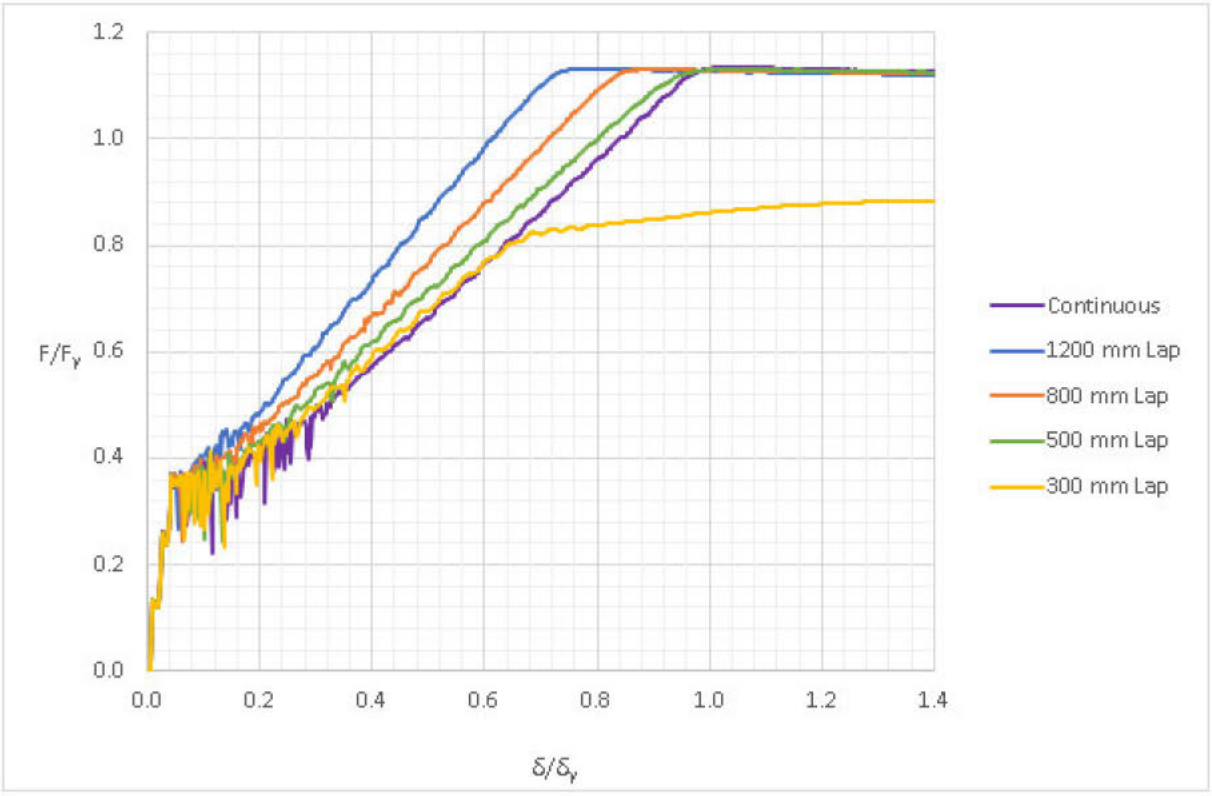

Figure 4.14: Fibre reinforced concrete with traditional steel bars load displacement curve for lapped reinforcement bars

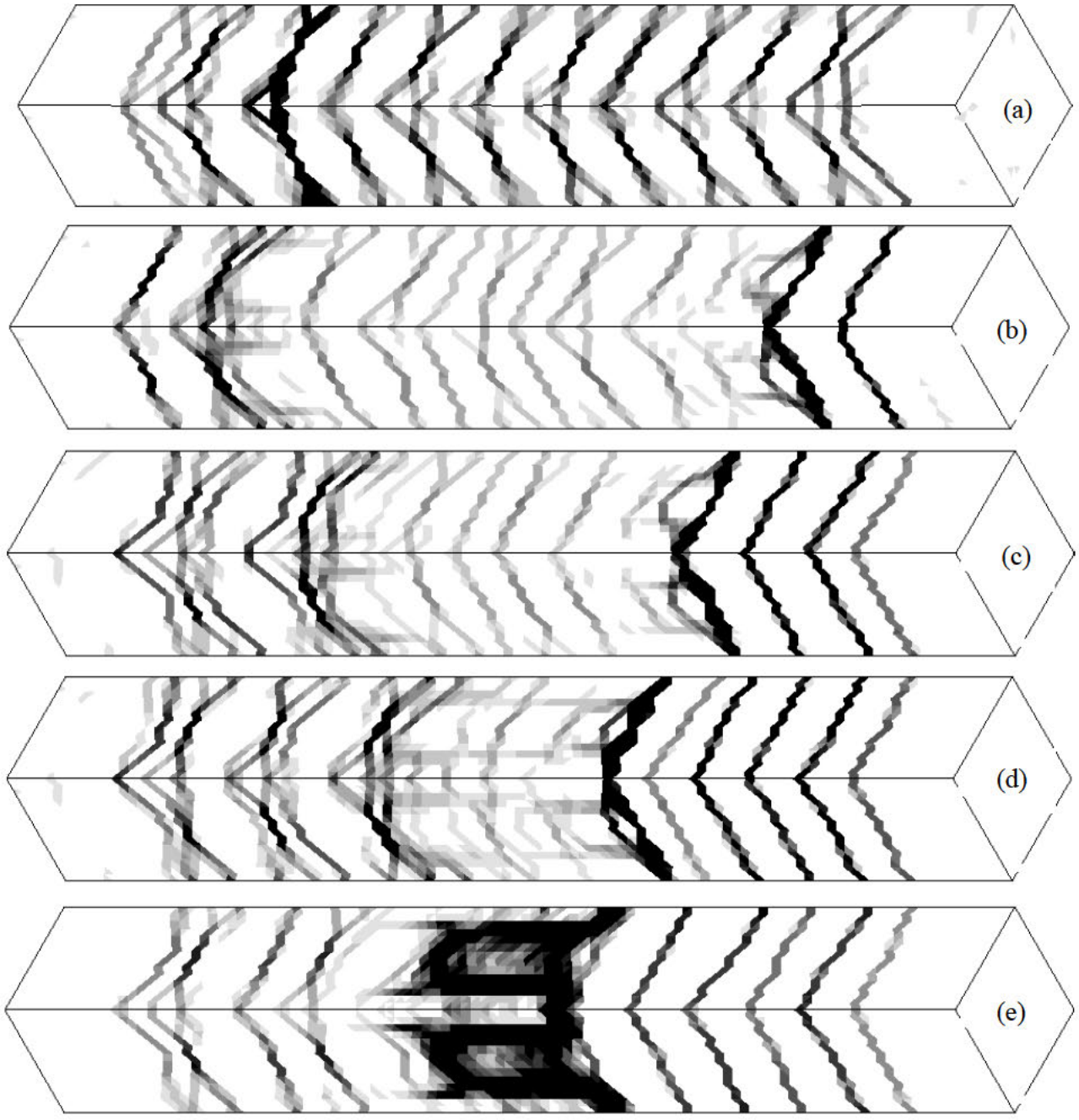

Figure 4.15: Fibre reinforced concrete with traditional steel bars lapped reinforcement bar contour plots showing maximum principal strain at a normalised displacement of 1.4 where black corresponds to a crack width of 0.3 mm – (a) continuous reinforcement; (b) 1200 mm lap; (c) 800 mm lap; (d) 500 mm lap; and (e) 300 mm lap

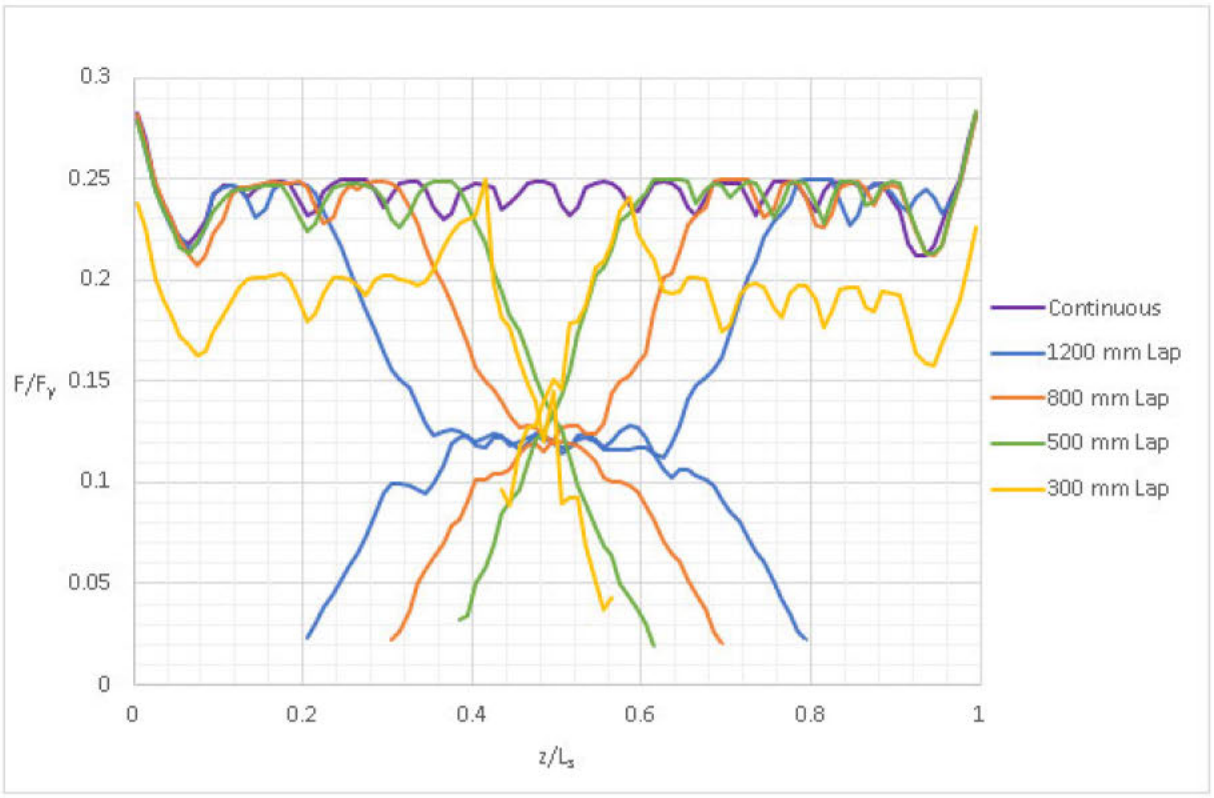

Figure 4.16: Steel force along lapped reinforcement bar for fibre reinforced concrete with traditional steel bars

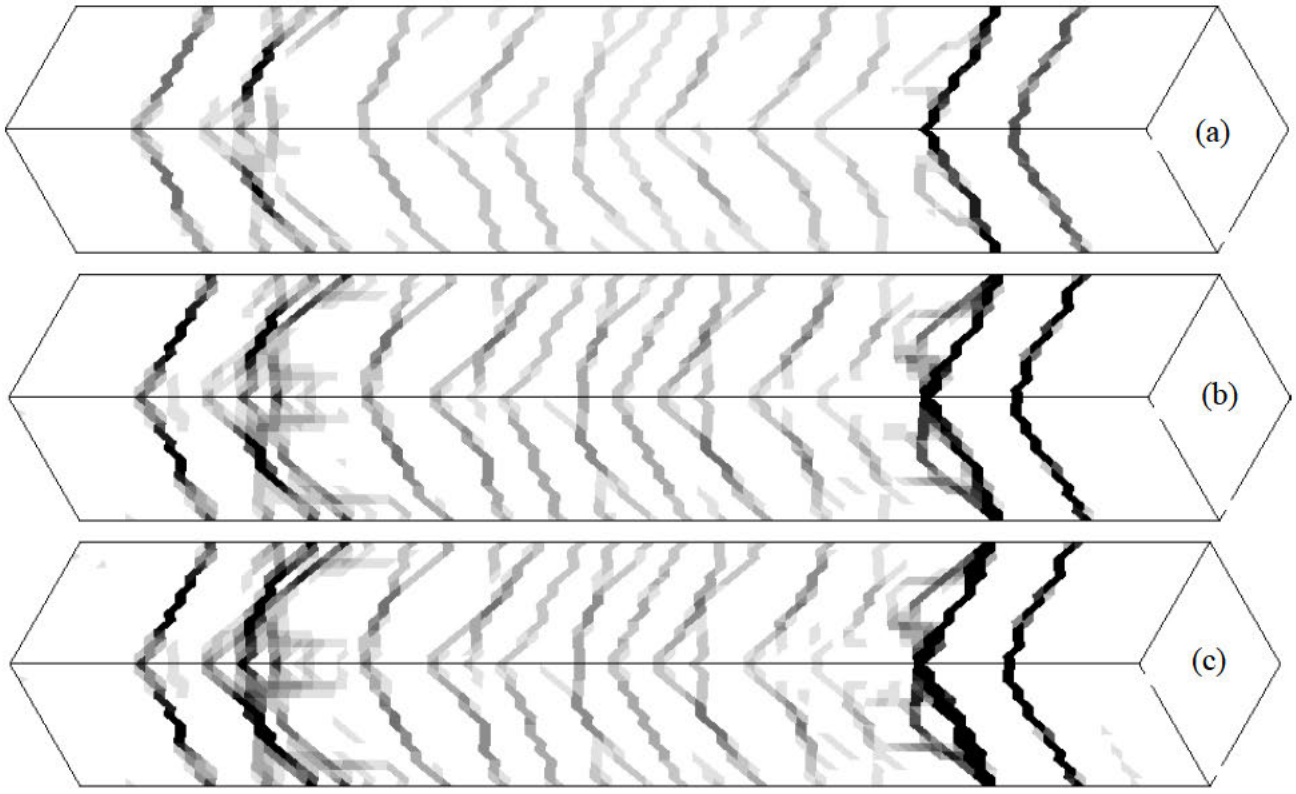

Figure 4.17: Fibre reinforced concrete with traditional steel bars long lap (1200 mm) contour plots showing maximum principal strain where black corresponds to a crack width of 0.3 mm at normalised displacements of – (a) before yield (0.4); (b) yield (0.7); and (c) end (1.4)

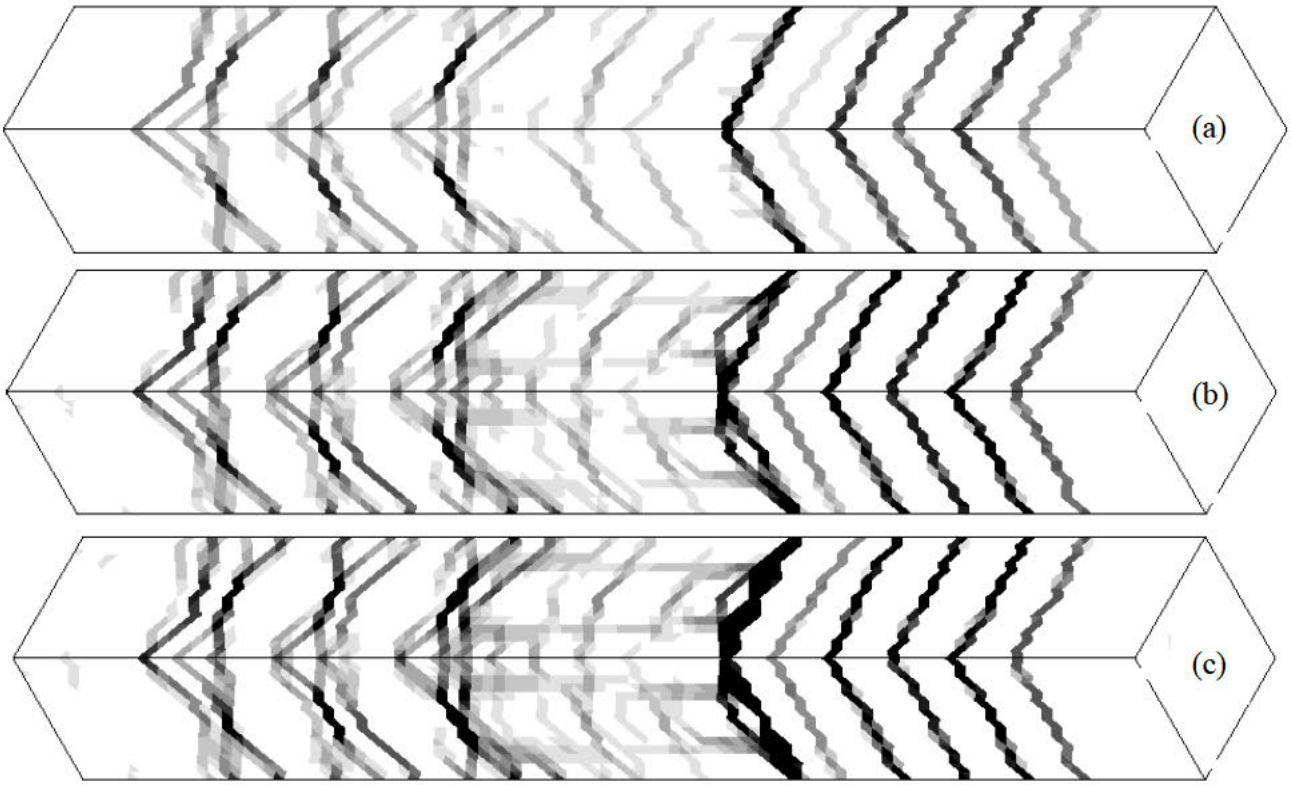

Figure 4.18: Fibre reinforced concrete with traditional steel bars short lap (500 mm) contour plots showing maximum principal strain where black corresponds to a crack width of 0.3 mm at normalised displacements of – (a) before yield (0.6); (b) yield (0.9); and (c) end (1.4)

4.4.3 Comparison

EC2 calculation was from BS EN 1992-1-1 (2004) and MC10 calculation was from CEB-FIP (2013).

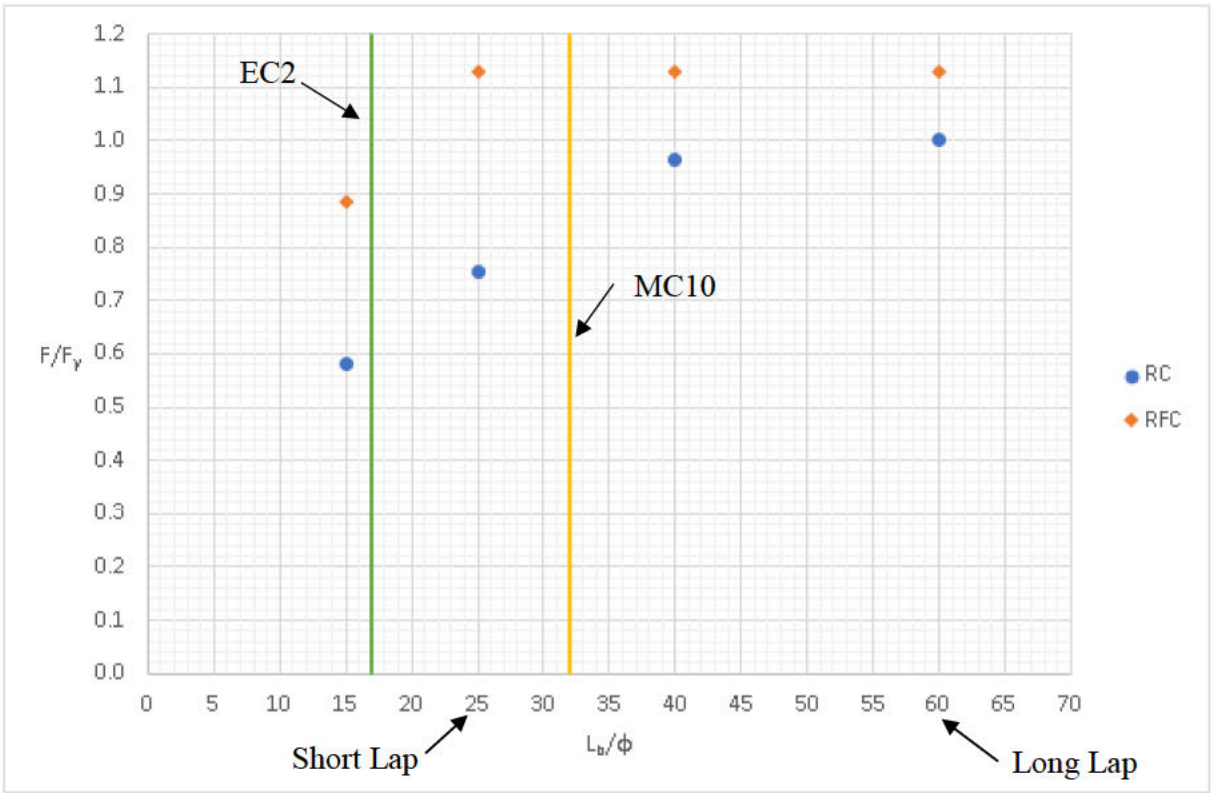

Figure 4.19: Comparison of maximum force for each lap

4.5 Discussion

With all modelling, simplifications are necessary to avoid excessive computational expense associated with large and complicated models. The simplifications make the modelling process more efficient, but in turn lead to limitations with the model. A designer must be aware of the simplifications made within any model so that the results can be interpreted for the real-life situation.

There are two main limitations in this model: modelling of rebar using beam elements and assumption of perfect bond conditions. Using beam elements instead of solid elements means that the model will overcompensate the volume of concrete compared to when the rebar is fully modelled. The assumption that there is perfect bond ignores the bond-slip which would occur from the reinforcement. These two model limitations could explain the sudden brittle failure that occurs for three of the lap lengths shown in Figure 4.9.

Modelling the reinforcement as a beam element means that there is a larger area of concrete in the model compared to the real-life situation which has been modelled. The reinforcement has effectively been modelled as a line instead of the full 20 mm diameter bar. This will increase the stiffness of the beam as there will be a higher percentage of concrete. The continuous reinforcement specimen will have an increase in stiffness of roughly 2 % and the longest lapped bar specimen (1200 mm) would have an increase in stiffness of roughly 3.2 %.

The modelling of the reinforcements interaction with concrete can be accomplished in a few different ways ranging in complexity as described in Section 2.6.3. For all analyses, the reinforcement was modelled with perfect bond which implies no bond-slip. Perfect bond causes the crack spacing to decrease and causes the concrete to crack immediately as the force has nowhere to go. However, as can be seen in the contour plots, there are spaces between the cracks which implies that there must be some bond-slip incorporated into this model even though perfect bond conditions have been modelled.

Bond slip is related to mesh size and a mesh study was undertaken on the continuous reinforcement to investigate the effect of the mesh size on the crack spacing. This was part of the verification of the model to ensure that the model was behaving the same way as expected. Figure 4.20 shows the load displacement response for the three mesh sizes which illustrates that the difference in response between the medium mesh and fine mesh is very small. This suggests that the results from the medium mesh are suitable for the purpose of the investigation whilst also saving computational time.

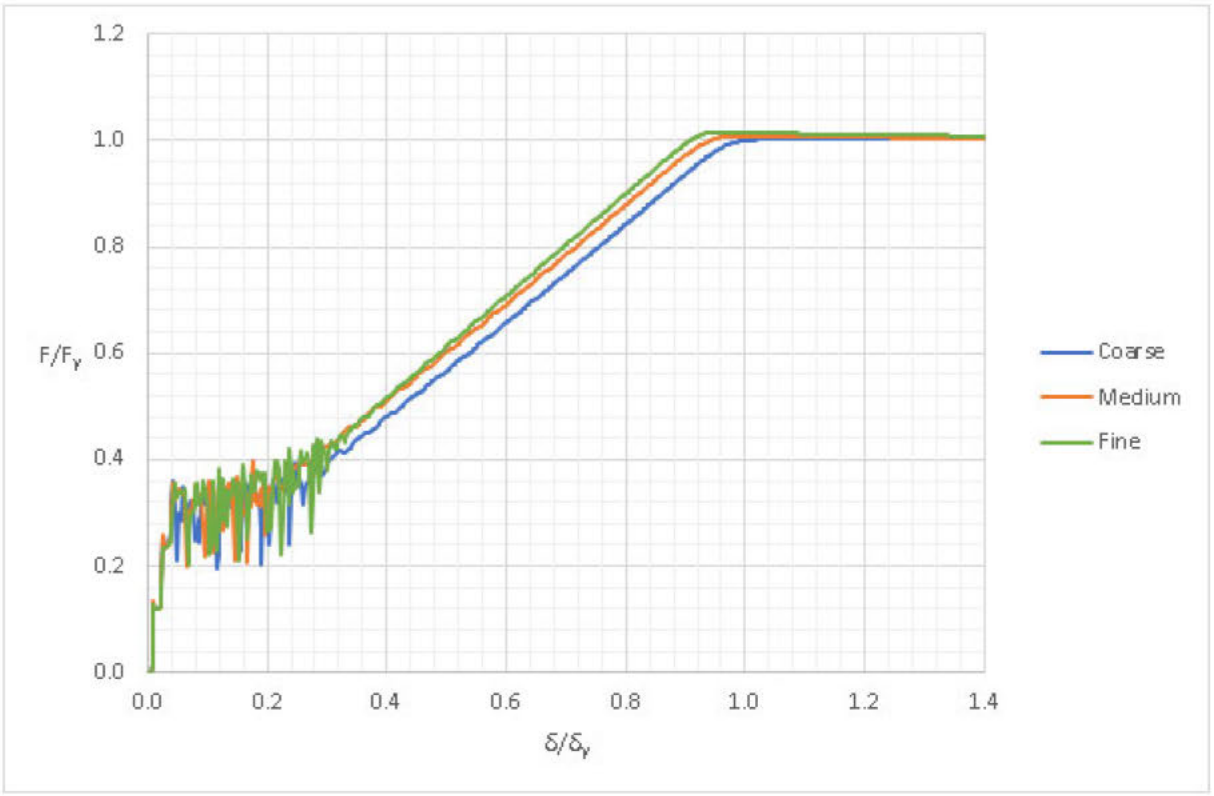

Figure 4.20: Reinforced concrete load displacement curve showing mesh independency

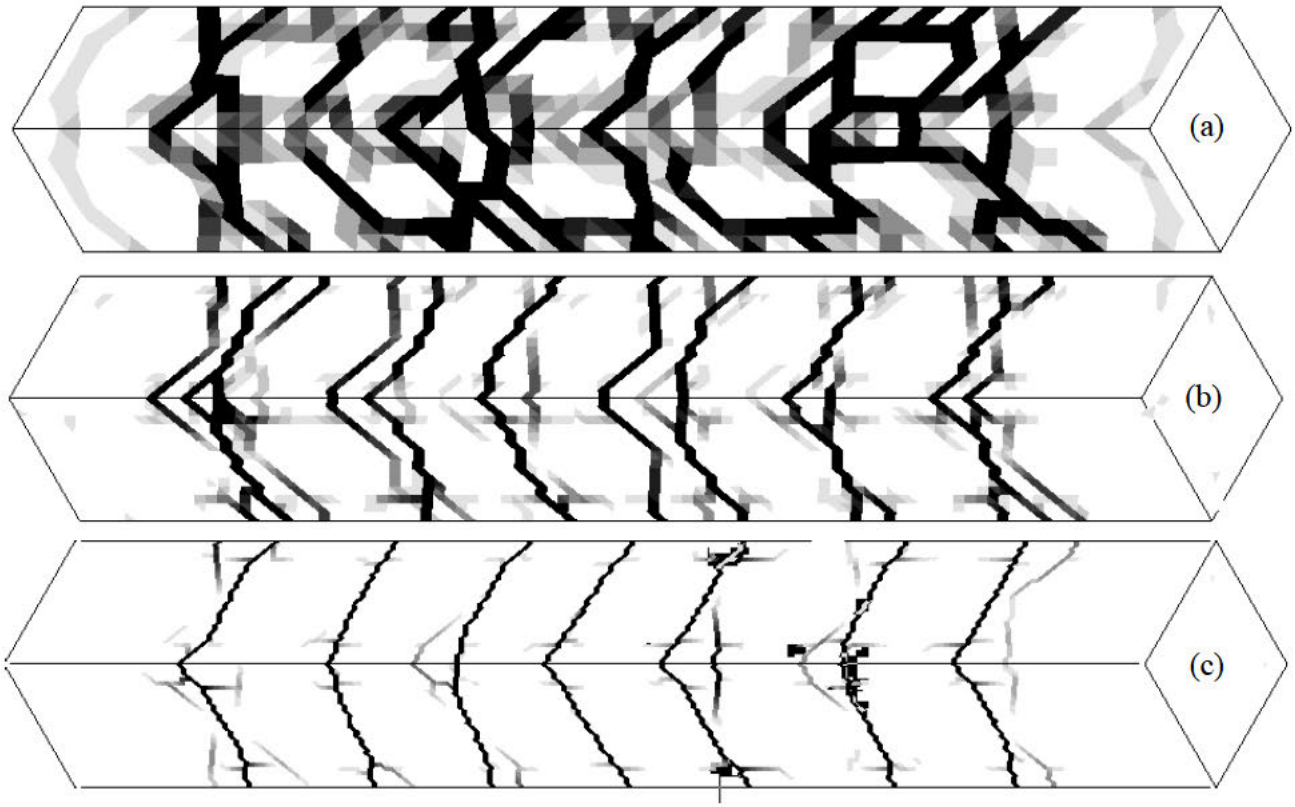

Figure 4.21: Reinforced concrete lapped reinforcement bar contour plots showing maximum principal strain at a normalised displacement of 1.4 where black corresponds to a crack width of 0.3 mm – (a) coarse mesh; (b) medium mesh; and (c) fine mesh

Figure 4.21 shows the contour plots for the three mesh sizes. The coarse mesh has larger cracks spaced closer together which highlights the perfect bond conditions which were expected. When the mesh size is decreased, the cracks become more distinct and spacing between the cracks can now be seen. For the fine mesh, the cracks have become very regular with clear spacings between each crack. These contour plots imply that when the mesh size is decreased, bond-slip has been incorporated into the model without purposely modelling it. Therefore the effect of bond slip on the layer around the concrete is dependent on the mesh size.

This leads to concerns when adding bond-slip into the model as the perfect bond model has some bond-slip when the mesh size is small enough. It would be erroneous to try and model bond-slip without including an allowance for the bond-slip incorporated with the mesh size change. This means that when adding bond slip to a model, it is necessary to adjust the amount so as not to overcompensate for how much there actually is in the real-life scenario.

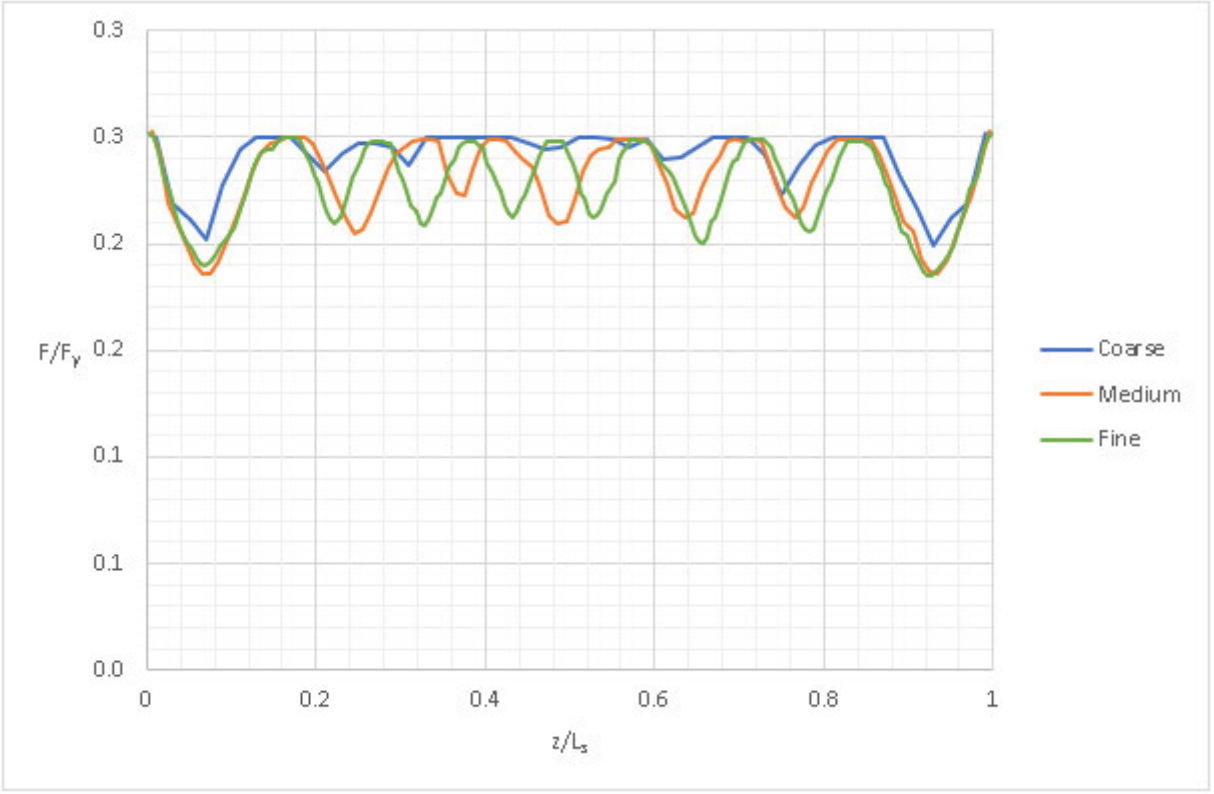

Figure 4.22: Steel force along one reinforcement bar for reinforced concrete straight reinforcement bars

Figure 4.22 shows the steel force along one reinforcement bar, again the coarse mesh acts more like a 'perfect bond' model. This can be explained by the concrete not being able to carry any tensile forces and the cracks are occurring very close to each other and the steel force therefore does not decrease by much. Whereas for both the coarse and fine mesh, the steel force decreases between cracks as the concrete is able to carry some of the tensile forces in these areas.

The mesh independency of the model can be seen by comparing the medium and fine mesh sizes. There are only very small differences between these two. One more crack appears in the contour plot for the fine mesh and the cracks are spaced very similarly, with the medium mesh having larger crack areas due to the perfect bond mechanism. This mesh study therefore confirmed the mesh independency of the model and allowed the subsequent analyses to be undertaken using the medium mesh size to save computational time and expense.

The timestep size was also investigated to analyse the effect of dynamic loading on the results. Dynamic effects can occur if the displacement is applied too fast and is best to be avoided as it would affect the results. To investigate if the timestep had an influence on the results, a verification on the continuous reinforcement model was undertaken using a timestep of 0.1 sec compared to a longer timestep of 1 sec.

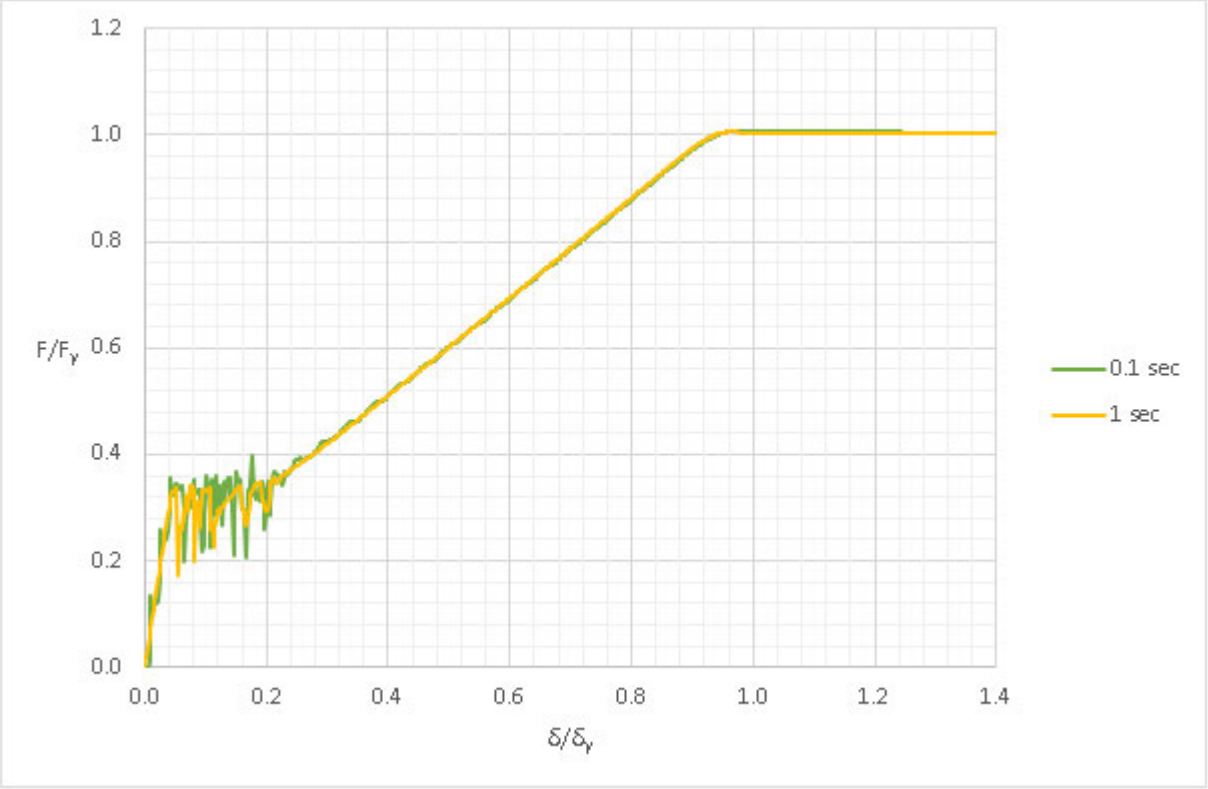

Figure 4.23: Reinforced concrete load displacement curve showing change in the timestep

Figure 4.23 shows that there is not much change between using a longer timestep compared to the shorter timestep of 0.1 sec. The dynamic effects from the faster timestep of 0.1 sec are very small and therefore have not had a considerable effect on the results. The contour plots for both timesteps are show in Figure 4.24 and are almost identical, as are the steel force graphs in Figure 4.25. Therefore, to save computational time, the timestep of 0.1 sec was used for all analyses.

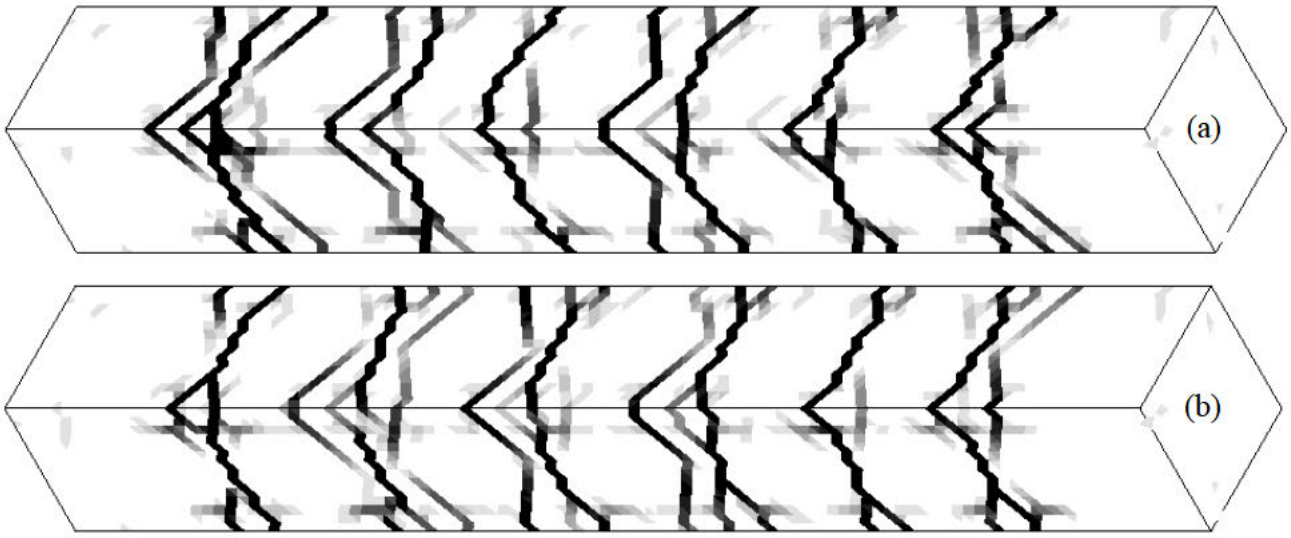

Figure 4.24: Reinforced concrete timestep change contour plots showing maximum principal strain at a normalised displacement of 1.4 where black corresponds to a crack width of 0.3 mm - (a) 0.1 sec; and (b) 1 sec

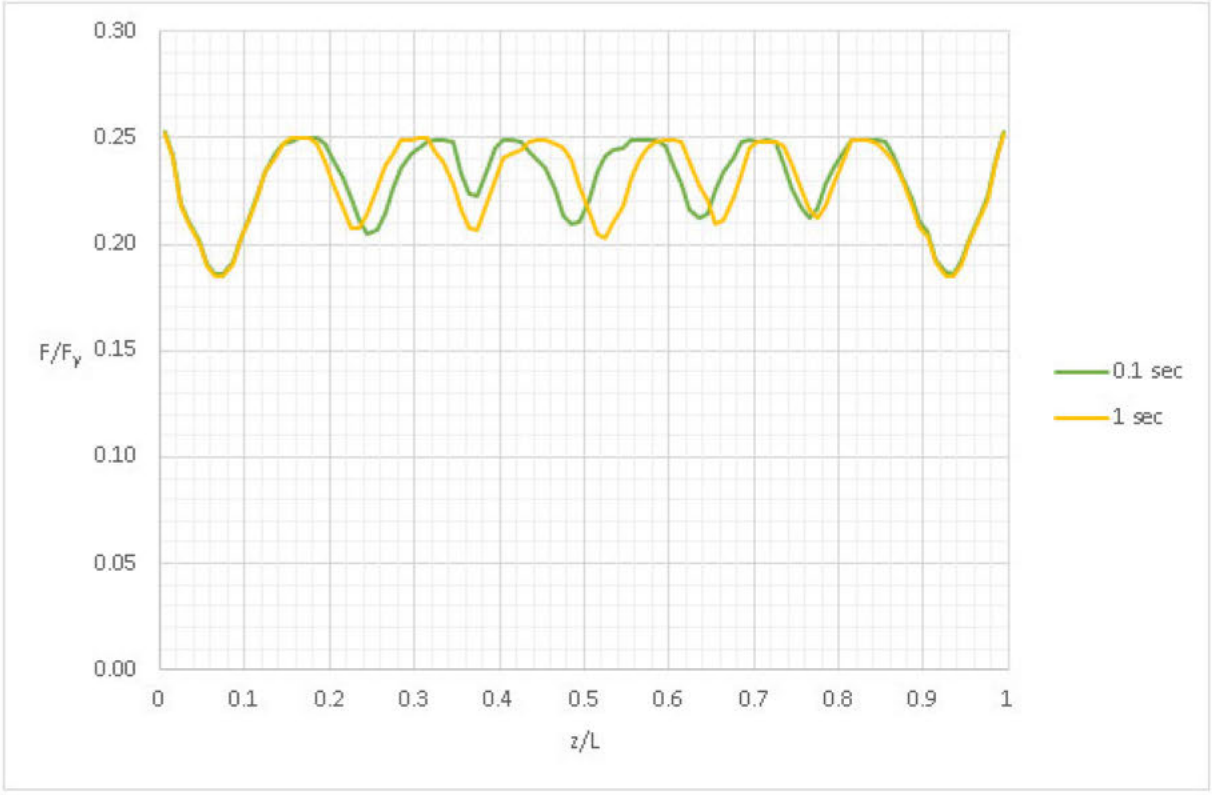

Figure 4.25: Steel force along one reinforcement bar for reinforced concrete change in timestep

A single element test was carried out to check the material input parameters used were correct and produced reasonable results. This involved subjecting a single cube element of different length L to uniaxial tension and confirming that the crack opening curve produced from the model corresponded to the same crack opening that the material parameters produced. Cubes of length 50 mm, 100 mm

and 200 mm were used for the single element tests – which correspond to small, medium and large respectively – with the geometry shown in Figure 4.26.

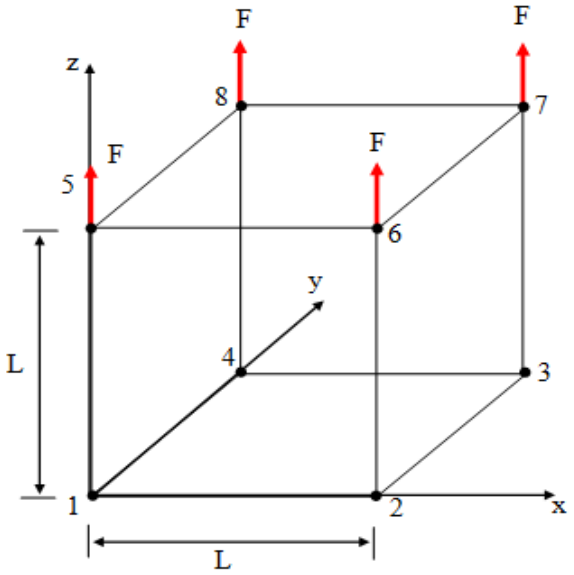

Figure 4.26: Single element geometry - 3D view

For both RC and RFC a force-displacement curve and a stress-crack opening curve were potted as shown in Figure 4.27 and Figure 4.28 for RC and in Figure 4.29 and Figure 4.30 for RFC.

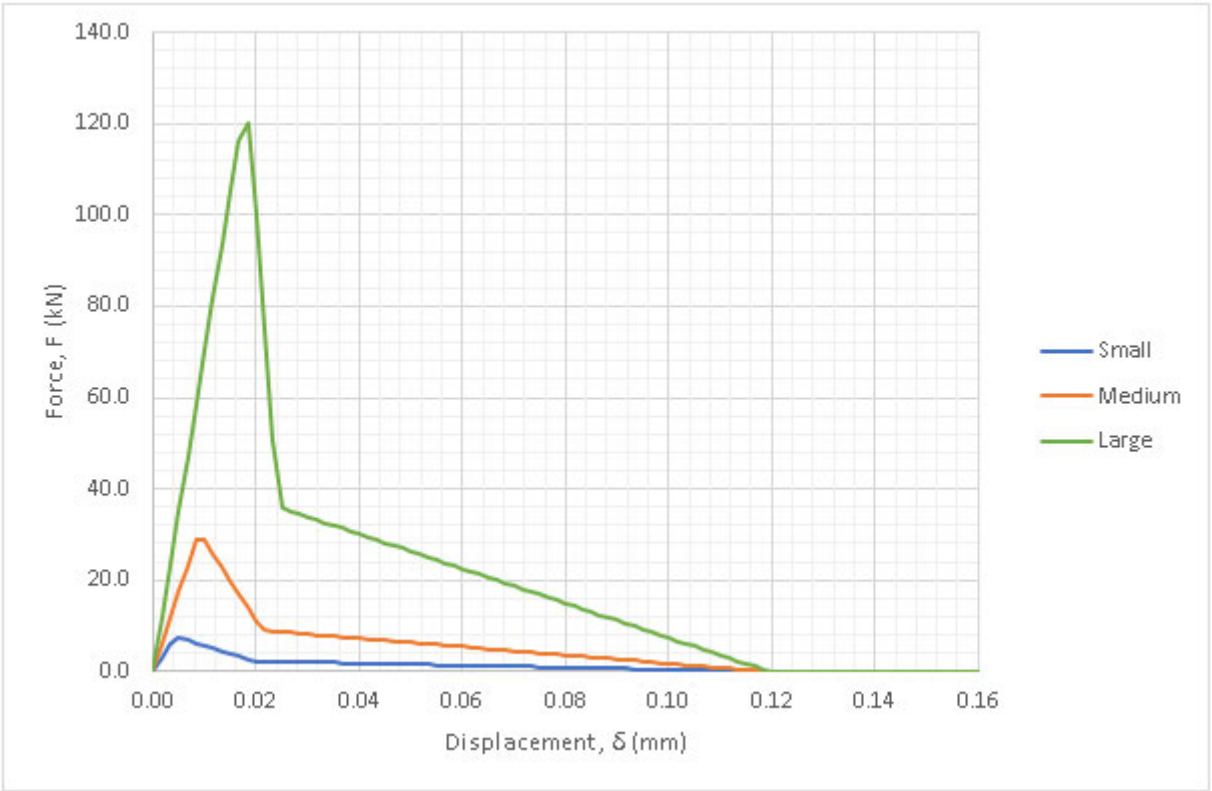

Figure 4.27: Force-displacement curve for RC

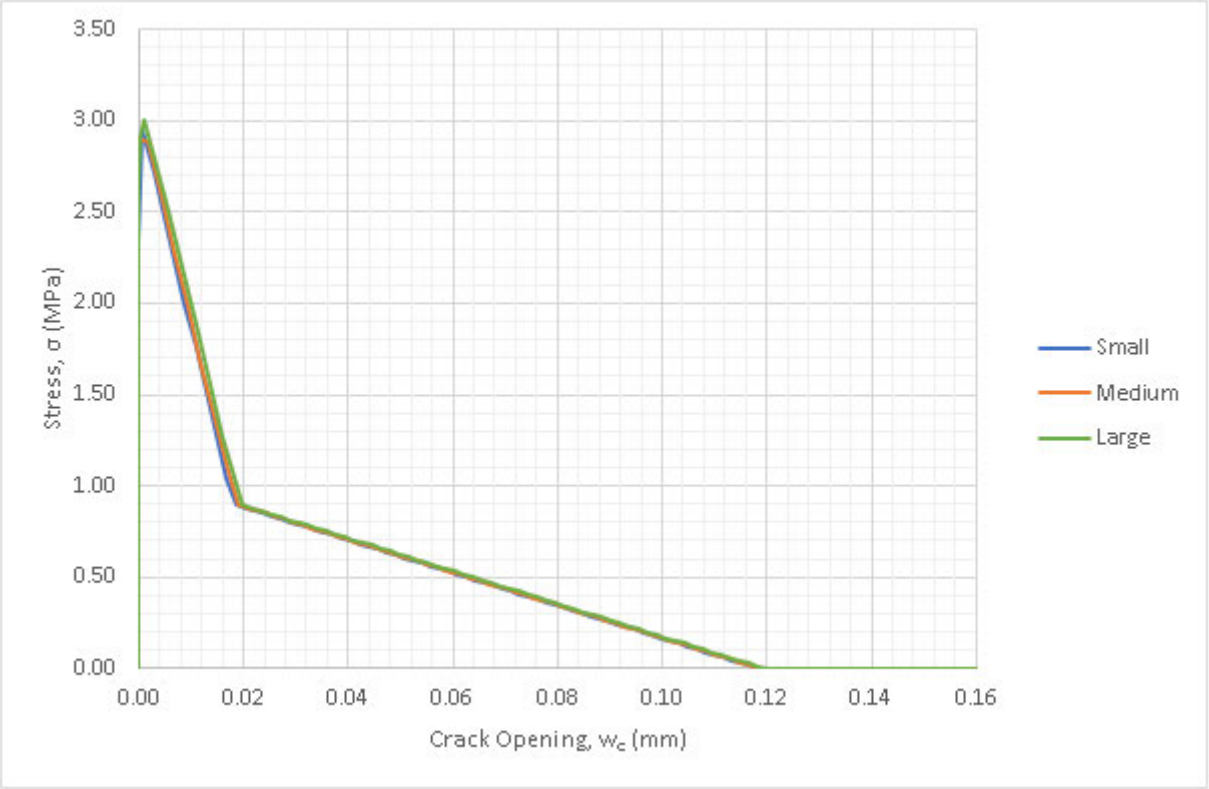

Figure 4.28: Stress-crack opening curve for RC

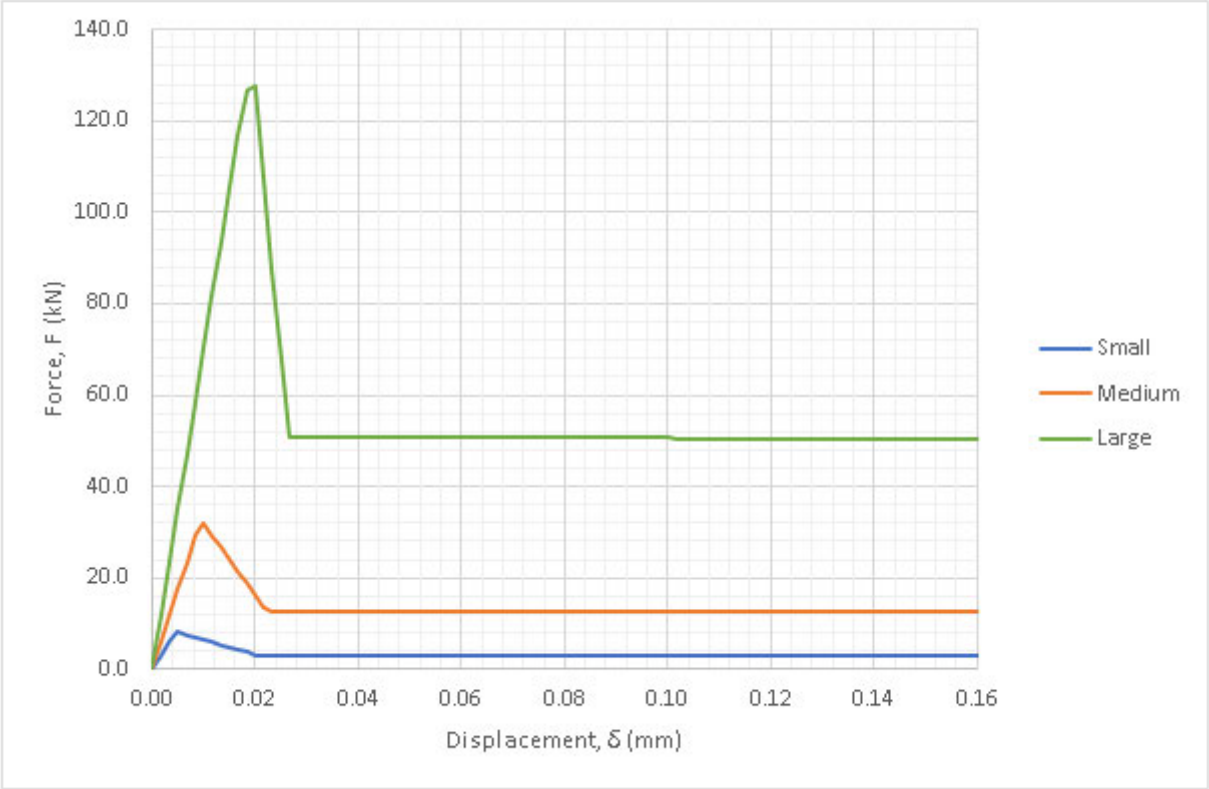

Figure 4.29: Force-displacement curve for RFC

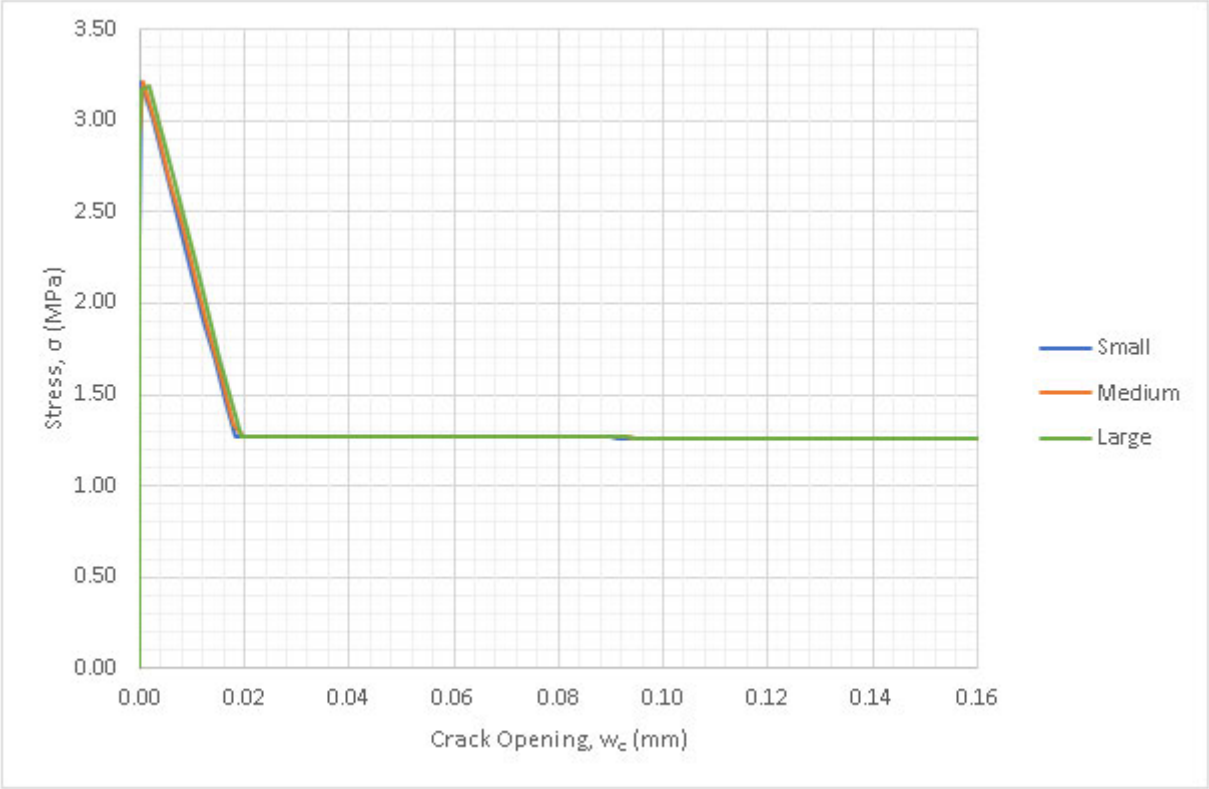

Figure 4.30: Stress-crack opening curve for RFC

The force – displacement plots shows the structural response of the element. As the cube doubles in size, the force increases by the square of the cube size. This graph can then be converted into a stress-crack opening curve by calculating the crack opening from Equation 4.6.

$$w_c = \delta - \delta_e \tag{4.6}$$

Where, δ_e is the elastic displacement of the element which is calculated from Equation 4.7.

$$\delta_e = \frac{\sigma}{E} \times L \tag{4.7}$$

The stress crack opening curve shows the material response of the element, which for both RC and RFC are the same for all three element sizes. This shows that the material parameters are unaffected by the size of the elements when modelling and confirms that the model is correctly applying the material parameters. Figure 4.28 and Figure 4.30 can be compared to Figure 3.2 which confirms that the model is correctly applying the material properties as expected as the curves are identical.

A validation of the model was done by checking the crack spacing aligned with the theory and design codes. The crack spacing changes considerably with the addition of fibres as can be seen by comparing the contour plots of Figure 4.10 and Figure 4.15. The RFC specimens have smaller crack spacings with the cracks not reaching the crack opening of 0.3 mm shown by the grey cracks. This aligns with the theory described in Section 2.4.1 as the addition of steel fibres will decrease the crack

spacing. The maximum crack spacing calculated using the rules in BS EN 1992-1-1 (2004) was 373 mm (calculation in Appendix B). This differs quite considerably from the crack spacings shown in the contour plots.

The crack spacing can be calculated from Equation 4.8.

$$s_r = \frac{L_s}{Number\ of\ Cracks} \tag{4.8}$$

Where, L_s is the specimen length. This equation will give a rough estimate of the average crack spacing for the continuous reinforcement specimens. The crack spacings from the model for RC and RFC are shown in Table 4.5.

Table 4.5: Crack spacing for different specimens

Specimen	Crack Spacing, s_r (mm)	
	RC	**RFC**
Continuous	330	200

The crack spacing results are less than the maximum allowable crack spacing calculated from EC2 which suggests that the design is acceptable. The crack spacing decreases with the addition of fibres. This implies that the RFC specimens are stronger.

The load displacement response for the specimens show that the only acceptable lap length for RC is the 1200 mm lap which is well above the MC10 design value. These results show that even for the EC2 design lap length, the reinforcement is unable to reach its yield strength before failure occurs. All three of the other lap length specimens show a sudden failure which represents the brittle failure discussed in Section 2.5.1.

Yield for the RC specimens is shown as 1 on the graphs. Figure 4.14 therefore shows that the RFC specimens are able to sustain a 12 % increase in load capacity, confirming that these RFC specimens are stronger and able to withstand a larger deformation before failure. The addition of fibres ensures that the brittle failure for lap lengths of 500 mm and 800 mm do not occur and both specimens are now able to reach yield before failure. However, the fibres are still not able to increase the strength for the 300 mm lap and it does not reach the reinforcement yield. Nonetheless, the 300 mm lap with fibres does not display the sudden brittle failure that was shown in the RC sample. Instead the sample does not lose the load capacity and continues to sustain load at a value of 90% of the reinforcement yield strength. Therefore, the fibres can stop the sudden brittle failure from occurring for all laps examined and increase the deformation capacity of the specimen.

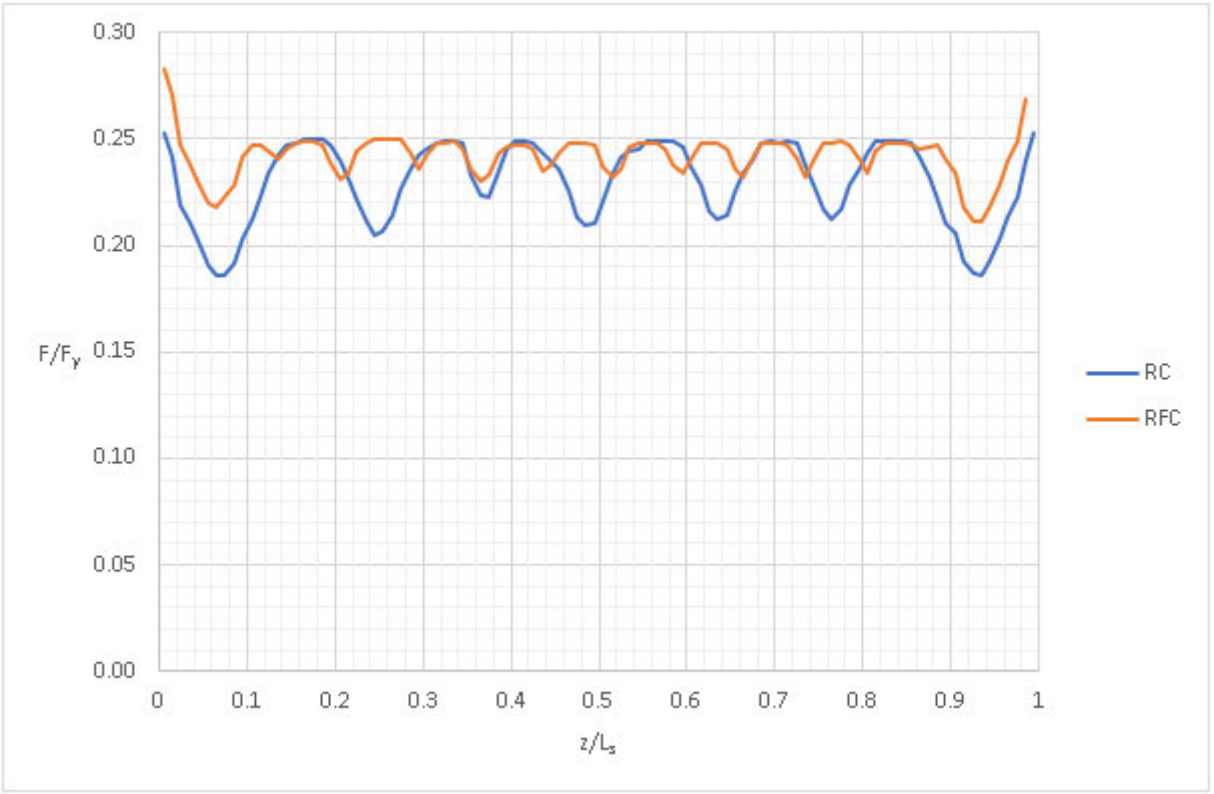

Figure 4.31: Continuous reinforcement steel force along one reinforcement bar for RC and RFC

Figure 4.31 shows the steel force graph for the continuous reinforcement for RC and RFC. The steel force has this behaviour due to the cracks that form along the bar. Where these cracks form, the steel force is carried fully by the reinforcement and then between the cracks the steel force is carried by both the reinforcement and the concrete. At these locations the steel force is less and is shown by the dips in the figure. The steel force reaches a maximum of 25 % of the reinforcement yield because the graph shows the force for only one bar. Four bars would then equate to 100 % of the reinforcement yield strength.

The steel force can be explained by Figure 4.32. Between cracks, the force of the steel will decrease whilst the force in the concrete increases and then at a crack, the concrete force decreases whereas the steel force increases again. At the cracks the steel force increases to the rebar strength as the concrete is no longer able to carry any of the tensile forces. The reason for the concrete being able to carry some of the tensile forces between the cracks is due to the bond between the reinforcement and the concrete. The force is transferred from the steel into the concrete via bond stresses. This is known as tension stiffening and has been explained in detail in Section 2.3.2.

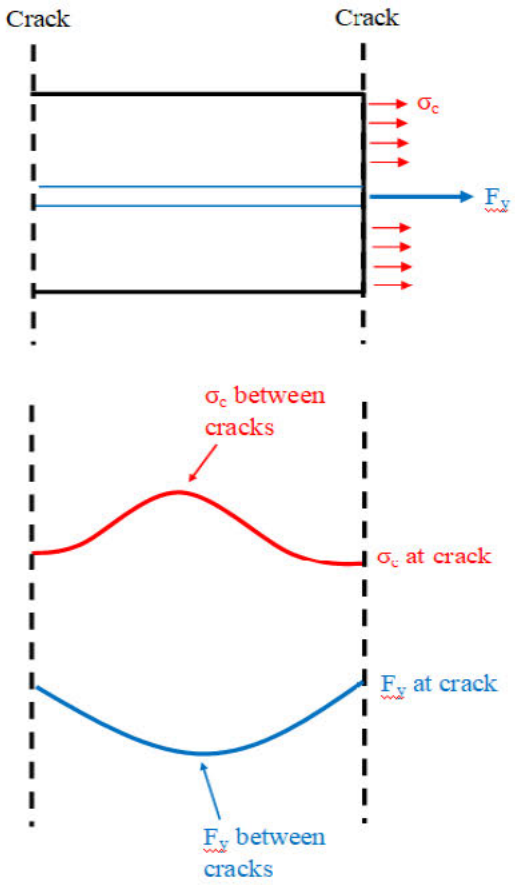

Figure 4.32: Steel force graph explanation

For the RFC, the reinforcement yield strength for all bars is around 12 % higher as seen in Figure 4.31 as the steel force maximum for one bar is 3 % higher. The steel force at the cracks does not reach this maximum yield strength shown by dimension Z in Figure 4.33. This difference in Z is due to fibres bridging the cracks and carrying some of the tensile forces, reducing the force that the steel needs to carry. The fibres can carry some of the tensile force at the cracks which implies the steel force will be lower and are also able to carry some of the force between the cracks which means that the concrete does not need to carry as much of the tensile forces.

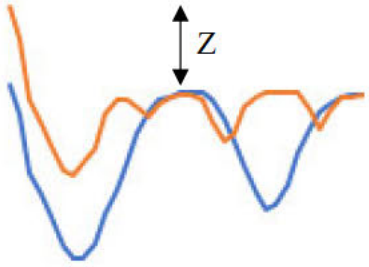

Figure 4.33: Close up of steel force graph

Figure 4.16 shows the steel force for the RFC specimens. Here the steel force is at the midpoint of the bar. The 1200 mm lap has a long section where the steel force of the two lapped bars are equal and this corresponds to half the value of the steel force for the one bar. This overlap could be explained by the transfer length where the force in the steel is transferring from one bar to the next. Lapped bars

need to have an adequately long lap length in order to have a long enough transfer length to sufficiently transfer the tensile forces from one bar to the next. This transfer length can just be seen for the 800 mm lap. For the RC specimens, the 1200 mm lap has a slight overlap which shows that it also has a very small transfer length. All other laps do not possess an adequate transfer length and are therefore not suitable for design.

Another interesting observation can be seen in Figure 4.11. Here the crossover between the reinforcement bars steel force is not at the midpoint and instead is at 40 % of the total length. This is unexpected as it would have been assumed that the reinforcement would transfer the force at the midpoint. A possible reason could be due to dynamic effects from pulling the specimen which may cause the force to transfer earlier. This only occurs for the RC specimens and an explanation is that the RFC specimens have a sufficient strength to allow the forces to transfer in the correct position.

The crack evolution plots show that the end cracks form first before yield with the cracks in the middle becoming more pronounced as yield occurs. At this point, the cracks in the middle of the bars become more defined. Distinct cracks form where the lapped bar ends, and these cracks are more strongly pronounced at the end closest to where the load is applied. This could be down to the dynamic effects of the load being applied too fast and this would cause the force transfer to be inconsistent.

4.6 Summary

The results of the nonlinear finite element modelling show that the addition of steel fibres can reduce the length of lapped reinforcement and withstand higher loads. The fibres removed the brittle failure that was seen in the RC specimens and the failure behaves in a more ductile manner. These results show that the lap length required by EC2 is not suitable for design as the reinforcement yield was not reached before a brittle and sudden failure occurred. In addition, the investigation confirmed the mesh independency of the CDPM2 material model as well as verifying that the model had been implemented correctly and was working as intended for the purpose of the study. The model was validated by confirming that the calculated rebar strength was reached ensuring that accurate results were produced. For the crack spacing, the validation confirmed that the model had a lower crack spacing than the maximum crack spacing allowed by EC2.

Therefore, these analyses conclude that steel fibres influence the performance of a reinforced concrete specimen and increase the strength by roughly 12 %. The deformation capacity is improved by the bridging effects of the fibres causing the failure to become more ductile.

5 Concrete Experiments

Small-scale experiments were performed in the laboratory to determine the compressive and tensile strength of concrete with and without steel fibres. Three different sets of concrete were designed:

- Set 1 – Normal Concrete
- Set 2 – Normal Concrete with 0.5% Volume Steel Fibres
- Set 3 – Normal Concrete with 1% Volume Steel Fibres

Compression tests were conducted on cubes to determine the compressive strength and tension splitting tests were performed on cylinders to determine the tensile strength. The cubes had dimensions 100 mm x 100 mm x 100 mm and the cylinders had dimensions 300 mm length by 150 mm diameter.

5.1 Concrete Mix Design

The concrete used in the experiments has been designed using the BRE Handbook (Teychenne et al., 1997). The concrete mix design forms showing all the parameters used in the design of each concrete set can be found in Appendix E.

The mixes were designed for a mean strength of 50 MPa at 28 days and assuming a cement strength of 42.5 MPa with 15 % extra material added in for spillage and waste. The resulting strength of concrete should be around 40 MPa which has been used in all analyses as seen in Chapter 4. Due to the small volume fraction of fibres, all three sets have the same mass of cement, water and aggregate. The constituents and masses used in the experiments are shown in Table 5.1.

Table 5.1: Mass of concrete constituents

Concrete Constituent	Mass of Constituents (kg)		
	Set 1 – Normal Concrete	**Set 2 – 0.5% Steel Fibres**	**Set 3 – 1% Steel Fibres**
Cement	9.7	9.7	9.7
Water	4.2	4.2	4.2
All-in Aggregate	37.5	37.5	37.5
Steel Fibres	-	0.85	1.7

5.2 Concrete Casting

The concrete was mixed using the yellow mixing drum shown in Figure 8.1 in Appendix F. Once the concrete was mixed it was placed into the cube and cylinder moulds in layers. Each layer was compacted using a vibrating bench to ensure all trapped air was expelled from the wet concrete. The concrete moulds used are shown in Figure 5.1. The concrete was left in these moulds for 24 hours

before being stripped and placed in the water bath. The samples were left in the water bath for 61 days before being tested. The steel fibres that were used in sets two and three are shown in Figure 5.2. The fibres have hooked ends and are 35 mm long with a 0.055 mm diameter.

Figure 5.1: Wet concrete in moulds

Figure 5.2: Steel fibres

5.3 Concrete Strength Tests

Concrete strength tests were conducted to aid the understanding of how the steel fibres affect the behaviour of concrete. Photographs from the experiments can be found in Appendix F.

5.3.1 Tension Splitting Test

The tension splitting test was used to determine the tensile strength at failure. A cylindrical sample of concrete was tested to destruction by applying a vertical compressive force. The cylinder was placed between two strips of timber with dimensions 12 mm x 3 mm along the top and bottom and the force applied until the concrete specimen cracked along its vertical diametric plane (Grassl, 2014). The splitting test on the cylinder specimens was performed using a displacement control at a rate of 0.2 mm/min. The tensile stress at failure was calculated from the maximum load that the cylinder withstands, defined in BS EN12390-6 (2009) as:

$$f_t = \frac{2F_{max}}{\pi LD} \tag{5.1}$$

Where, F_{max} is the maximum load at failure measured in newtons (N), L is the length of the cylinder in millimetres (mm) and D is the diameter of the cylinder in millimetres (mm).

5.3.2 Compression Test

The compression test was conducted on the concrete cube samples to determine the compressive strength of the concrete. This test was performed by gradually increasing the vertical force on the sample until failure occurs. The stress which the sample failed at is taken as the maximum

compressive stress of the concrete (Grassl, 2014). The compression test was performed using load control. The machine has a standard rate for the load control of 20 N/mm^2/min, which was used for all cube tests. The maximum load sustained by the cube before failure was used to calculate the compressive strength of the concrete. BS EN12390-3 (2009) defines the compressive strength as:

$$f_c = \frac{F_{max}}{A_c} \tag{5.2}$$

Where, F_{max} is the maximum load at failure measured in newtons (N), and A_c is the cross-sectional area in square millimetres (mm^2).

5.4 Results and Discussion

The average tensile strength was calculated for each set and the results are shown in Table 5.2

Table 5.2: Splitting test results showing maximum load and tensile strength for each set

	Set 1 - Plain	Set 2 – 0.5% Fibres	Set 3 – 1% Fibres
Maximum Load (N)	208.2	174.7	159.1
Tensile Strength (MPa)	2.95	2.47	2.25

Figure 5.3 shows the three different sets of concrete at failure. The normal concrete had a sudden failure which resulted in a complete fracture down the centre. The other two sets show cracking but due to the fibres the samples do not break. Here the fibres bridge the cracks and therefore the concrete cylinder is still able to sustain some load. Figure 5.3(c) shows an interesting failure where the top of the cylinder experienced crushing at the location of the timber strip. This failure is most likely due to the way the experiment was conducted instead of the way the concrete performed.

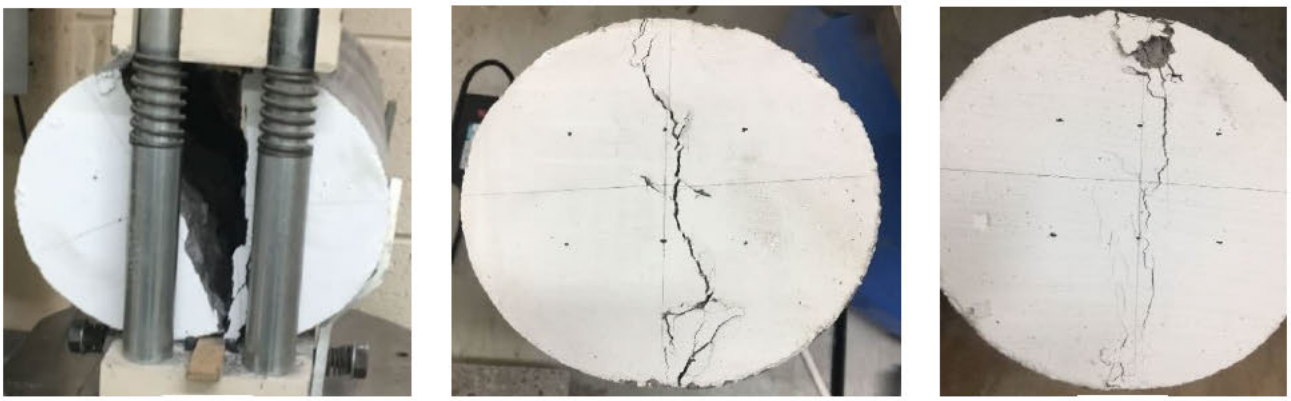

(a) (b) (c)

Figure 5.3: Failure of concrete cylinders during splitting test for (a) set 1 - normal concrete; (b) set 2 - 0.5 % fibres; and (c) set 3 – 1 % fibres

The tensile strength expected for the normal concrete was 3 MPa which was almost reached by the samples. Both sets with fibres had a lower tensile strength which does not correlate to the theory predictions as discussed in Section 2.2 and 2.4. Nevertheless, the bridging behaviour of the fibres was clearly seen by the crack response, which has been illustrated by the load-displacement curve shown in Figure 5.4. The samples without fibres had a sudden failure and the concrete completely split in half. The samples with fibres were able to combat this sudden failure due to the bridging action of the fibres. These samples had a slower failure and after the first cracking occurred the sample continued to sustain a load which decreased as time went on.

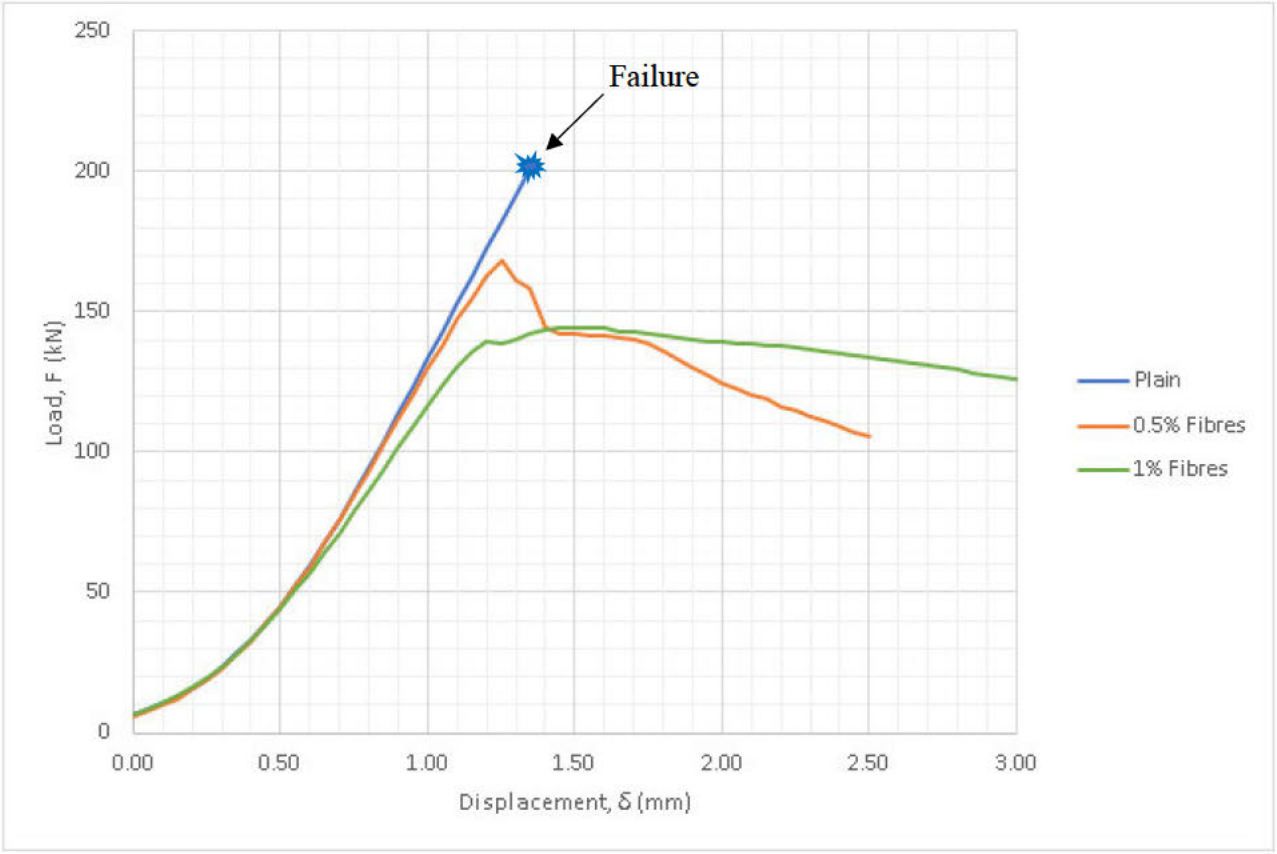

Figure 5.4: Load-displacement curve for the three concrete sets

The average compressive strength was calculated for each set and the results are shown in Table 5.3.

Table 5.3: Compression test results showing maximum load and tensile strength for each set

	Set 1 - Plain	Set 2 – 0.5% Fibres	Set 3 – 1% Fibres
Maximum Load (N)	426.5	257.8	228.3
Compressive Strength (MPa)	42.6	25.8	22.8

The concrete was designed for a compressive strength of 40 MPa which the plain concrete managed to reach. However, the concrete sets with fibres had almost half the strength which was unexpected.

The failure of the cube samples is shown in Figure 5.5.

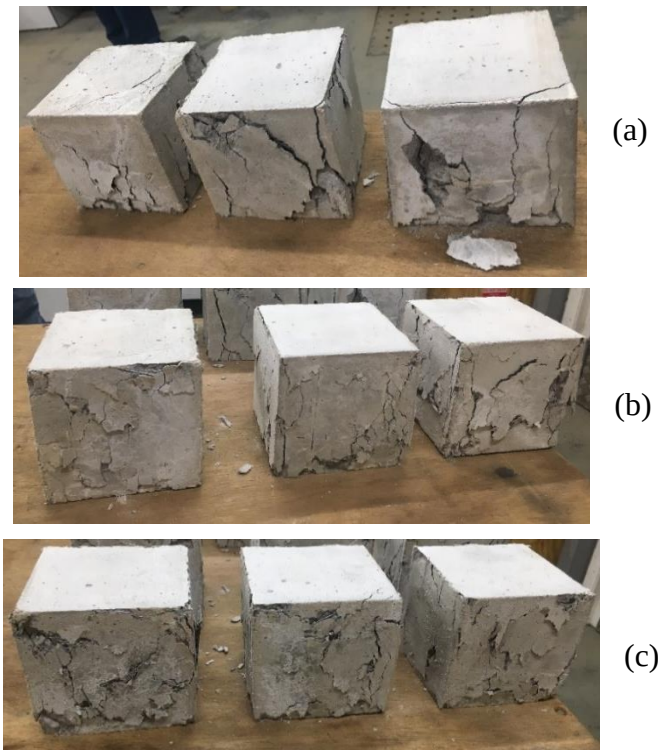

Figure 5.5: Failure of concrete cylinders during compression test for (a) set 1 - normal concrete; (b) set 2 - 0.5 % fibres; and (c) set 3 – 1 % fibres

The inconsistencies in the experiments could be due to several factors. Firstly, the mixing of the concrete was very slow, and it is possible that the fibres were not properly mixed or distributed evenly within the concrete. Another reason might be because of the limited proportions of coarse aggregate in the mix (see Figure 8.7 and Figure 8.8 in Appendix F) and this could have affected the strength and the bond of the fibres to the concrete.

5.5 Summary

The results from the small-scale experiments confirmed the bridging effect of the fibres. They showed how the fibres work in transferring the load once a concrete member has cracked and how they then influence the deformation behaviour of the concrete specimen. However, the results show inconsistencies with the theory as the sets with fibres had a lower tensile and compressive strength when fibres are meant to increase the tensile strength of a concrete specimen. The reasons for this can be explained by the mixing and distribution of the steel fibres as well as the type of aggregate that was used. It is therefore very important when using steel fibres to have strict quality control on the concrete mix design to ensure that the mix has the required strength and that the fibres have been evenly distributed. The results clearly show the difficult nature of fibres and how the casting of the concrete is crucial in achieving the expected strength gain.

6 Conclusions

6.1 General Conclusions

The aim of this project was to investigate the influence of steel fibres on the strength and deformation capacity of reinforced concrete connections using nonlinear finite element analysis. This aim was achieved by subjecting a reinforced concrete connection to tension by prescribing a displacement to one end using the finite element programme LS-DYNA.

The main investigation examined the behaviour of reinforcement lap lengths and explored the differences in the design codes required values. The required lap length for MC10 was larger than for EC2 and the analyses showed that only a lap length much larger (1200 mm) than the MC10 required value was able to withstand the load and allow the reinforcement to reach its yield strength. The addition of steel fibres revealed that the three lap lengths greater than EC2 were able to reach the reinforcement yield strength and were able to withstand the load, implying that the strength had been increased. The lap length smaller than EC2 (300 mm) still exhibited the brittle failure that was seen without the addition of fibres. Even though the other laps reached reinforcement yield, there was no transfer length for the small lap (500 mm) and only a very small transfer length for the one above (800 mm), thereby showing that these laps were still at the lower limit of the quantity of reinforcement that needed to be provided.

The concrete experiments assessed how steel fibres affect the strength and failure response of plain concrete cubes and cylinders and concluded that the fibres decreased the strength. This unexpected result has been accounted for by the concrete mixing and distribution of fibres and emphasises the importance that the mixing procedure has. Nevertheless, the experiments improved the failure response as the fibre concrete had a more ductile failure, indicating a higher deformation capacity. These experiments gave an indication of how steel fibres behave in concrete but since these experiments were not conducted on reinforced concrete connections, conclusions cannot be made on how the fibres would improve the connection response in experiments. Separate experiments would need to be undertaken to investigate and compare the connection response to the modelling results.

In conclusion, steel fibres have a promising influence on reinforced concrete connections as the specimens had a higher load capacity and ductility implying that both the strength and deformation capacity had increased. The investigation did highlight however, that in reality the fibres are not always able to provide this higher strength and great care must be taken when using them in construction.

6.2 Suggestions for Further Work

This investigation focused on understanding how straight reinforcement laps behave with the addition of steel fibres. Reinforced concrete connections can use a variety of different reinforcement combinations and shapes and an interesting addition would be to analyse how looped reinforcement bars behave with steel fibres and compare these to the results achieved here.

Due to the simplifications used as explained in Section 4.5 it would be of interest to model the bond-slip that would occur between the reinforcement and concrete – allowing for the bond-slip that was achieved in the 'perfect bond' model executed here. It would also be beneficial to model the reinforcement using the techniques explained in Section 2.6.3 such as the shared nodes with the ribs modelled using a fine mesh and see the effect on the results. Modelling the rebar as solid elements would be a useful analysis to understand how much the beam element model overcompensates the concrete volume.

As explained in the general conclusions, experiments on the reinforced concrete connections modelled in the analyses would provide an interesting investigation on the practical use of fibres. This would allow the distribution and mixing of the fibres with the reinforcement bars to be examined in greater detail. However, experiments on this scale would be expensive and time consuming.

Steel fibres are rarely used in industry due to their unpredictable behaviour, but they have very advantageous properties and are becoming more popular especially in areas prone to earthquakes. It would therefore be relevant to assess how steel fibres respond when under seismic loading and how they affect the structural integrity of a building that may be subject to earthquake loading.

7 References

Aslani, F. and Nejadi, S. (2012). Bond characteristics of steel fibre reinforced self-compacting concrete. *Canadian Journal of Civil Engineering*, 39(7), pp.834-848.

Bischoff, P. (2001). Effects of shrinkage on tension stiffening and cracking in reinforced concrete. *Canadian Journal of Civil Engineering*, 28(3), pp.363-374.

Bischoff, P. (2003). Tension Stiffening and Cracking of Steel Fiber-Reinforced Concrete. *Journal of Materials in Civil Engineering*, 15(2), pp.174-182.

Bolander, J. *Fiber Reinforced Concrete: Cracking and Post-cracking Strength Estimations.*

Bright, N. and Roberts, J. (2010). *Structural Eurocodes - Extracts from the Structural Eurocodes for Students of Structural Design*. 3rd ed. British Standards Institution.

BS EN 12390-3:2009. *Testing Hardened Concrete*, Part 3: Compressive Strength of Test Specimens.

BS EN 12390-6:2009. *Testing Hardened Concrete*, Part 6: Tensile Splitting Strength of Test Specimens.

BS EN 1992-1-1:2004 + A1:2014. *Eurocode 2: Design of Concrete Structures*, Part 1-1: General rules and rules for buildings.

Cairns, J. (2015). Bond and anchorage of embedded steel reinforcement in fib Model Code 2010. *Structural Concrete*, 16(1), pp.45-55.

CEB-FIP. (2013). *CEB-FIP Model Code for Concrete Structures 2010*, fib, Ernst & Sohn.

Chen, W. (2007) *Plasticity in Reinforced Concrete*, J. Ross Publishing, pp. 4-26.

Grassl, P. (1999). *Splicing of Reinforcement Loops in Beams - Experiments and Non-linear Finite Element Analyses*, Division of Concrete Structures, Chalmers University of Technology, Göteborg, Sweden.

Grassl, P. and Jirásek, M. (2006). Damage-plastic model for concrete failure. *International Journal of Solids and Structures*, 43(22-23), pp.7166-7196.

Grassl, P., Xenos, D., Nyström, U., Rempling, R. and Gylltoft, K. (2013). CDPM2: A damage-plasticity approach to modelling the failure of concrete. *International Journal of Solids and Structures*, 50(24), pp.3805-3816.

Grassl, P. (2014), *Construction Materials Lecture Notes*, Civil Engineering Year 1, University of Glasgow, School of E, Glasgow, Scotland.

Grassl, P. (2016), *User manual for MAT_CDPM (MAT_273) in LS-DYNA*, Available at: https://petergrassl.com/Research/DamagePlasticity/CDPMLSDYNA/index.html [Accessed 18 Oct. 2018].

Grassl, P. (2018), *Structural Concrete Lecture notes*, Structural Concrete Year 5, University of Glasgow, School of Engineering, Glasgow, Scotland.

Jirásek, M. and Bažant, Z. (2002). *Inelastic analysis of structures*. Chichester: Wiley.

Livermore Software Technology Corporation (2018a). *LS-DYNA Keyword User's Manual* [Online] vol. 1, Available at: http://www.lstc.com/download/manuals [Accessed 10 Oct 2018].

Livermore Software Technology Corporation (2018b). *LS-DYNA Keyword User's Manual* [Online] vol. 2 – Material Models, Available at: http://www.lstc.com/download/manuals [Accessed 10 Oct 2018].

Livermore Software Technology Corporation (2018c). *LS-DYNA Theory Manual*, [Online] Available at : http://www.lstc.com/download/manuals [Accessed 21 Nov 2018].

Livermore Software Technology Corporation (2019). *What are the differences between implicit and explicit? — LS-DYNA Support*. [online] Dynasupport.com. Available at: https://www.dynasupport.com/faq/general/what-are-the-differences-between-implicit-and-explicit [Accessed 3 Jan. 2019].

Lockhart, E. (2017). *Modelling the Failure of Reinforced Concrete Subjected to Dynamic Loading Using CDPM2 in LS-DYNA*, University of Glasgow, School of Engineering, MEng Thesis, Glasgow, Scotland.

MacLeod, I. (2005). *Modern structural analysis*. London: Thomas Telford Limited.

Maidl, B.R. & Dietrich, J. 1995, *Steel fibre reinforced concrete*, Ernst & Sohn, Berlin.

Micallef, M. and Vollum, R. (2017). *The Behaviour of Long Tension Reinforcement Laps*, Department of Civil and Environmental Engineering, Imperial College London, London.

Naaman, A. (1987). *High Performance Fiber Reinforced Cement Composites.*

Rypl, D. (2016). *Triangulation of 3D Domains User Guide*, Czech Technical University in Prague, Faculty of Civil Engineering, Department of Mechanics, Prague, Czech Republic.

Schwer, L. (2014). *Modeling Rebar: The Forgotten Sister in Reinforced Concrete Modeling*.

Schaller, C. (ed.), Thacker, B., Doebling, S., Hemez, F., Anderson, M., Pepin, J. and Rodriguez, E. (2004) *Concepts of Model Verification and Validation*, Los Alamos National Laboratory, University of California.

Teychenne, D., Franklin, R. and Erntroy, H. (1997). *Design of normal concrete mixes*. Watford: Building Research Establishment.

8 Appendices

Appendix A – Reinforcement Lap Length Calculations

The following calculations show how the lap lengths were calculated for both the Eurocode 2 and 2010 Model Code equations.

Eurocode 2

$\emptyset = 20$ mm

$f_{cm} = 40$ MPa

$\alpha_{ct} = 1$ (recommended value)

$\gamma_c = 1$

$f_{ck} = f_{cm} - 8 = 40 - 8 = 32$ MPa

$$f_{ctm} = 0.3 \times (f_{ck})^{2/3}$$

$$f_{ctm} = 0.3 \times (32)^{2/3} = \mathbf{3\ MPa}$$

$\eta_1 = 1.0$ (for 'good' bond conditions)

$\eta_2 = 1.0$ (for $\phi \leq 32$ mm)

$$f_{bm} = 2.25\eta_1\eta_2 f_{ctm}$$

$$f_{bm} = 2.25 \times 1.0 \times 1.0 \times 3.0 = \mathbf{6.8\ MPa}$$

$f_{yk} = 500$ MPa

$\gamma_s = 1$

$$\sigma_y = f_{yd} = \frac{f_{yk}}{\gamma_s}$$

$$\sigma_y = f_{yd} = \frac{500}{1.0} = \mathbf{500\ MPa}$$

$$L_{b,rqm} = \left(\frac{\emptyset}{4}\right)\left(\frac{\sigma_y}{f_{bm}}\right)$$

$$L_{b,rqm} = \left(\frac{20}{4}\right)\left(\frac{500}{6.8}\right)$$

$$L_{b,rqm} = \mathbf{368\ mm}$$

For straight bar in tension:

$\alpha_1 = 1.0$

$\alpha_2 = 1 - 0.15\frac{(c_d - \emptyset)}{\emptyset}$

For straight bars, $c_d = \min(\frac{a}{2}, c_1, C)$

$C = 30$ mm

$c_1 = 30$ mm

$\frac{a}{2} = \frac{150}{2} = 75$ mm

$\therefore c_d = 30$ mm

$\Longrightarrow \alpha_2 = 1 - 0.15\frac{(30-20)}{20} = 0.925$

$\alpha_3 = 1 - K\lambda$ (in tension)

Take $K = 0$ (conservative assumption) $\quad \therefore \alpha_3 = 1.0$

$\alpha_5 = 1 - 0.04p = 1.0$ (conservative assumption)

$\alpha_6 = \left(\frac{\rho_1}{25}\right)^{0.5} = 1.0$

$$L_b = \alpha_1\alpha_2\alpha_3\alpha_5\alpha_6 L_{b,rqm}$$

$$L_b = 1.0 \times 0.925 \times 1.0 \times 1.0 \times 1.0 \times 368$$

$$\therefore L_b = \mathbf{340\ mm}$$

2010 Model Code

$f_{cm} = 40$ MPa

$f_{stm} = 500$ MPa (for good bond conditions)

$\emptyset = 20$ mm

$c_{min} = \min\left(\frac{c_s}{2}, c_x, c_y\right) = 30$ mm

$c_{max} = \max\left(\frac{c_s}{2}, c_x\right) = 55$ mm (as $c_s = 110$ mm)

$k_m = 0$ (as $c_s < 8c_y$)

$$f_{stm} = 54\left(\frac{f_{cm}}{25}\right)^{0.25}\left(\frac{25}{\emptyset}\right)^{0.2}\left(\frac{L_b}{\emptyset}\right)^{0.55}\left[\left(\frac{c_{min}}{\emptyset}\right)^{0.25}\left(\frac{c_{max}}{c_{min}}\right)^{0.1} + k_m k_{tr}\right]$$

$$500 = 54\left(\frac{40}{25}\right)^{0.25}\left(\frac{25}{20}\right)^{0.2}\left(\frac{L_b}{20}\right)^{0.55}\left[\left(\frac{30}{20}\right)^{0.25}\left(\frac{55}{30}\right)^{0.1} + 0\right]$$

$$\therefore L_b = \mathbf{635\ mm}$$

Appendix B – Crack Spacing Calculation

The maximum crack spacing was calculated from the equations in Eurocode 2.

For a member in tension:

$h = 250$ mm

$b = 250$ mm

$d = 210$ mm

$$A_{ct,eff} = A_{cb,eff} = \big(2.5(h - d)\big) \times b$$

$$A_{ct,eff} = A_{cb,eff} = \big(2.5(250 - 210)\big) \times 250$$

$$A_{ct,eff} = A_{cb,eff} = 25000 \text{ mm}^2$$

$$A_{c,eff} = A_{ct,eff} + A_{cb,eff}$$

$$A_{c,eff} = 100 \times 250 + 100 \times 250$$

$$A_{c,eff} = 50000 \text{ mm}^2$$

$A_s = 1256 \text{ mm}^2$ (4 x 20 mm diameter bars)

$$\rho_{s,eff} = \frac{A_s}{A_{c,eff}}$$

$$\rho_{s,eff} = \frac{1256}{50000}$$

$$\rho_{s,eff} = 0.02512$$

$\emptyset = 20$ mm

$C = 30$ mm

$k_1 = 0.8$ (for high bond bars)

$k_2 = 1.0$ (for pure tension)

$k_3 = 3.4$

$k_4 = 0.425$

$$S_{r,max} = k_3 C + k_1 k_2 k_4 \frac{\emptyset}{\rho_{s,eff}}$$

$$S_{r,max} = 3.4 \times 30 + 0.8 \times 1.0 \times 0.425 \times \frac{20}{0.02512}$$

$$\boldsymbol{S_{r,max} = 373 \text{ mm}}$$

Appendix C – Input File

The input file used in all analyses was as follows:

```
*KEYWORD  50000000
*TITLE
 Simulation of straight lapped connection subjected to tension
$
*Parameter
$---+----1----+----2----+----3----+----4----+----5----+----6----+----7----+----8
r Tstart    0.0     r Tend     0.1        r DtMax   100.e-3 r MaxDisp   6.e-3
$        |         |         |         |         |         |         |         |
r TSSFAC    0.8     i LCTM      9         r TconP     30.0
$---+----1----+----2----+----3----+----4----+----5----+----6----+----7----+----8
$
*Parameter_Expression
$---+----1----+----2----+----3----+----4----+----5----+----6----+----7----+----8
$        |         |         |         |         |         |         |         |
 r TDplot   Tend/20
 r TASCII TDplot/30.
 r Tend2   2.0*Tend
$
*CONTROL_ENERGY
    |    2         2         2         2
$---+----1----+----2----+----3----+----4----+----5----+----6----+----7----+----8
*CONTROL_SHELL
  20.0             1        -1         1         2         2         1
$---+----1----+----2----+----3----+----4----+----5----+----6----+----7----+----8
*CONTROL_TIMESTEP
$   DTINIT    TSSFAC      ISDO    TSLIMT     DT2MS      LCTM     ERODE     MS1ST
    0.0000       0.8         0     0.000     0.000     &LCTM
$---+----1----+----2----+----3----+----4----+----5----+----6----+----7----+----8
$
*CONTROL_TERMINATION
   &Tend
$
$
*CONTROL_OUTPUT
$  NPOPT NEECHO NREFUP IACCOP OPIFS IPNINT IKEDIT IFLUSH
    |  1,   3,      ,       ,     ,    50
```

The data was output into files by adding the following into the input file:

```
$---+----1----+----2----+----3----+----4----+----5----+----6----+----7----+----8
$$$$$$$$$$$$$$$$$$$$$$$$$$$$$$$$$$$$$$$$$$$$$$$$$$$$$$$$$$$$$$$$$$$$$$$$$$$$$$$
$                                   TIME HISTORY                                 $
$$$$$$$$$$$$$$$$$$$$$$$$$$$$$$$$$$$$$$$$$$$$$$$$$$$$$$$$$$$$$$$$$$$$$$$$$$$$$$$
$
*DATABASE_ELOUT
$---+----1----+----2----+----3----+----4----+----5----+----6----+----7----+----8
$       dt
   &TASCII
$
*DATABASE_HISTORY_BEAM_SET
$---+----1----+----2----+----3----+----4----+----5----+----6----+----7----+----8
$    setid
        1
.

*DATABASE_GLSTAT
$       dt
   &TASCII
$
*DATABASE_MATSUM
$       dt
   &TASCII
$
*DATABASE_NODFOR
$       dt
   &TASCII
*DATABASE_SPCFORC
$#      dt
   &TASCII
$---+----1----+----2----+----3----+----4----+----5----+----6----+----7----+----8
*DATABASE_BINARY_D3PLOT
$       dt
   &TDplot
$
$
$---+----1----+----2----+----3----+----4----+----5----+----6----+----7----+----8
*DATABASE_EXTENT_BINARY
$    neiph     neips    maxint    strflg    sigflg    epsflg    rltflg    engflg
        5                              1         1         1
$   cmpflg    ieverp    beamip
            0
$---+----1----+----2----+----3----+----4----+----5----+----6----+----7----+----8
$
*Include
material.k
$
*Include
mesh.k
```

The ends of the rebar were strengthened by adding the following into the input file:

```
*PART
boxsolid
$---+----1----+----2----+----3----+----4----+----5----+----6----+----7----+----8
$        |         |         |         |         |         |         |         |
$      pid     secid       mid     eosid      hgid      grav    adpopt      tmid
       1         1         1         0         0         0         0         0
*SECTION_SOLID
$    secid    elform       aet
       1        10         0
$
*PART
reinforcement
$---+----1----+----2----+----3----+----4----+----5----+----6----+----7----+----8
$        |         |         |         |         |         |         |         |
$      pid     secid       mid     eosid      hgid      grav    adpopt      tmid
       2         2         2         0         0         0         0         0
$
reinforcement
$---+----1----+----2----+----3----+----4----+----5----+----6----+----7----+----8
$        |         |         |         |         |         |         |         |
$      pid     secid       mid     eosid      hgid      grav    adpopt      tmid
       3         3         2         0         0         0         0         0
$
$
*SECTION_BEAM_TITLE
Section reinforcement
$---+----1----+----2----+----3----+----4----+----5----+----6----+----7----+----8
$        |         |         |         |         |         |         |         |
$    secid    elform      shrf   qr/irid       cst     scoor       nsm
       2         1       1.0         2         1       0.0       0.0
$        |         |         |         |         |         |         |         |
$      ts1       ts2       tt1       tt2     nsloc     ntloc
     0.020     0.020       0.0       0.0       0.0       0.0
$
Section reinforcement
$---+----1----+----2----+----3----+----4----+----5----+----6----+----7----+----8
$        |         |         |         |         |         |         |         |
$    secid    elform      shrf   qr/irid       cst     scoor       nsm
       3         1       1.0         2         1       0.0       0.0
$        |         |         |         |         |         |         |         |
$      ts1       ts2       tt1       tt2     nsloc     ntloc
     0.040     0.040       0.0       0.0       0.0       0.0
```

The boundary conditions were applied using the following in the input file:

```
$---+----1----+----2----+----3----+----4----+----5----+----6----+----7----+----8
*Boundary_Prescribed_Motion_Set
$---+----1----+----2----+----3----+----4----+----5----+----6----+----7----+----8
$       ID       DOF       VAD      LCID        SF       VID     DEATH     BIRTH
        2         3         2       111       1.0
$
*BOUNDARY_SPC_SET
$---+----1----+----2----+----3----+----4----+----5----+----6----+----7----+----8
$       ID       CID      DOFX      DOFY      DOFZ     DOFRX     DOFRY     DOFRZ
        2         0         1         1         0         0         0         0
$
*BOUNDARY_SPC_SET
$---+----1----+----2----+----3----+----4----+----5----+----6----+----7----+----8
$       ID       CID      DOFX      DOFY      DOFZ     DOFRX     DOFRY     DOFRZ
        1         0         1         1         1         0         0         1
```

The rebar was constrained in the solid element using the CONSTRAINED_BEAM_IN_SOLID keyword as follows:

```
*CONSTRAINED_BEAM_IN_SOLID
$---+----1----+----2----+----3----+----4----+----5----+----6----+----7----+----8
$       |         |         |         |         |         |         |         |
$    slave    master     sstyp     mstyp                           nquad      cdir
        2         1         1         1                                      0
$       |         |         |         |         |         |         |         |
$    start       end               axfor
        0.        0.                0.
$
*CONSTRAINED_BEAM_IN_SOLID
$---+----1----+----2----+----3----+----4----+----5----+----6----+----7----+----8
$       |         |         |         |         |         |         |         |
$    slave    master     sstyp     mstyp                           nquad      cdir
        3         1         1         1                                      0
$       |         |         |         |         |         |         |         |
$    start       end               axfor
        0.        0.                0.
$ applied Y-direction displacement
*DEFINE_CURVE
 111, 0, 1., 1., 0., 0.
  0.0,     0.0
  &Tend,   &MaxDisp
  &Tend2,  &MaxDisp
$
$
$ maximum time increment
*DEFINE_CURVE
9,0,1.,1.,0.,0.
   0.0,  &DtMax
 &Tend,  &DtMax
 &Tend2, &DtMax
$
*END
```

Appendix D – Material File

The material file for the Reinforced Concrete specimens was as follows:

```
$ Material
$ Mat 273 (units: Newtons-m-Pa)
*MAT_CDPM
$---+----1----+----2----+----3----+----4----+----5----+----6----+----7----+----8
$       |         |         |         |         |         |         |         |
$      MID       RHO         E        PR       ECC       QH0        FT        FC
         1    2.40E3     35.E9       0.2                          3.0e6     40.e6
$       |         |         |         |         |         |         |         |
$       HP        AH        BH        CH        DH        AS        DF       FC0
      0.01
$       |         |         |         |         |         |         |         |
$     TYPE        BS        WF       WF1       FT1    STRFLG   FAILFLG       EFC
        1             117.8e-6                                          1.e-3
$
*MAT_PLASTIC_KINEMATIC_TITLE
#Reinforcement
$---+----1----+----2----+----3----+----4----+----5----+----6----+----7----+----8
$       |         |         |         |         |         |         |         |
$#     mid        ro         e        pr      sigy      etan      beta
         2    7.85E3    200.E9       0.3    500.E6         0       0.0
$       |         |         |         |         |         |         |         |
$#     src       srp        fs        vp
       0.0       0.0       0.0       0.0
```

The material file for the Fibre Reinforced Concrete with Traditional Steel Fibres specimen was as follows:

```
$ Material
$ Mat 273 (units: Newtons-m-Pa)
*MAT_CDPM
$---+----1----+----2----+----3----+----4----+----5----+----6----+----7----+----8
$       |         |         |         |         |         |         |         |
$      MID       RHO         E        PR       ECC       QH0        FT        FC
         1    2.40E3     35.E9       0.2                          3.0e6     40.e6
$       |         |         |         |         |         |         |         |
$       HP        AH        BH        CH        DH        AS        DF       FC0
      0.01
$       |         |         |         |         |         |         |         |
$     TYPE        BS        WF       WF1       FT1    STRFLG   FAILFLG       EFC
        1             117.8e-6                                          1.e-3
$
*MAT_PLASTIC_KINEMATIC_TITLE
#Reinforcement
$---+----1----+----2----+----3----+----4----+----5----+----6----+----7----+----8
$       |         |         |         |         |         |         |         |
$#     mid        ro         e        pr      sigy      etan      beta
         2    7.85E3    200.E9       0.3    500.E6         0       0.0
$       |         |         |         |         |         |         |         |
$#     src       srp        fs        vp
       0.0       0.0       0.0       0.0
```

Appendix E – Concrete Mix Design Forms

The concrete mix designs form used in the design of the three sets of concrete are shown on the next three pages. Each mix design has quantities for three cubes and three cylinders along with 15% extra material added in for waste.

[3 cubes & 3 cylinders]

Concrete mix design form

Job title ..NORMAL CONCRETE..

Stage	Item		Reference or calculation	Values	
1	1.1	Characteristic strength	Specified	..... N/mm² at 28 days	
				Proportion defective ..... %	
	1.2	Standard deviation	Fig 3	..... N/mm² or no data	..... N/mm²
	1.3	Margin	C1 or Specified	(k = ...) ..... × ..... =	..... N/mm²
					..... N/mm²
	1.4	Target mean strength	C2	..... + ... =	50 N/mm²
	1.5	Cement strength class	Specified	42.5/~~52.5~~	
	1.6	Aggregate type: coarse Aggregate type: fine		~~Crushed~~/uncrushed ~~Crushed~~/uncrushed	
	1.7	Free-water/cement ratio	Table 2, Fig 4	0·44	
	1.8	*Maximum free-water/ cement ratio*	*Specified*	..... Use the lower value	0·44
2	2.1	Slump or Vebe time	Specified	Slump 60-180 mm or Vebe time 0-3 s	
	2.2	Maximum aggregate size	Specified		20 mm
	2.3	Free-water content	Table 3	.....	195 kg/m³
3	3.1	Cement content	C3	195 ÷ 0·44 =	443 kg/m³
	3.2	*Maximum cement content*	*Specified*	..... kg/m³	
	3.3	*Minimum cement content*	*Specified*	..... kg/m³	
				use 3.1 if ≤ 3.2 use 3.3 if > 3.1	443 kg/m³
	3.4	Modified free-water/cement ratio		.....	
4	4.1	Relative density of aggregate (SSD)		2·6 known/~~assumed~~	
	4.2	Concrete density	Fig 5		2360 kg/m³
	4.3	Total aggregate content	C4	2360 − 443 − 195 =	1722 kg/m³
5	5.1	Grading of fine aggregate	Percentage passing 600 µm sieve		70 %
	5.2	Proportion of fine aggregate	Fig 6		34 %
	5.3	Fine aggregate content	C5	1722 × 0·34 =	585 kg/m³
	5.4	Coarse aggregate content	C5	1722 − 585 =	1137 kg/m³

Quantities	Cement (kg)	Water (kg or litres)	Fine aggregate (kg)	Coarse aggregate (kg) 10 mm	20 mm	40 mm
per m³ (to nearest 5 kg)	445	195	585	380	760	–
per trial mix of 0·0189 m³	9·7	4·2	12·7	8·3	16·5	–

└ total aggregate = 37·5kg

Items in italics are optional limiting values that may be specified (see Section 7).
Concrete strength is expressed in the units N/mm². 1 N/mm² = 1 MN/ m² = 1 MPa. (N = newton; Pa = pascal.)
The internationally known term 'relative density' used here is synonymous with 'specific gravity' and is the ratio of the mass of a given volume of substance to the mass of an equal volume of water.
SSD = based on the saturated surface-dry condition.

[15% for waste included]

[3 cubes & 3 cylinders]

Concrete mix design form

Job title 0.5% STEEL FIBRES

Stage	Item		Reference or calculation	Values
1	1.1	Characteristic strength	Specified	..... N/mm² at 28 days
				Proportion defective ..... %
	1.2	Standard deviation	Fig 3	..... N/mm² or no data ..... N/mm²
	1.3	Margin	C1 or Specified	(k = ...) ..... × ..... = ... N/mm²
				..... N/mm²
	1.4	Target mean strength	C2	..... + ... = 50 N/mm²
	1.5	Cement strength class	Specified	42.5/~~52.5~~
	1.6	Aggregate type: coarse Aggregate type: fine		~~Crushed~~/uncrushed ~~Crushed~~/uncrushed
	1.7	Free-water/cement ratio	Table 2, Fig 4	0.44
	1.8	*Maximum free-water/ cement ratio*	*Specified*	..... Use the lower value: 0.44
2	2.1	Slump or Vebe time	Specified	Slump 60-180 mm or Vebe time 0-3 s
	2.2	Maximum aggregate size	Specified	20 mm
	2.3	Free-water content	Table 3	195 kg/m³
3	3.1	Cement content	C3	195 ÷ 0.44 = 443 kg/m³
	3.2	*Maximum cement content*	*Specified*	..... kg/m³
	3.3	*Minimum cement content*	*Specified*	..... kg/m³
				use 3.1 if ≤ 3.2 use 3.3 if > 3.1: 443 kg/m³
	3.4	Modified free-water/cement ratio		.....
4	4.1	Relative density of aggregate (SSD)		2.6 ~~known~~/assumed
	4.2	Concrete density	Fig 5	2360 kg/m³
	4.3	Total aggregate content	C4	2360 − 443 − 195 = 1722 kg/m³
5	5.1	Grading of fine aggregate	Percentage passing 600 µm sieve	70 %
	5.2	Proportion of fine aggregate	Fig 6	34 %
	5.3	Fine aggregate content	C5	1722 × 0.34 = 585 kg/m³
	5.4	Coarse aggregate content	C5	1722 − 585 = 1137 kg/m³

Quantities	Cement (kg)	Water (kg or litres)	Fine aggregate (kg)	Coarse aggregate (kg) 10 mm	20 mm	40 mm
per m³ (to nearest 5 kg)	445	195	585	380	760	~~/~~
per trial mix of 0.0189 m³	9.7	4.2	12.7	8.3	16.5	~~/~~

└ total aggregate = 37.5 kg

Items in italics are optional limiting values that may be specified (see Section 7).
Concrete strength is expressed in the units N/mm². 1 N/mm² = 1 MN/ m² = 1 MPa. (N = newton; Pa = pascal.)
The internationally known term 'relative density' used here is synonymous with 'specific gravity' and is the ratio of the mass of a given volume of substance to the mass of an equal volume of water.
SSD = based on the saturated surface-dry condition.

[15% for waste included]

0.5% steel fibres = 0.85 kg

[3 cubes & 3 cylinders]

Concrete mix design form

Job title 1% STEEL FIBRES

Stage	Item		Reference or calculation	Values
1	1.1	Characteristic strength	Specified	✓ N/mm² at 28 days
				Proportion defective ✓ %
	1.2	Standard deviation	Fig 3	✓ N/mm² or no data ✓ N/mm²
	1.3	Margin	C1 or Specified	(k = ✓) ✓ × ✓ = ✓ N/mm²
				✓ N/mm²
	1.4	Target mean strength	C2	✓ + ✓ = 50 N/mm²
	1.5	Cement strength class	Specified	42.5/~~52.5~~
	1.6	Aggregate type: coarse		~~Crushed~~/uncrushed
		Aggregate type: fine		~~Crushed~~/uncrushed
	1.7	Free-water/cement ratio	Table 2, Fig 4	0.44
	1.8	*Maximum free-water/ cement ratio*	*Specified*	✓ Use the lower value: 0.44
2	2.1	Slump or Vebe time	Specified	Slump 60 - 180 mm or Vebe time 0-3 s
	2.2	Maximum aggregate size	Specified	20 mm
	2.3	Free-water content	Table 3	✓ 195 kg/m³
3	3.1	Cement content	C3	195 ÷ 0.44 = 443 kg/m³
	3.2	*Maximum cement content*	*Specified*	✓ kg/m³
	3.3	*Minimum cement content*	*Specified*	✓ kg/m³
				use 3.1 if ≤ 3.2 use 3.3 if > 3.1 443 kg/m³
	3.4	Modified free-water/cement ratio		✓ ✓
4	4.1	Relative density of aggregate (SSD)		2.6 ~~known~~/assumed
	4.2	Concrete density	Fig 5	2360 kg/m³
	4.3	Total aggregate content	C4	2360 - 443 - 195 = 1722 kg/m³
5	5.1	Grading of fine aggregate	Percentage passing 600 µm sieve	70 %
	5.2	Proportion of fine aggregate	Fig 6	34 %
	5.3	Fine aggregate content	C5	1722 × 0.34 = 585 kg/m³
	5.4	Coarse aggregate content	C5	1722 - 585 = 1137 kg/m³

Quantities	Cement (kg)	Water (kg or litres)	Fine aggregate (kg)	Coarse aggregate (kg) 10 mm	20 mm	40 mm
per m³ (to nearest 5 kg)	445	195	585	380	760	✓
per trial mix of 0.0189 m³	9.7	4.2	12.7	8.3	16.5	✓

total aggregate = 37.5kg

Items in italics are optional limiting values that may be specified (see Section 7).
Concrete strength is expressed in the units N/mm². 1 N/mm² = 1 MN/ m² = 1 MPa. (N = newton; Pa = pascal.)
The internationally known term 'relative density' used here is synonymous with 'specific gravity' and is the ratio of the mass of a given volume of substance to the mass of an equal volume of water.
SSD = based on the saturated surface-dry condition.

[15% for waste included]

1% steel fibres = 1.7 kg

Appendix F – Concrete Experiment Photographs

Additional photographs from the concrete experiments described in Chapter 5 are shown here to show how the experiments were conducted in more detail.

Concrete Mixing

Figure 8.1: Concrete mixing drum

(a) (b) (c)

Figure 8.2: Concrete mixes. (a) set 1 ; (b) set 2 ; (c) set 3

Figure 8.3: Concrete tamping on vibrating table

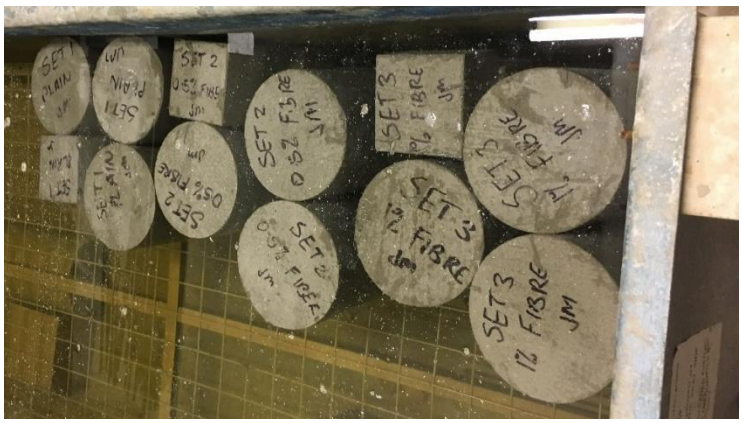

Figure 8.4: Concrete samples curing in water bath

Figure 8.5: Concrete cube samples ready for testing

Figure 8.6: Concrete cylinder samples ready for testing

Concrete Testing

Figure 8.7: Plain concrete cube after compression test

Figure 8.8: Half of plain concrete cylinder after splitting test

Figure 8.9: Steel fibres bridging the crack on a steel fibre cylinder set

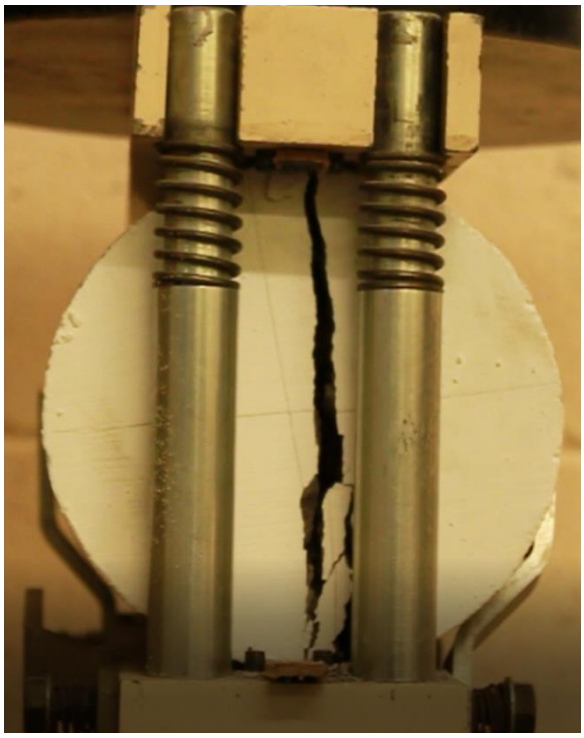

Figure 8.10: Normal concrete cylinder after splitting test

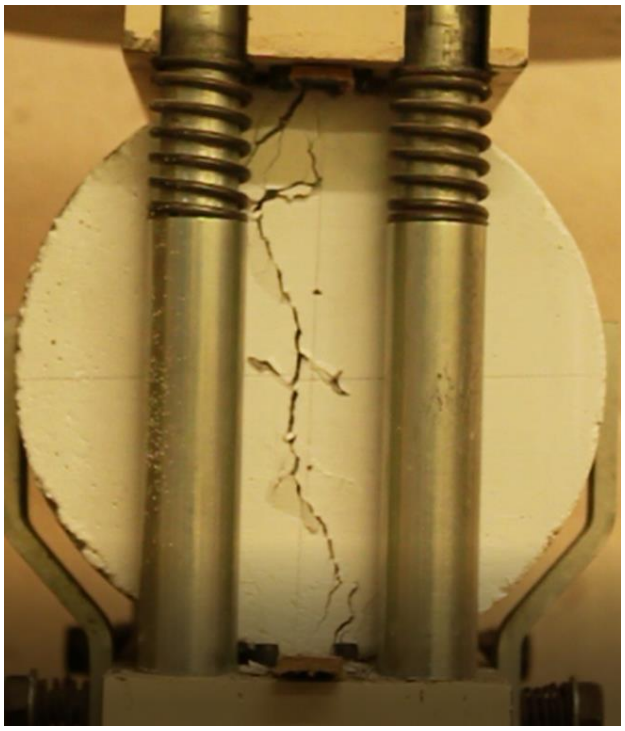

Figure 8.11: 0.5 % steel fibre concrete after splitting test

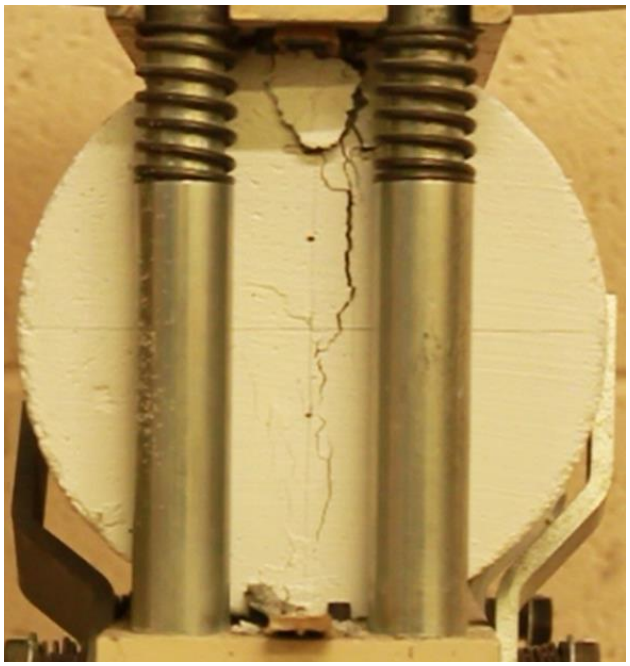

Figure 8.12: 1 % steel fibre concrete after splitting test